

**A STUDY OF FLAT LINEAR INDUCTION MACHINES**

**A STUDY OF FLAT LINEAR INDUCTION MACHINES**

by

**PAUL J. NOLAN, B.E.**

**A Thesis**

**Submitted to the Faculty of Graduate Studies**

**in Partial Fulfillment of the Requirements**

**for the Degree**

**Master of Engineering**

**McMaster University**

MASTER OF ENGINEERING  
(Electrical Engineering)

McMASTER UNIVERSITY  
Hamilton, Ontario

TITLE: A Study of Flat Linear Induction Machines

AUTHOR: Paul J. Nolan, B.E. (National University of Ireland)

SUPERVISOR: R.T.H. Alden, M.A.Sc., Ph.D. (University of Toronto)

NUMBER OF PAGES: xi , 148

## ACKNOWLEDGEMENTS

The author expresses his sincere appreciation to Professor R.T.H. Alden who supervised this work for his continuous encouragement and guidance.

Thanks are also due to Professor C.K. Campbell for permission to use his computational facilities.

The financial support of the National Research Council (grant A7879) is acknowledged.

## ABSTRACT

Of greatest interest in the field of linear motion electrical machines are, the flat linear induction motor and liquid metal pump. The former has feasibility in high speed transportation while the latter is becoming of increasing importance in metallurgical processes.

This thesis examines and extends the traditional representation for the usual sheet secondary classification and then presents a common theory which also allows composite secondary machines to be analysed. An idealized model is developed consisting of a number of regions representing air gaps, iron segments, and secondary conductors. A general solution for the field quantities is obtained. The concept of wave impedance and a transfer matrix approach allow a wide variety of configurations to be analysed. Unlike previous work the approach developed here allows for simultaneous investigation of lateral variation and skin effect. In the limiting cases where in turn skin effect and lateral variation are neglected the solutions are in agreement with known results.

TABLE OF CONTENTS

PAGE

CHAPTER 1:	INTRODUCTION	
1.1	The Linear Induction Machine .....	1
1.2	Review .....	11
1.3	Object of the Thesis .....	16
1.4	Governing Equations .....	16
CHAPTER 2:	ANALYSIS OF THE THIN FINITE WIDTH SHEET MACHINE	
2.1	Introduction .....	25
2.2	Model and Assumptions .....	25
2.3	Governing Equations .....	27
2.4	General Solution .....	33
2.5	The Ideal Machine .....	35
2.6	Finite Width Machine .....	43
CHAPTER 3:	ANALYSIS UNDER THE INFINITE WIDTH ASUMPTION	
3.1	Introduction .....	57
3.2	Skin Effect in the Travelling Wave Case ...	57
3.3	Normal Forces due to Skin Effect .....	66
3.4	Model and Assumptions .....	68
3.5	Equations and General Solution .....	70
3.6	Magnetic Field and Current Density Distribution .....	74
3.7	Performance of the Through Flux Machine ...	80
CHAPTER 4:	GENERALIZED ANALYSIS OF THE FLAT LINEAR INDUCTION MACHINE USING AN ANALOGUE CIRCUIT	
4.1	Introduction .....	87
4.2	Model and Assumptions .....	88

TABLE OF CONTENTS Continued.

	<u>PAGE</u>
4.3 Field Equations and Analogue Circuit .....	90
4.4 General Solution .....	96
4.5 Traction and Levitation Forces .....	99
4.6 Representation of Slotted Stator .....	103
4.7 Discussion .....	107
CHAPTER 5: SIMULTANEOUS TREATMENT OF FLUX PENETRATION AND LATERAL EDGE EFFECT USING A WAVE IMPEDANCE APPROACH	
5.1 Introduction .....	108
5.2 Assumptions .....	108
5.3 General Development .....	110
5.4 Penetration Effect in the Infinite Depth Case	113
5.5 Transfer Matrix and General Solution .....	116
5.6 Boundary Conditions at Stator Surface ....	121
5.7 Reduction of General Solution in limiting cases	124
5.8 Discussion .....	128
CHAPTER 6: CONCLUSIONS	
6.1 Summary of the Thesis .....	130
6.2 Specific Contributions of this work .....	132
6.3 Suggestions for future work in this area ..	138
APPENDIX 1:	
Current density distribution due to three-phase distributed winding .....	140
APPENDIX II:	
Vector phasor quantities .....	142
REFERENCES .....	143

## FIGURE CAPTIONS

<u>Figure</u>		<u>Page</u>
1.1	Conventional squirrel cage induction machine .....	2
1.2	Unrolled squirrel cage machine .....	2
1.3	Induced current paths in sheet secondary	2
1.4	Lateral instability in sheet secondary machine .....	4
1.5	Main classes of linear induction machines	4
1.6	Open-sided machine .....	5
1.7	Double-sided machine .....	5
1.8	Doubly-excited machine .....	5
1.9	Composite secondary .....	7
1.10	End connections in flat machine .....	7
1.11	Tubular machine .....	7
1.12	Classification of linear induction machine	9
1.13	Typical layouts of linear machines as train drives .....	14
1.14	Reference direction for stress tensors ..	23
2.1	General model for two dimensional analysis	26
2.2-a	Elementary loops for Ampere's law .....	28
2.2-b	General end section .....	28
2.3	Equivalent circuit for 'ideal machine' ..	37
2.4	"Ideal machine's" force-speed characteristic .....	37
2.5	Maximum efficiency's dependence on Goodness	40
2.6	Phasor relationships in the ideal machine	42
2.7	Dependence of lateral variation of flux-density on $a/\lambda$ .....	44

<u>Figure</u>		<u>Page</u>
2.8	Dependence of lateral variation of flux-density on S.G .....	45
2.9	Induced current streamlines .....	47
2.10	Dependence of Demagnetising Coefficient on $\lambda/a$ and S.G .....	50
2.11	Force attenuation factor due to finite width effect .....	53
2.12	Lateral variation of flux-density in induction pump with side conductors ...	55
2.13	Lateral variation of flux-density in machine with lateral asymmetric secondary	56
3.1	Co-ordinate system for analysis of skin effect .....	58
3.2	Frequency dependence of travelling wave skin depth .....	62
3.3	Flux distribution in open sided machine	64
3.4	Flux distribution in open sided machine with conducting medium .....	65
3.5	Model for analysis under infinite width approximation .....	69
3.6	Distribution of $\Gamma_1$ for different $c / \lambda$ values.....	76
3.7	Distribution of $\Gamma_2$ for different $c / \lambda$ values.....	78
3.8	Force attenuation factor due to flux penetration effect .....	81
3.9	Dependence of Demagnetising Coefficient on S.R and $c/\lambda$ .....	83
3.10	Phasor diagrams for machine in presence of flux penetration effect .....	85

<u>Figure</u>		<u>Page</u>
4.1	General multiregion representation of linear machines under the infinite width assumption .....	89
4.2	Equivalent anisotropic medium properties	89
4.3	Infinitesimal section used in formulation of equations .....	91
4.4	Analogue circuit for infinitesimal section .....	91
4.5	$\pi$ and T analogue circuits .....	98
4.6-a	Control volume for force calculation ..	100
4.6-b	Model used in investigating sense of normal force (attraction or repulsion)	100
4.7-a	Representation of stator region .....	104
4.7-b	Thin slice of tooth region .....	104
5.1	Multiregion representation of finite width machine .....	109
5.2-a	Variation of skin depth with secondary width .....	117
5.2-b	Variation of skin depth with wavelength	118
5.2-c	Variation of skin depth with magnetic Reynold's number .....	119
5.3	Primary current sheet distributions ...	123
5.4	Truncation error in Fourier Series representation .....	123
5.5	Equivalence of closed form and series solutions .....	127
 <u>Table</u>		
1.1	Magnetic Reynold's number.....	21
3.1	Travelling wave skin depth.....	61

## NOMENCLATURE

(M.K.S. system of units)

A	magnetic vector potential
B	magnetic flux density
$\phi$	magnetic flux
E	electric field intensity
H	magnetic field intensity
J	induced current density
$J_A$	applied current density
h	linear sheet current density
$\lambda$	wavelength
$\beta$	wave number
$\omega$	angular supply frequency
a	mid width of secondary
c	mid thickness of secondary
g	mid thickness of effective air gap
$\sigma$	conductivity
$\mu$	permeability
V	velocity of secondary
$u_s$	synchronous velocity
S	slip
R	Magnetic Reynolds' number
G	Laithwaite "Goodness factor"
f	force density
$f_s$	surface force density
p	Poynting vector
$T_{ij}$	magnetic stress tensor
$\kappa$	$\beta\sqrt{1 + j R}$
$\gamma$	$= \beta\sqrt{1 + j S R}$
$\psi$	current stream function

$$\alpha_n = \frac{2n-1}{2a} \pi$$

$$\gamma_n = \sqrt{\alpha_n^2 + \gamma_0^2}$$

[T] transfer matrix

$Z_0$  Characteristic Wave impedance

$Y_0$  Characteristic Wave admittance

$l_x, l_y, l_z$  unit vectors in x,y,z direction

subscript

1,2,3 vector components in x,y,z directions respectively

$\sim$  phasor quantity

avg average values

superscripts

\* complex conjugate

CHAPTER I  
INTRODUCTION

1.1 The Linear Induction Machine:

The simplest way of introducing linear induction machines to the engineer is to consider their development from the conventional squirrel cage machine. A typical squirrel cage induction machine is shown in Fig. 1.1

As is well known, the effect of the polyphase currents distributed over the stator in the rotating machine is to produce a rotating magnetic field. Induced voltages are set up in the rotor conductors. The interaction of the resulting rotor currents in the magnetic field results in the torque.

The first stage in the development is to consider the machine being unrolled as shown in Fig. 1.2. In this case we expect a linearly travelling field to be set up. Let us neglect, for the present time, any modification in the magnetic field caused by the unrolling process. By applying the same principles a force and output power should be available.

It should be understood that the principles involved would not be changed if the squirrel cage secondary were replaced by a continuous sheet conductor. In fact it may even be a conducting liquid - such is the arrangement used in liquid metal pumps.

In the squirrel cage the induced currents flow in the definite

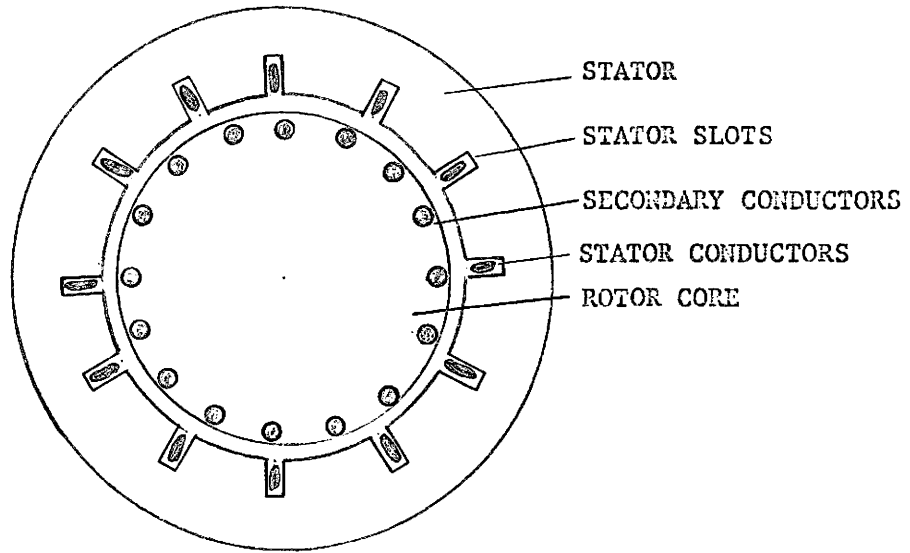


FIG 1.1 : Conventional squirrel cage induction machine

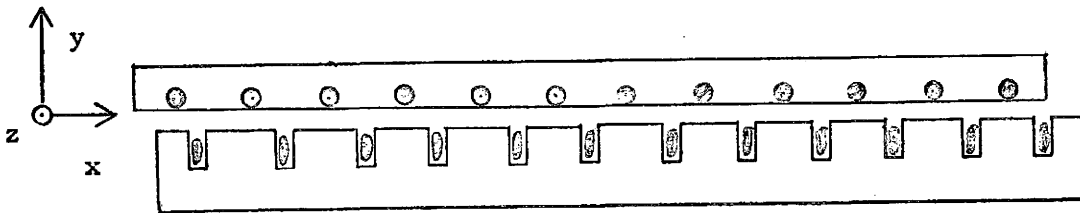


FIG 1.2 : Unrolled squirrel cage machine

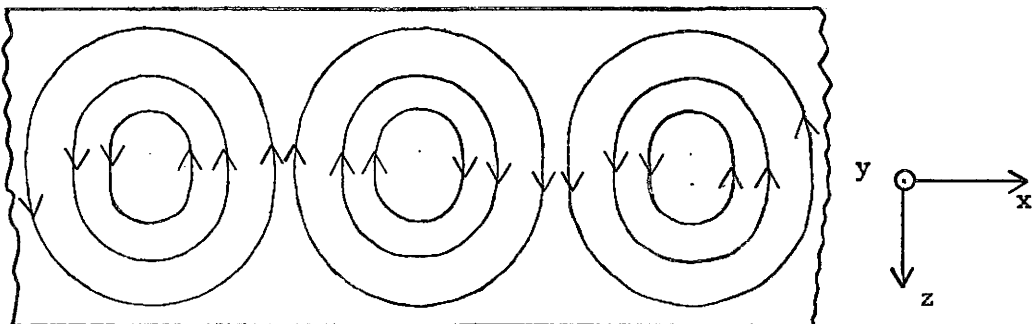


FIG 1.3 : Induced current paths in sheet secondary

paths described by the secondary conductors. In the case of the sheet secondary the induced current paths are not so well defined. The induced currents in this case flow in roughly elliptical paths as shown in Fig. 1.3. Due to the non-uniform current density distribution over the width we also get non-uniform flux and force density distributions. This is referred to as the "lateral edge effect".

If the secondary is asymmetrically positioned as shown in Fig. 1.4, a force tending to increase the eccentricity results. This lateral instability results from shaded pole action in the  $z$  direction. Because of the different resistances at the end sections the induced current tends to be displaced towards the larger extending end. This results in an uneven flux distribution and shaded pole action.

It is obvious from Fig. 1.2 that for continuous motion, either the unrolled stator or rotor must be elongated. These shall henceforth be called primary and secondary respectively. Consequently we get two broad classifications of linear induction machines as shown in Fig. 1.5. These are the short primary and the short secondary machine. Generally the short primary arrangement is less expensive to build and has higher efficiency. If the primary is the moving part some means of power pick-up must be incorporated. The alternative is to use a sectionalised primary in which different sections can be switched in.

Probably the simplest linear induction machine is that shown in Fig. 1.6. It is classified as an "open sided machine". Skin effect in a relatively thick secondary plays an important part in determining the performance of the machine. The study of the skin effect

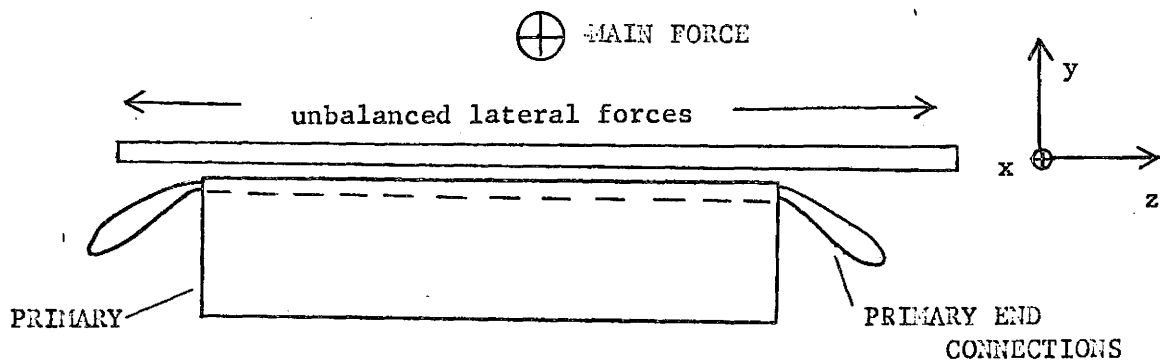
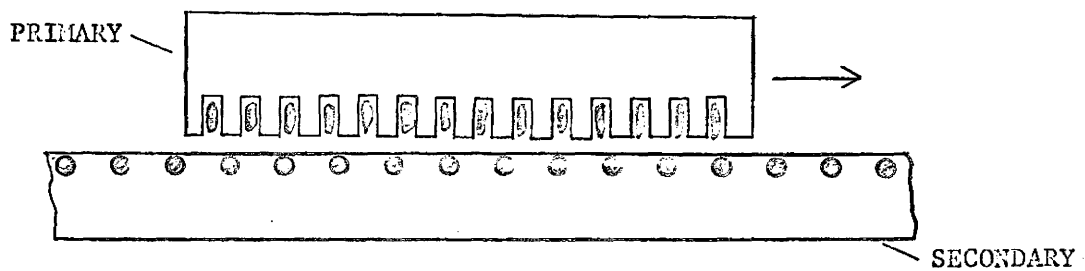
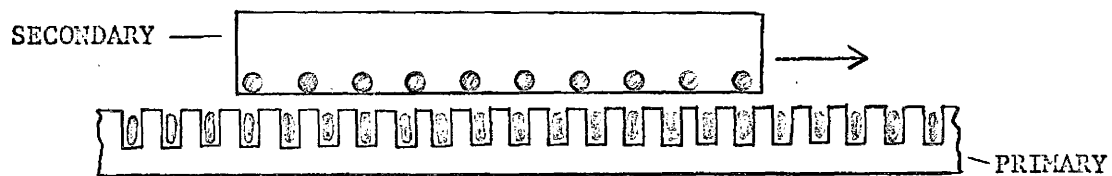


FIG 1.4 : Lateral instability in sheet secondary machine.



(a) Short primary arrangement



(b) Short secondary arrangement

FIG 1.5 : Main classes of linear induction machines

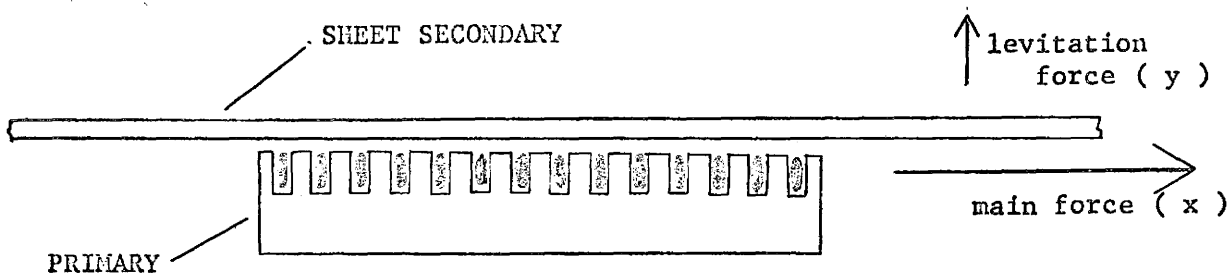


FIG 1.6 : Open-sided machine

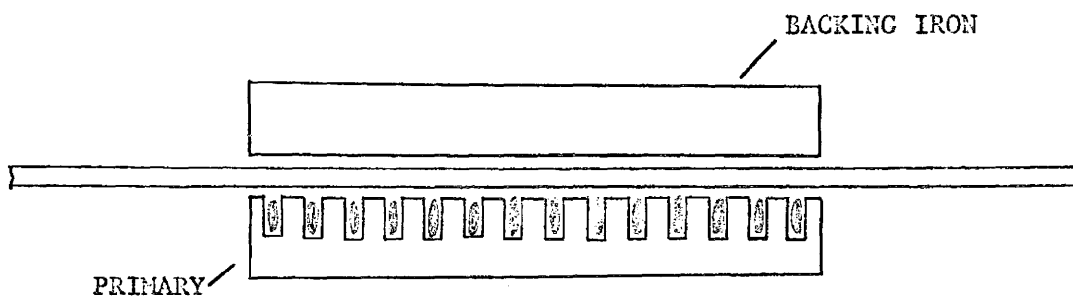


FIG 1.7 : Double-sided machine

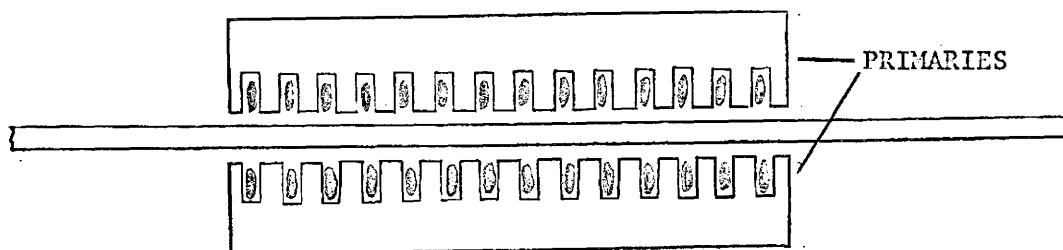


FIG 1.8 : Doubly excited machine.

in the secondary and attenuation in the large air gap with regard to the output characteristic of the machine is referred to as "the flux penetration effect". Recently forces normal to the direction of motion have been considered. In the machine in Fig. 1.6 this force is a levitation force. The force can be interpreted in terms of shaded pole action in the normal direction. The induced currents at different heights can be shown to have different phase angles. The net effect is that there is a travelling field upwards. The levitation force can thus be considered to result from induction motor action in the y direction.

Because the flux must return through the air, the magnetic circuit of Fig. 1.6 is poor. It can be improved by placing a slab of iron at the back of the sheet as shown in Fig. 1.7. This is referred to as a double sided machine. Further improvement can be effected by having a doubly excited machine. (Fig. 1.8). This is the most common flat linear induction machine. Referring to Fig. 1.7, it is obvious that as regards the electromagnetic action the backing iron can be integral with the conducting secondary. Such an arrangement is called a composite secondary. Other forms would be the developed cage machine or having a conducting plate with an array of iron slugs as depicted in Fig. 1.9.

The question of forces in the normal direction is now complicated by magnetic pull besides the levitation force in the opposite direction. This magnetic pull also helps lateral stability since the magnetic pull force would oppose the decentrallizing force due to shaded pole action.

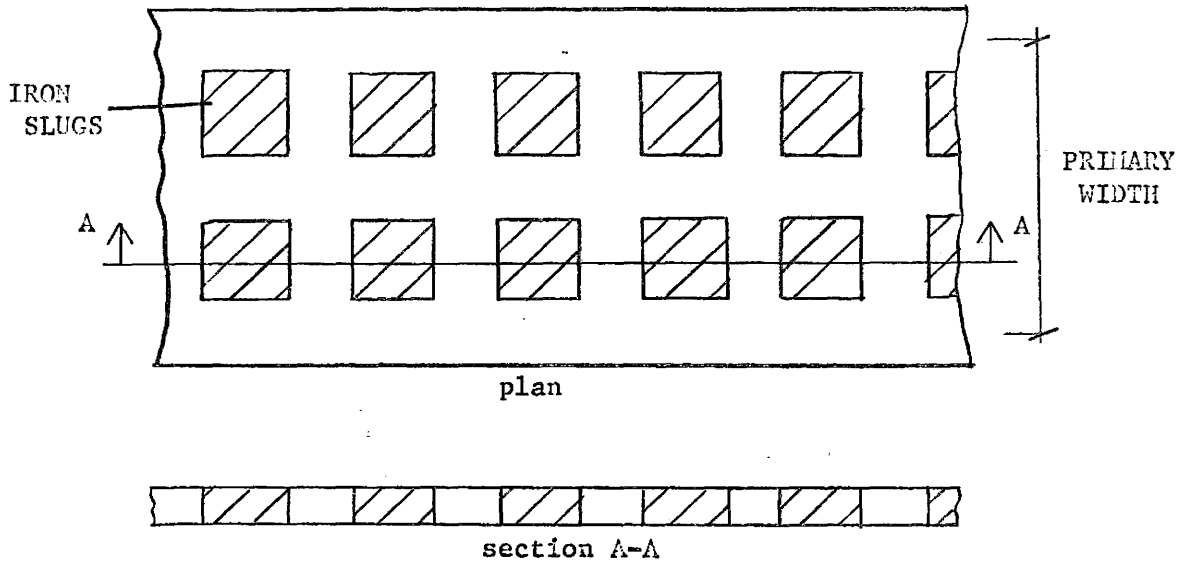


FIG 1.9 : Composite secondary

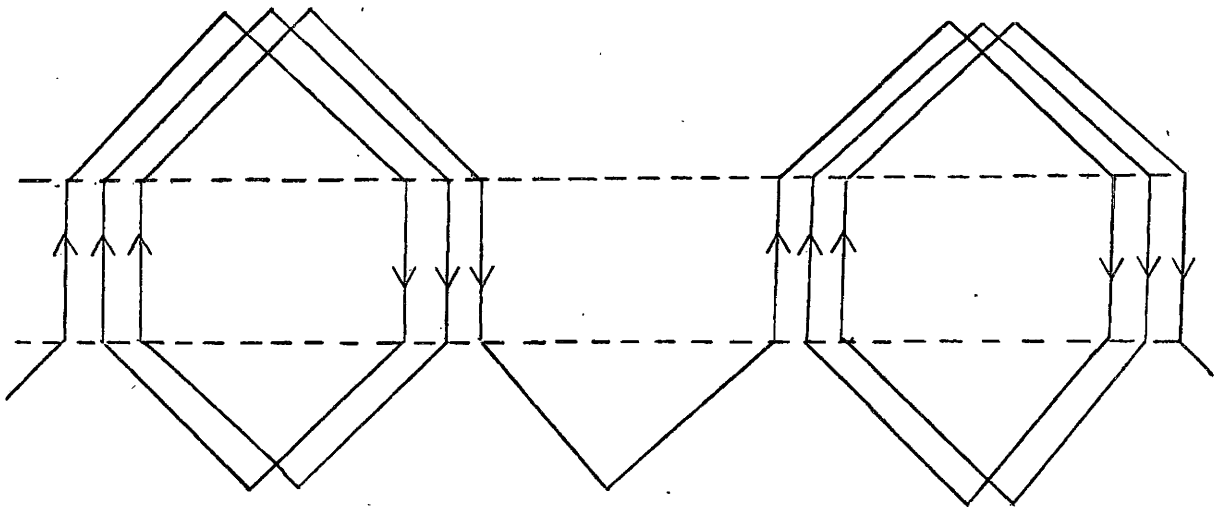


FIG 1.10 : End connections in flat machine.

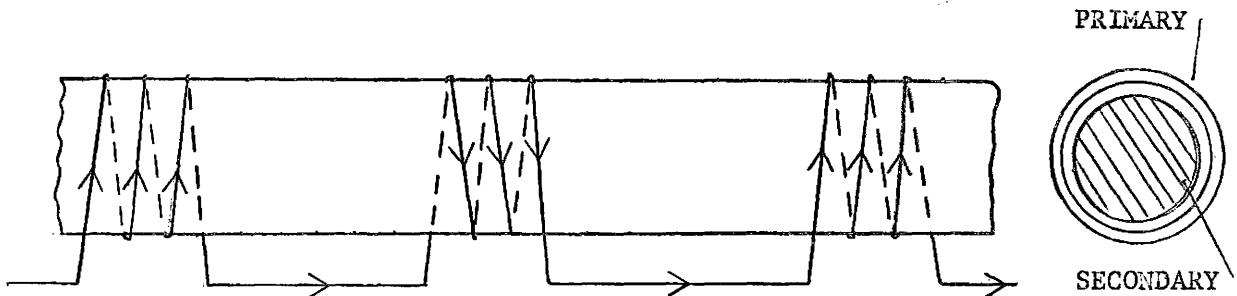


FIG 1.11 Tubular machine

With reference to the doubly excited machine there are two possible arrangements. The flat linear machine generally has corresponding top and bottom windings carrying in phase currents. The alternative is to connect corresponding top and bottom coils in anti-phase. In the former the currents in top and bottom combine additively to produce normal flux or through flux. The latter arrangement results in cancellation as regards normal flux but reinforcement as regards transverse flux production. This very logically leads into the other main classification of linear machine which can again be developed by considering topological changes to the squirrel cage machine of Fig. 1.1.

Upon rerolling in the transverse direction the unrolled stator of Fig. 1.2 we obtain the tubular machine (Fig. 1.11). It has an end turn advantage. In the flat form all the conductors of a particular phase winding have to travel through approximately a pole pitch until they again become active (Fig. 1.10). Due to the overlap in the tubular case only one end connection is required. Due to the large effective air gap - the flux passes through the tube axially - it is desirable that the secondary contain ferromagnetic material.

The above is by no means an exhaustive list of the different kinds of linear machines. It is merely intended to serve as a general introduction to the concepts and terminology used. Fig. 1.12 shows the classification of flat linear induction machines. For further information on linear induction machines in general, the reader is referred to review papers on the subject. (1),(4),(15),(16)

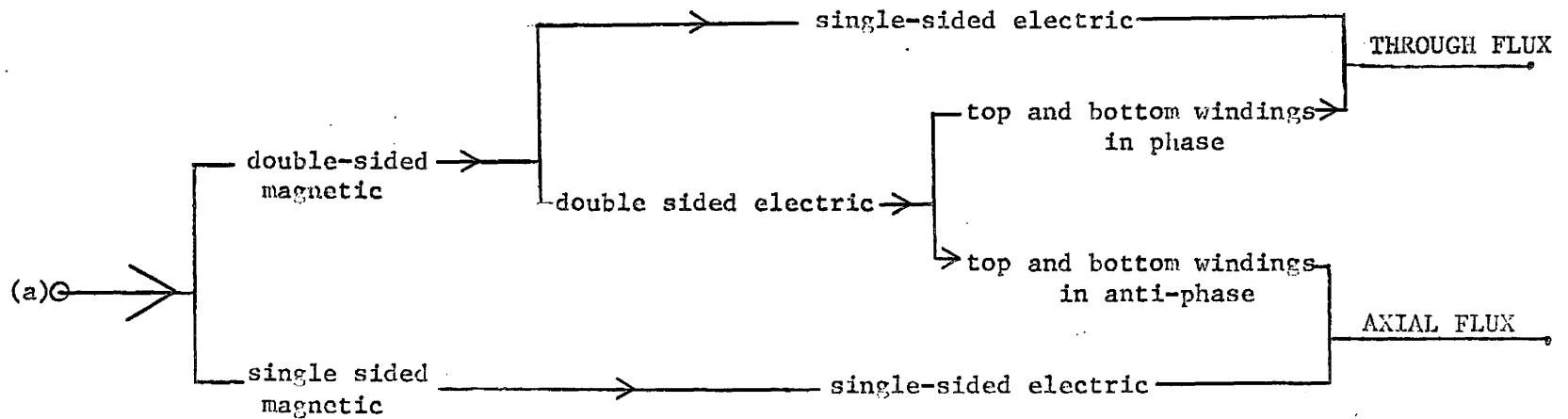
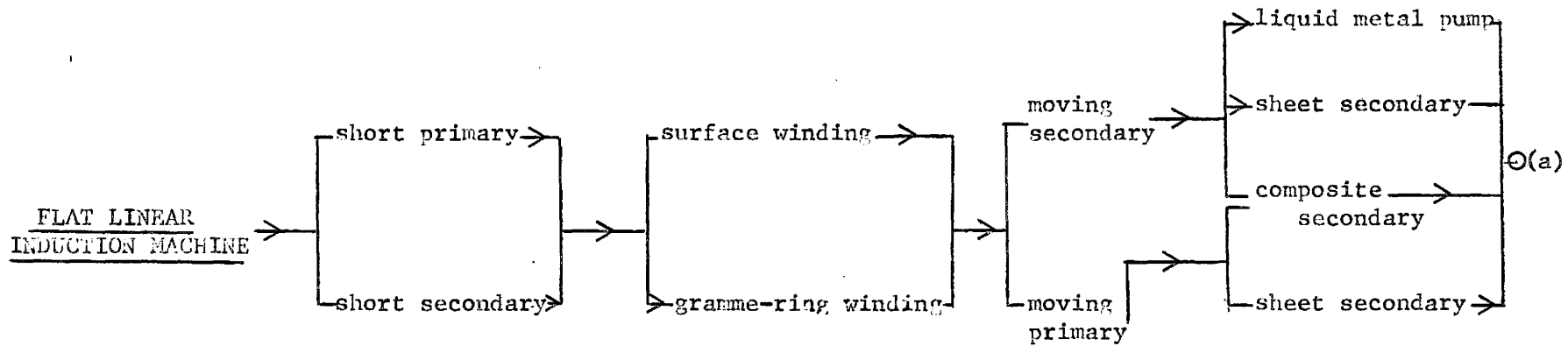


FIG 1.12 : Classification of linear induction machines .

So far we have assumed that the unrolling process gives us a linearly travelling field. In addition we must consider the unwanted parasitic components of flux and flux density that are set up. These result from the inherent imbalance of the primary circuit and the transients occurring at the edges. Even in the absence of the secondary the unrolled stator presents different impedances to the different phases due to the asymmetry caused by the ends. Consequently unbalanced current will flow producing in the general case forward and backward travelling fields and a standing field. Even in the case of a balanced current set a pulsating component of flux exists. The flux cannot only contain a travelling wave component. There must also be a standing wave component since the total flux must be zero at both ends. Study of the above is referred to as "finite length effect", "end effects", "entry and exit edge effect" or "longitudinal end effect."

Generally some modification must be made to the arrangement to cancel the effects of the unwanted field components. Such modifications include compensating windings, grading of end section windings etc. Generally in multi-wavelength machines the end effects can be neglected.

Also whether or not the machine is series or parallel connected can make a marked difference to the operation. In conventional rotating machines the difference is only to change the impedance of the machine. In this case the distribution of flux and mmf does not change only the magnitude is changed. This is not the case in linear

induction machines due to the above mentioned asymmetry. Series connection is generally preferred in short primary machines and parallel connection in short secondary machines for convenience in power supply.

## 1.2 Review:

The rotating field machine was developed in 1885. The first known reference to linear induction machines appeared in 1890 in a patent relating to induction machines. This was followed in 1895 by a patent specifically proposing linear induction machines for use in weaving looms. In 1905 came two proposals for railway use - one proposing the sectionalised stationary primary arrangement and the second suggesting the short moving primary arrangement. The latter idea is the ancestor of systems being currently examined (1).

The first use in liquid metal pumping was due to L. Chabb (2) who in 1915 proposed an induction pump for mercury. It had no practical application at the time and was soon forgotten. Albert Einstein and Leo Szillard had a patent in 1928 for an induction pump used for circulating liquid sodium in a refrigeration plant (2).

From the beginning of the century until about 1940 interest seems to have declined. In 1946 came the first large scale machine. This was the Westinghouse "Electropult" - a linear motor arrangement for launching aircraft. (3) The machine was of the short moving primary type. However unlike most other machines the secondary consisted of wound conductors. A constant thrust was accomplished by varying the secondary resistance. The project was abandoned due to the high cost.

In the early fifties came the need for the pumping of sodium and potassium in nuclear reactors. Due to radioactive contamination, mechanical pumps are undesirable. Both of these liquid metals are good conductors so consequently liquid metal pumps were proposed.

Flat linear induction pumps were most popular in this application. (1),(4) Feasibility and design studies have also been carried out on M.H.D. induction generators. These can be viewed as pumps operating above the synchronous velocity. (5),(6)

At the same time much work was being carried out in the U.S.S.R. on liquid metal pumps for use in metallurgical processes.

The main reason why induction machines are preferred to conduction is that the latter involve contact with the liquid metal. Contact has associated with it, chemical reaction and heat transfer problems. (2)

In 1947 Laithwaite began research on linear motors with regard to their application for shuttle propulsion in weaving looms. Over the past twenty years or so he has contributed enormously in this area. Besides linear induction machines he has contributed significantly to knowledge of all induction machines. (1),(7)-(14)

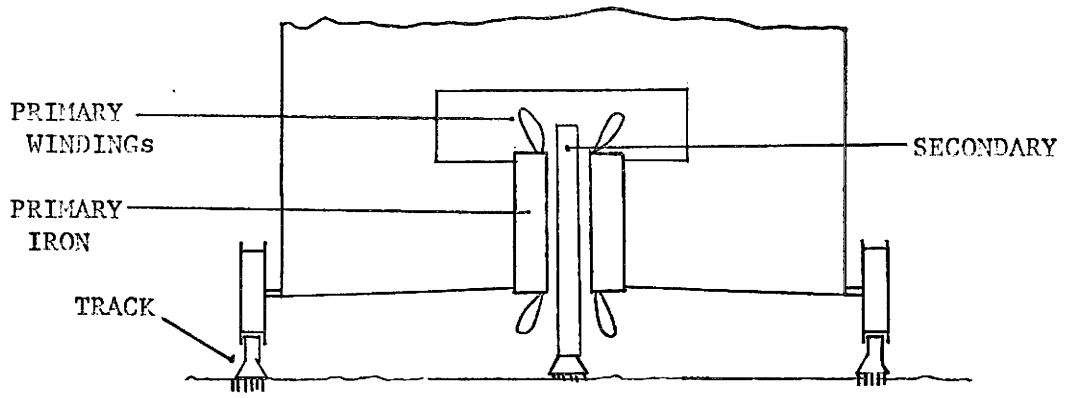
Other pioneering work has been done by Poloujadoff at the University of Grenoble. (15), (16), (17), (18). This work has been mainly concerned with the transportation application of flat linear induction machines. Much research is currently being carried out on experimental transportation machines: - Urba motor, Aerotrains, Gorton machine (7) etc.

The main reason for the present research in linear machines is the blatant need for revolutionary development in inter-city and urban transportation.

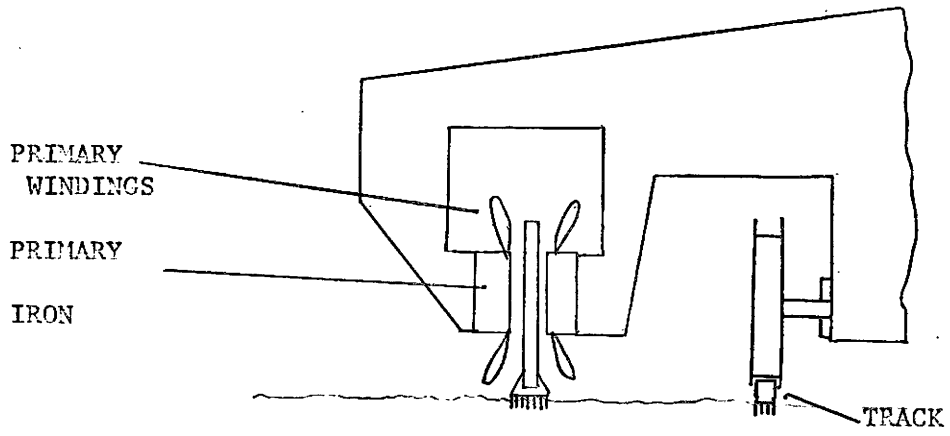
Some of the advantages of a drive using linear induction motors are (7), (15), (19): -

- (1) Conventional systems use a drive that depends on adhesion between wheels and track. The adhesion force decreases with speed. The maximum speed is limited to about 250 m.p.h.. No such limit exists in the linear drive case. Also much steeper inclines can be negotiated.
- (2) There are no centrifugal forces in linear machines since there are no rotating parts. Consequently there is no limit on speed due to centrifugal forces.
- (3) There is no mechanical contact required between the vehicle and track. An air suspension system has been proposed in (15). The normal forces in a composite secondary machine, though usually attractive, have recently been shown to be repulsive under certain conditions.
- (21). The use of this repulsive or levitation force to give a frictionless drive has been considered. In Fig. 1.13 some typical track layouts are shown.

Apart from the high initial cost of track other factors must be considered. The efficiency may be lower than that of an alternative system and, except in the case where the electric power is generated on board, speed control is a problem. With solid state frequency conversion there is a possibility that power could be picked up at any frequency - even d.c. and converted to give any desired frequency. A limited speed



(a)



(b)

FIG 1.13 : Typical layouts of linear machines as train drives.

control is also possible by changing the pole pitch by switching in different primary coil arrangements. (7) Another possibility is to have collection at variable frequency. (7)

As in many other engineering examples the use of linear induction machines had preceded the development of accurate analytic solutions of the problems involved. Generally speaking the general trend in the analysis is to divide the problem into the following three classes:

- (1) Flux penetration and lateral edge effects are neglected. The end edge effect (entry/exit effect) is considered.
- (2) Lateral and end edge effects are neglected. Flux penetration effect is analysed.
- (3) Flux penetration and end edge effects are neglected. Lateral edge effect is considered.

Pump problems are divided into two classes. One examines electromagnetic phenomena under the assumption of a given velocity profile. The velocity profile is usually considered flat. The second class is the study of hydrodynamic phenomena. Considering the first classification there is no difference between a liquid metal pump and a sheet secondary induction motor.

One of the early works on flat linear induction pumps is due to Blake (4). The ideal machine was considered. Laithwaite (10) introduced the concept of "Goodness".

The first classification has been considered by Okhremenko (22), (23), (24), Wang (25), Wang and Dudzinsky (26), and Veski (27).

The second classification has been considered by Okhremenko (22), (23), (24), Verte (27), Poloujadoff (16), Vlauev (28), and Bolton (29), (30).

The third classification, the end effect has been considered by Laithwaite (7), (9), (11), (1), Raschepkin (31), (32), Nasar (33) and Cerini and Elliott (34).

Besides the above main classifications overall design considerations have been considered by Laithwaite (7), (9), (36), Watt (35) and Verte (2).

The above list is by no means complete but is a representative section of the published work and shows the current state of the art.

### 1.3 Object of the thesis:

The object of this work is to lay down a common basis for the study of multi-wavelength linear induction machines. Flux penetration and lateral edge effects are to be considered but, owing to the large number of wavelengths, end effects may be neglected. A model is to be developed which is applicable to both linear motors and liquid metal pumps (under the assumption of a flat velocity profile). Both composite and sheet secondary machines are to be considered.

### 1.4 Governing Equations

Maxwells' equations under certain approximations regarding the velocity, frequency and material properties give the equations. Further the Lorentz force law, Poynting vector and Maxwell stresses are in-

roduced for force calculation.

The approximations are (44): -

- (1) Non-relativistic case i.e.  $V^2 \ll C^2$  is assumed. ( $V$  is a characteristic velocity and  $C$  the velocity of light).
- (2) Negligible displacement current compared with conduction current.
- (3) Neglect of space charge effects.

Field equations:

In the laboratory reference frame Maxwells' equations are:

$$\nabla \times E = - \frac{\partial B}{\partial t}$$

$$\nabla \times H = J$$

$$\nabla \cdot J = 0$$

$$\nabla \cdot B = 0$$

The Lorentz transformation under these approximations take the form: -

$$E' = E + V \times B$$

$$B' = B$$

$$H' = H$$

$$J' = J$$

The above shows the relationship between the quantities in the rest frame of the secondary (or any reference frame in fact) and the quantities in the laboratory rest frame. Only the electric field intensity is affected by the transformation.

The constitutive equation and Ohms' law are: -

$$\begin{aligned} B' &= \mu H' \\ J' &= \sigma E' \end{aligned}$$

The above must be applied in the rest frame of the medium.

The following are the boundary conditions to be satisfied at an interface.

$$E'_a \times n = E'_b \times n$$

$$B'_a \cdot n = B'_b \cdot n$$

$$H'_a \times n = H'_b \times n + h'$$

The primes in above refer to any reference frame which does not move normal to the interface. a and b refer to the two media separated by the interface. n is the normal vector to the surface. h' is the current sheet density at the interface.

The above equations in vector point form can be changed to integral form. In this form they are more closely associated with their discoveries. Using the divergence and Stokes' law we obtain:

$$\int_S B \cdot ds = 0$$

$$\oint E \cdot dl = - \int_S \frac{\partial B}{\partial t} \cdot ds \quad (\text{Faraday})$$

$$\oint H \cdot dl = \int_S J \cdot ds \quad (\text{Ampere})$$

The magnetic transport equation:

By combining Maxwells' equations we get the equation describing the distribution of field quantities.

From Maxwells' equations we have:

$$\nabla \times H = J$$

$$\nabla \times B = \mu J$$

from Ohms' law:

$$J = \sigma(E + V \times B)$$

(the velocity is assumed constant with time)

Substituting:

$$\nabla \times \nabla \times B = \mu\sigma(\nabla \times E + \nabla \times V \times B)$$

Now  $\nabla \times \nabla \times B = -\nabla^2 B + \nabla(\nabla \cdot B)$  and  $\nabla \cdot B = 0$ . Consequently upon substituting  $-\frac{\partial B}{\partial t} = \nabla \times E$ .

$$\nabla^2 B = \mu\sigma\left(\frac{\partial B}{\partial t} - \nabla \times V \times B\right)$$

$$\frac{\partial B}{\partial t} = \frac{1}{\mu\sigma} \nabla^2 B + \nabla \times V \times B.$$

In the absence of velocity the above represents a pure diffusion process. In this case the field lines diffuse or slip through the material at rate determined by  $1/\sigma\mu$  (the magnetic diffusivity). If the second term dominates the field lines do not slip through the material but are transported along with it.

If we write  $x = L_0 x^*$ ,  $V = V_0 V^*$  etc. where  $L_0$  and  $V_0$  are characteristic

values - asterisked quantities are normalised we obtain:

$$\frac{\partial B}{\partial t} = \frac{1}{\mu_0 \sigma L_0^2} \nabla^{*2} B + \frac{V_0}{L_0} \{ \nabla^* \times V^* \times B \}$$

$$\frac{\partial B}{\partial t} = \frac{1}{\mu_0 \sigma L_0^2} \{ \nabla^{*2} B + \mu_0 \sigma V_0 L_0 \nabla^* \times V^* \times B \}$$

Upon examination, it is seen that the ratio of magnetic convection to diffusion contribution is  $\mu_0 \sigma V_0 L_0$ . By analogy with the fluid mechanics case where the Reynolds number is the ratio of inertial to viscous forces, this quantity is called the Magnetic Reynolds number. The Magnetic Reynolds number will also be seen to represent the ratio of the induced magnetic field to the net field.

Typical values are shown in table 1.1.

#### Power and force equations:

The instantaneous rate of energy flow through a volume is given:

$$\int_s \mathbf{p} \cdot d\mathbf{s} = \int_s (\mathbf{E} \times \mathbf{H}) \cdot d\mathbf{s}$$

$\mathbf{p}$  is called the Poynting vector. The above equation is only valid in its entire integral form - there is no assurance that  $\mathbf{p}$  represents the local power density as pointed out in (43). However in much of our work the concept will prove very useful as the  $\mathbf{p}$  vector will be found constant over certain surfaces.

metal	frequency (hertz)	wavelength.			
		.1m	.2m	.4m	1.0m
<u>liquid iron</u>	25	.024	.096	.384	2.39
	60	.058	.230	.922	5.76
	400	.384	1.54	6.14	38.4
<u>mercury</u>	25	.050	.200	.800	5.00
	60	.120	.480	1.92	12.0
	400	.800	3.20	12.8	80.0
<u>sodium</u>	25	.520	2.08	8.32	52.0
	60	1.25	4.99	19.9	125.
	400	8.32	33.3	133.	832.
<u>aluminium</u>	25	1.77	7.08	28.3	177.
	60	4.25	16.9	67.9	425.
	400	28.3	113.	453.	2830.
<u>copper</u>	25	2.89	11.6	46.4	290.
	60	6.96	27.8	111.	696.
	400	46.4	186.	742.	4640

TABLE 1.1 : Magnetic Reynolds number.

In most of the published work on linear induction machines the assumption of a non-magnetic secondary was made.

All liquid metals are also non-magnetic (the Curie point is below the melting point in all cases).

Consequently the force density is given by the Lorentz force law:

$$f = J \times B$$

$f$  is the force density. In the case of a magnetic secondary, magnetic as well as electromagnetic forces have to be accounted for. Maxwells' magnetic stress( $T$ ) is the most useful principle in this case (41), (44).

Under the approximations listed we obtain:

$$T_{ij} =$$

$$\begin{vmatrix} \frac{1}{2}(B_1H_1 - B_2H_2 - B_3H_3) & B_1H_2 & B_1H_3 \\ B_2H_1 & \frac{1}{2}(B_2H_2 - B_1H_1 - B_3H_3) & B_2H_3 \\ B_3H_1 & B_3H_2 & \frac{1}{2}(B_3H_3 - B_1H_1 - B_2H_2) \end{vmatrix}$$

(first subscript indicates the surface, the second indicates the direction of the stress - see fig. 1.14)

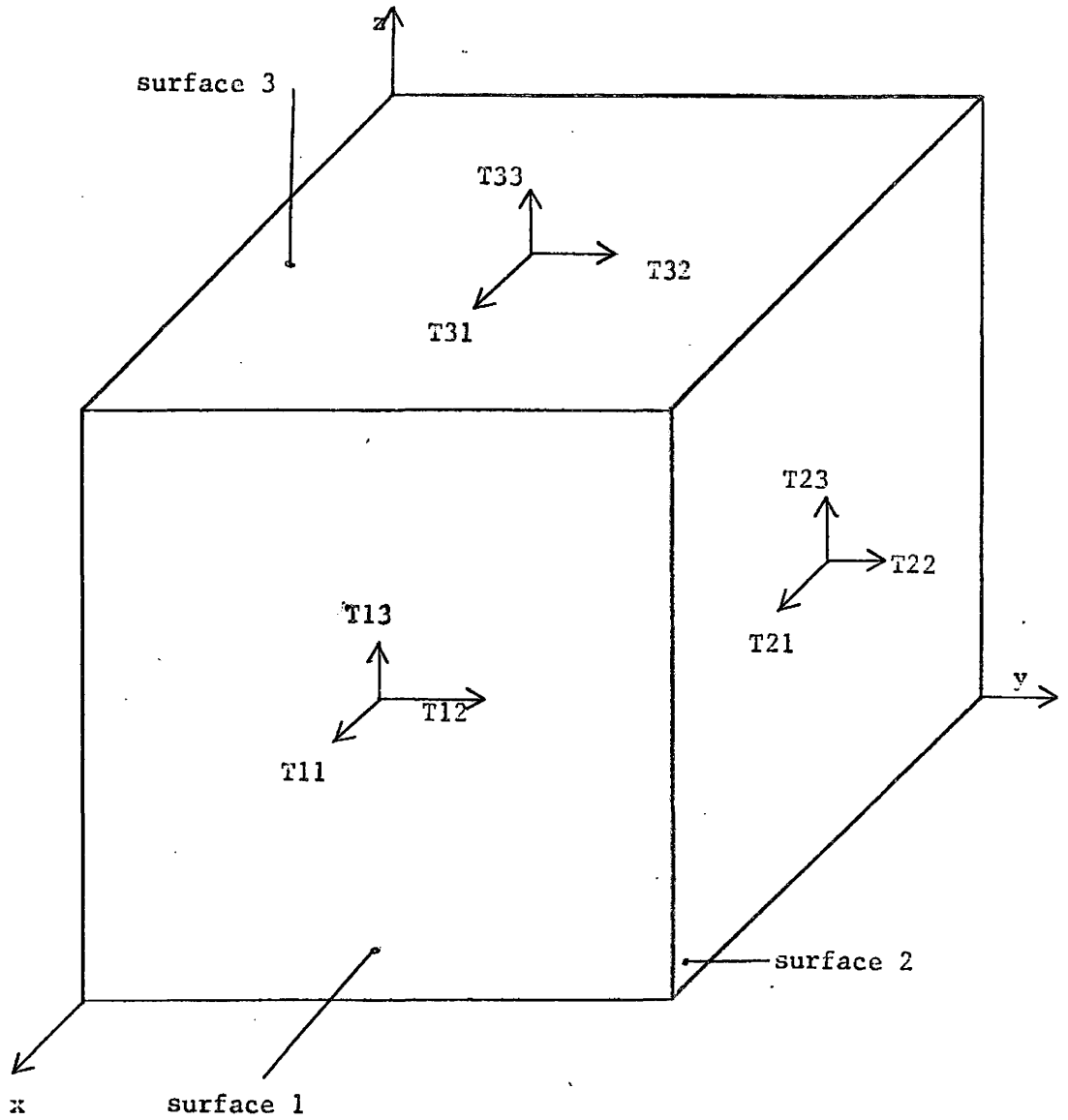


FIG 1.14 : Reference direction for stress tensors.

The total force on a control volume can be expressed as the integral of the stresses over the surface.

$$F_i = \int_s T_{ji} dA_j.$$

In cases where the stress tensor does not vary over a surface we shall find it convenient to talk about surface force density.

## CHAPTER II

### ANALYSIS OF THE THIN FINITE WIDTH SHEET MACHINE

#### 2.1 Introduction

The most common linear induction machine is the double-sided sheet secondary machine in which corresponding top and bottom primary coils carry in-phase currents. In cases where the secondary and air gaps are thin relative to the wavelength, the normal component of flux density can be considered constant in the y direction (depth). Under this assumption the lateral edge (finite width) effect can be analysed using a two-dimensional approach.

The only component of induced current density contributing to output power is that in the direction of the primary conductors (the z direction). The return paths in the x direction result in a non uniform flux redistribution and lateral forces. Consequently the shape of the induced current paths are of fundamental importance in determining the performance and therefore it is desirable that these paths and the non-uniform flux distribution be found so that the machine's behaviour in the presence of the lateral edge effect can be predicted.

#### 2.2 Model and Assumptions

The model is as shown in Fig.2.1. For generality the sheet secondary is assumed to be laterally assymmetric.

The following are the main assumptions:

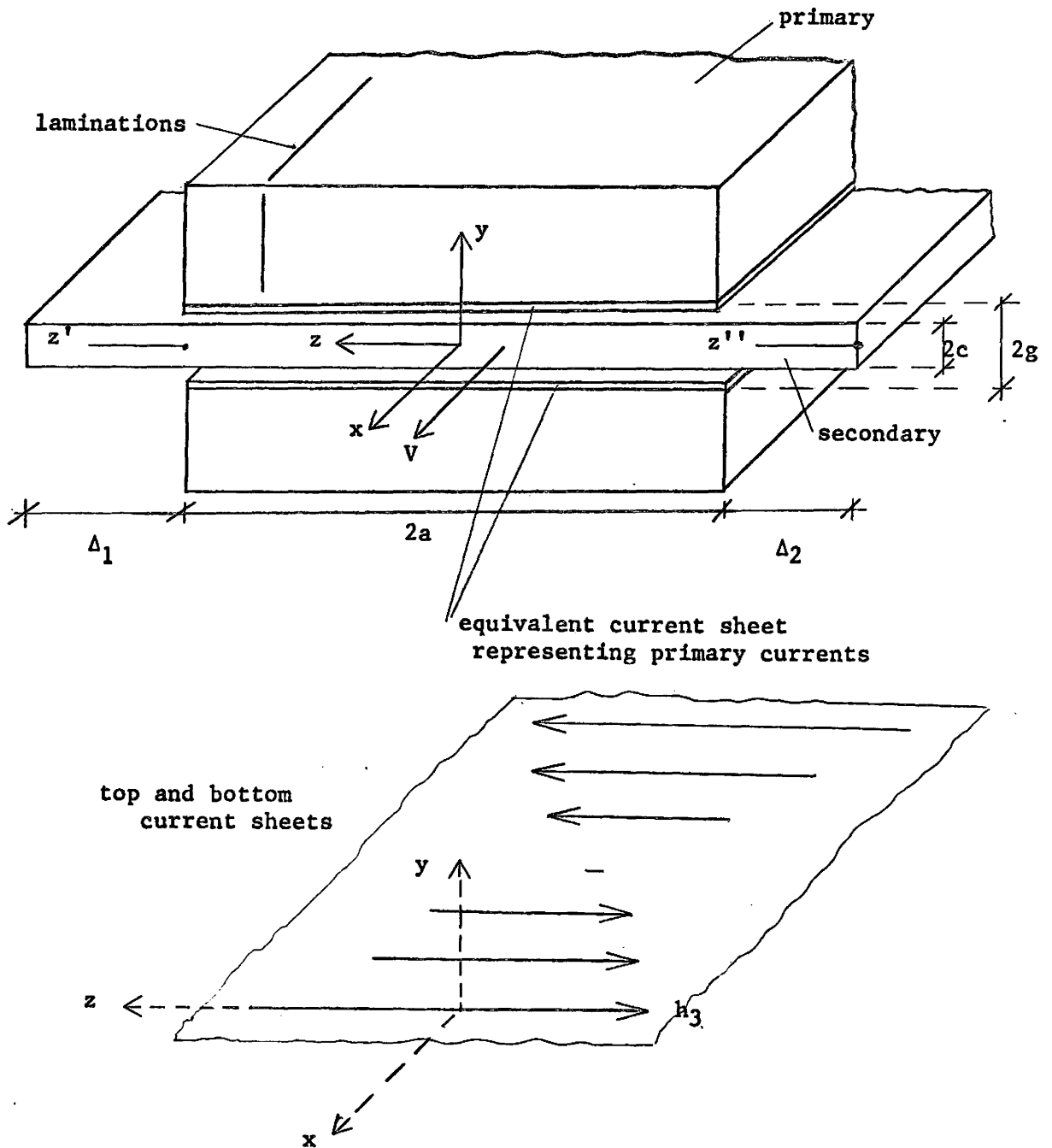


FIG. 2.1 : General model for two dimensional analysis

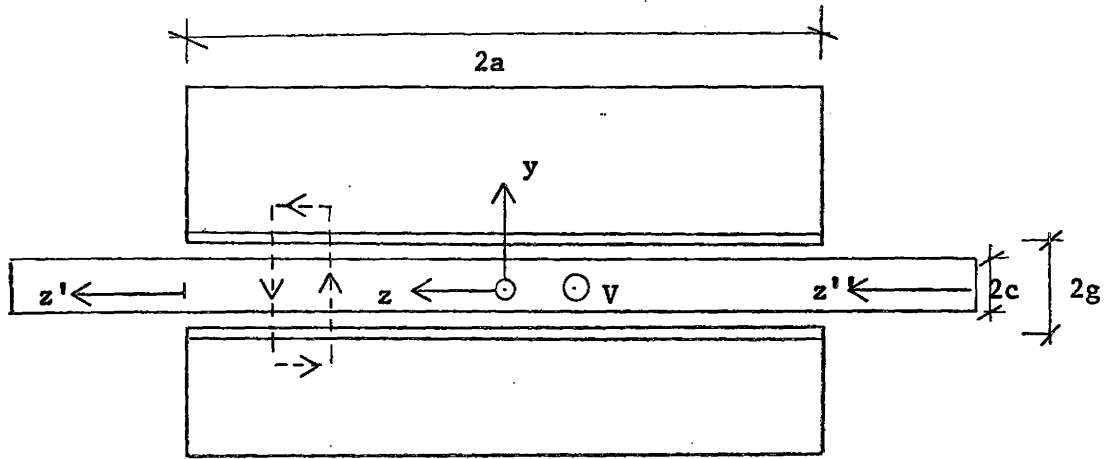
1. The normal component of flux density ( $B_2$ ) is not a function of  $y$ . As shall be seen later, this assumption is valid for double-sided machines where the ratio of gap thickness to wavelength is small.
2. The permeability and resistance of the stator is infinite. The assumption of infinite resistance is not strictly accurate (as pointed out by Bolton (29)). This is because the return currents (currents in the  $x$  direction) produce a flux in the  $z$  direction. This direction is normal to the laminations and consequently there will be induced currents in the stator blocks. The assumption will be kept however for tractability of the results.
3. The effect of slotting is neglected. The excitation is replaced by linear current sheets backing smooth iron surfaces. Only the fundamental component of the current sheets is considered.
4. The machine is many wavelengths long so the longitudinal edge effect can be neglected.
5. The field exists only in the "active portion" i.e. over the stator width. Fringing of the field beyond these limits is ignored.

### 2.3 Governing Equations:

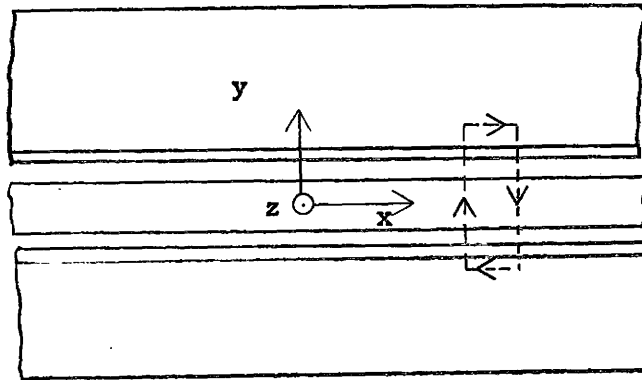
For convenience we separately consider the centre zone or active region and the end zones where the field is assumed zero. The reference frame for all quantities is that of the laboratory. A list of the symbols appears on page  $x$ . Vector-phasor quantities are used throughout the development. Their properties are discussed in Appendix 2.

#### (a) Active Region:

Applying Amperes circuital rule to the elementary paths shown in Fig. 2.2-a



(i) Loop used in formulation of equation 2.1



(ii) Loop used in formulation of equation 2.2

FIG. 2.2-a : Elementary loops for Ampere's law

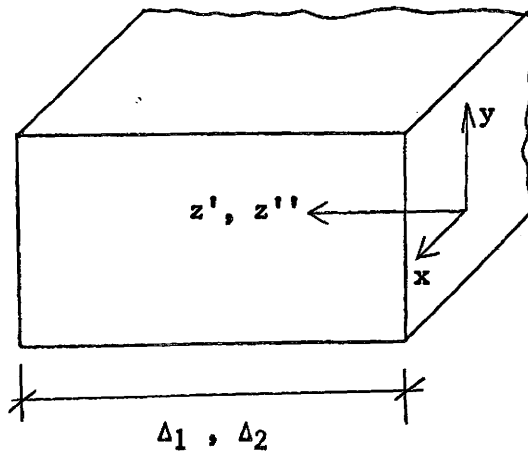


FIG. 2.2-b : General end section

we obtain:

$$2g[H_{\nu 2z} - H_{\nu 2z+\Delta z}] = 2c \Delta z J_{\nu 1} \quad \dots 2.1$$

$$2g[H_{\nu 2x} - H_{\nu 2x+\Delta x}] = 2 \Delta x h_{\nu 3} - 2 \Delta x c J_{\nu 3} \quad \dots 2.2$$

where  $h_{\nu 3}$  is the phasor representing the fundamental component of the primary current sheets.

The mmf component in the stator blocks is considered negligible due to their infinite permeability.

Using the first term of the Taylor series expansion and simplifying yields:

$$-\frac{\partial H_{\nu 2}}{\partial y} = \frac{c}{g} J_{\nu 1} \quad \dots 2.3$$

$$-\frac{\partial H_{\nu 2}}{\partial x} = \frac{h_{\nu 3}}{g} - \frac{c}{g} J_{\nu 3} \quad \dots 2.4$$

and 
$$\therefore J_{\nu 1} = -\frac{g}{c} \frac{\partial H_{\nu 2}}{\partial z} \quad \dots 2.5$$

$$J_{\nu 3} = \frac{g}{c} \frac{\partial H_{\nu 2}}{\partial x} + \frac{h_{\nu 3}}{c} \quad \dots 2.6$$

From Maxwell's relationship  $\nabla \times E = -\frac{\partial B}{\partial t}$  we obtain:

$$-\frac{\partial B_{\nu 2}}{\partial t} = \frac{\partial E_{\nu 1}}{\partial z} - \frac{\partial E_{\nu 3}}{\partial x} \quad \dots 2.7$$

The Lorentz transformation for electric field is:

$$\vec{E}' = \vec{E} + \vec{V} \times \vec{B}$$

where the prime indicates the value in the moving secondary reference frame.

Consequently we obtain:

$$E'_{\nu 1} = E_{\nu 1} \quad \dots 2.8$$

$$E'_{\nu 3} = E_{\nu 3} + V B_{\nu 2} \quad \dots 2.9$$

Consequently we get the expression for the induced current density:

$$J_{\nu 1} = \sigma E_{\nu 1} \quad \dots 2.10$$

$$J_{\nu 3} = \sigma (E_{\nu 3} + V B_{\nu 2}) \quad \dots 2.11$$

Substituting in (2.7) for  $E_{\nu 1}$  and  $E_{\nu 3}$  we obtain:

$$-\sigma \frac{\partial B_{\nu 2}}{\partial t} = \frac{1}{\sigma} \left\{ \frac{\partial J_{\nu 1}}{\partial z} - \frac{\partial J_{\nu 3}}{\partial x} \right\} + V \frac{\partial B_{\nu 2}}{\partial x} \quad \dots 2.12$$

Substituting for  $J_{\nu 1}$  and  $J_{\nu 3}$  results in:

$$-\sigma \frac{\partial B_{\nu 2}}{\partial t} = \frac{g}{c} \left\{ -\frac{\partial^2 H_{\nu 2}}{\partial z^2} - \frac{\partial^2 H_{\nu 2}}{\partial x^2} \right\} - \frac{1}{c} \frac{\partial h_{\nu 3}}{\partial x} + V \frac{\partial B_{\nu 2}}{\partial x} \quad \dots 2.13$$

Using the properties  $\frac{\partial}{\partial x} = -j\beta$ ,  $\frac{\partial}{\partial t} = j\omega$  and the constitutive equation

$B = \mu_0 H$  we obtain upon rearranging:

$$\frac{g}{c} \left\{ \frac{\partial^2 \tilde{B}_2}{\partial z^2} + \frac{\partial^2 \tilde{B}_2}{\partial x^2} \right\} = j \omega \mu_0 \sigma \left( 1 - \frac{V\beta}{\omega} \right) \tilde{B}_2 + j \frac{\beta \mu_0}{c} h_3 \quad \dots 2.15$$

This can be written:

$$\frac{\partial^2 \tilde{B}_2}{\partial z^2} = \gamma_0^2 \tilde{B}_2 - \beta^2 \tilde{B}_{20} \quad \dots 2.16$$

where  $\gamma_0^2 = \beta^2 (1 + j S G)$

S is the slip =  $1 - \frac{V\beta}{\omega}$

$G = \frac{c}{g} R$ , where R is the magnetic Reynold's number =  $\frac{\mu_0 \sigma \omega}{\beta^2}$ .

G is called the Laithwaite Goodness Factor.

$\tilde{B}_{20}$  is the flux density corresponding to the same primary current with the secondary removed (or slip = 0). Referring to expression 2.4 we obtain:

$$j \beta H_2 = \frac{1}{g} h_3 \quad \dots 2.17$$

Consequently :

$$\tilde{B}_2 = -j \frac{\mu_0 h_3}{\beta g} = \tilde{B}_{20} \quad \dots 2.18$$

### (b) Secondary End Regions

Consider the general end section. (Fig. 2.2-b) where the normal component of flux density is assumed zero. In this region Maxwell's equation

$\nabla \times H = J$ , reduces to :

$$0 = \frac{\partial J_1}{\partial z} - \frac{\partial J_3}{\partial x} \quad \dots 2.19$$

Differentiating the above with respect to x yields:

$$0 = \frac{\partial^2 J_1}{\partial x \partial z} - \frac{\partial^2 J_3}{\partial x^2}$$

From the continuity equation  $\nabla \cdot J = 0$  we obtain:

$$\frac{\partial J_1}{\partial x} + \frac{\partial J_3}{\partial z} = 0 \quad \dots 2.20$$

we get, upon substitution:

$$\frac{\partial^2 J_3}{\partial x^2} + \frac{\partial^2 J_3}{\partial z^2} = 0 \quad \dots 2.21$$

which is Laplace's equation in two dimensions.

Similarly it can be shown:

$$\frac{\partial^2 J_1}{\partial x^2} + \frac{\partial^2 J_1}{\partial z^2} = 0 \quad \dots 2.22$$

The following are the boundary conditions to be satisfied at the interfaces at both end sections:

- (i) continuity of normal (z) component of current density.
- (ii) continuity of tangential component of electric field intensity.
- (iii)  $J_3 = 0$  at extreme boundaries.

## 2.4 General Solution:

The general solution of (2.16) is:

$$B_{\sim 2} = B_{\sim c} + B_{\sim -} e^{+\gamma_0 z} + B_{\sim +} e^{-\gamma_0 z} \quad \dots 2.23$$

where  $B_{\sim c} = \frac{\beta^2}{\gamma} B_{\sim 20}$  and substituting for  $B_{\sim 20}$  from 2.18

$$= -j \frac{\beta^2}{\gamma_0} \frac{\mu_0 h_3}{\beta g}$$

$B_{\sim -}$  and  $B_{\sim +}$  are arbitrary constants.

The corresponding expressions for  $J_{\sim 1}$ ,  $J_{\sim 3}$  (given by 2.5 and 2.6 and substituting for  $h_{\sim 3}$  from above) are:

$$J_{\sim 1} = \frac{g}{c} \frac{\gamma_0}{\mu_0} \{ B_{\sim +} e^{-\gamma_0 z} - B_{\sim -} e^{+\gamma_0 z} \} \quad \dots 2.24$$

$$J_{\sim 3} = -\frac{g}{c} \frac{\beta}{\mu_0} \{ S G B_{\sim c} + j(B_{\sim +} e^{-\gamma_0 z} + B_{\sim -} e^{+\gamma_0 z}) \} \quad \dots 2.25$$

The solution in the inactive zones is:

$$J_{\sim 3} = A_{\sim} \text{Cosh } \beta z + B_{\sim} \text{Sinh } \beta z \quad \dots 2.26$$

and from the continuity equation we obtain:

$$J_{\sim 1} = -j \{ A_{\sim} \text{Sinh } \beta z + B_{\sim} \text{Cosh } \beta z \} \quad \dots 2.27$$

Upon substituting the conditions  $J_{\sim 3} = 0$  at  $z' = \Delta_1$  and  $z'' = \Delta_2$  we obtain:

for  $z > a$

$$J_{\nu 3} = \frac{\text{Sinh } \beta(\Delta_1 - z')}{\text{Sinh } \beta\Delta_1} J_{\nu 3a} \quad \dots 2.28$$

$$J_{\nu 1} = j \frac{\text{Cosh } \beta(\Delta_1 - z')}{\text{Sinh } \beta\Delta_1} J_{\nu 3a} \quad \dots 2.29$$

for  $z < -a$

$$J_{\nu 3} = \frac{\text{Sinh } \beta z''}{\text{Sinh } \beta\Delta_2} J_{\nu 3-a} \quad \dots 2.30$$

$$J_{\nu 1} = \frac{\text{Cosh } \beta z''}{\text{Sinh } \beta\Delta_2} J_{\nu 3-a} \quad \dots 2.31$$

where  $J_{\nu 3a}$  and  $J_{\nu 3-a}$  are the current densities at  $z=\pm a$  respectively.

It shall be found convenient to determine the quantity  $Z = \frac{E_1}{J_3}$  at the interfaces separating the active from the end zones.

Consequently we obtain:

$$Z_{a+} = \left. \frac{E_1}{J_3} \right|_{z=a} = j \rho' \text{Coth } \beta\Delta_1 \quad \dots 2.32$$

$$Z_{a-} = \left. \frac{E_1}{J_3} \right|_{z=-a} = -j \rho' \text{Coth } \beta\Delta_2 \quad \dots 2.33$$

where  $\rho'$  is the resistivity of the end sections. In the general sheet secondary case  $\rho' = \rho$ . By putting  $\Delta_1 = \Delta_2$  and  $\rho' \neq \rho$  we can represent a linear induction pump with short circuiting side conductors at  $z = \pm a$ .

Calculating the same quantities for the centre portion we obtain:

$$Z_{a+} = \frac{\gamma_0 \rho \{B_{\nu+} e^{-\gamma_0 a} - B_{\nu-} e^{\gamma_0 a}\}}{\beta \{S G B_{\nu 20} + j(B_{\nu+} e^{-\gamma_0 a} + B_{\nu-} e^{\gamma_0 a})\}} \quad \dots 2.34$$

$$Z_{a-} = -\frac{\gamma_0 \rho \{B_{\nu+} e^{\gamma_0 a} - B_{\nu-} e^{-\gamma_0 a}\}}{\beta \{S G B_{\nu 20} + j(B_{\nu+} e^{\gamma_0 a} + B_{\nu-} e^{-\gamma_0 a})\}} \quad \dots 2.35$$

Equating the above we obtain the following matrix relationship:

$$\begin{bmatrix} (\rho \gamma_0 + j \beta Z_{a-}) e^{\gamma_0 a} & -(\rho \gamma_0 - j \beta Z_{a-}) e^{-\gamma_0 a} \\ -(\rho \gamma_0 + j \beta Z_{a+}) e^{-\gamma_0 a} & (\rho \gamma_0 - j \beta Z_{a+}) e^{\gamma_0 a} \end{bmatrix} \begin{bmatrix} B_{\nu+} \\ B_{\nu-} \end{bmatrix} = \beta S G B_{\nu c} \begin{bmatrix} Z_{a-} \\ Z_{a+} \end{bmatrix} \quad 2.36$$

Substituting for  $Z_{a+}$  and  $Z_{a-}$  yields:

$$\begin{bmatrix} (\gamma_0 + \beta \frac{\rho}{\rho} \text{Coth } \beta \Delta_2) e^{\gamma_0 a} & -(\gamma_0 - \beta \frac{\rho}{\rho} \text{Coth } \beta \Delta_2) e^{-\gamma_0 a} \\ -(\gamma_0 - \beta \frac{\rho}{\rho} \text{Coth } \beta \Delta_1) e^{-\gamma_0 a} & (\gamma_0 + \beta \frac{\rho}{\rho} \text{Coth } \beta \Delta_1) e^{\gamma_0 a} \end{bmatrix} \begin{bmatrix} B_{\nu+} \\ B_{\nu-} \end{bmatrix} = \beta \frac{\rho}{\rho} S G B_{\nu c} \begin{bmatrix} \text{Coth } \beta \Delta_2 \\ \text{Coth } \beta \Delta_1 \end{bmatrix} \quad 2.37$$

## 2.5 The Ideal Machine:

It follows from 2.36 that if  $Z_{a+}$  and  $Z_{a-}$  are zero the  $B_{\nu+}$  and  $B_{\nu-}$  terms are also zero. This case corresponds to having large end sections in the case of a sheet secondary machine or to the case of infinitely conducting side bus bars in the case of an induction pump.

In this case the solution reduces to:

$$B_{\sim 2} = \frac{1}{1 + j S G} B_{\sim 20} \quad \dots 2.38$$

where  $B_{\sim 20}$  is the no load flux density i.e. the flux density existing when the slip is zero (the primary current being constant).

The primary voltage can be expressed in terms of  $B_{\sim 2}$  and the current in terms of  $h_{\sim 3}$ . (Actually it is the difference between the applied voltage and the voltage drop across primary impedance that determines

$B_{\sim 2}$  }

Consequently we can write:

$$V = K_1 B_2$$

$$I = K_2 h_3$$

$K_1$ ,  $K_2$  are constants determined by the number of phases, slots per phase, number of conductors slot, etc. etc. It is not necessary to determine their value at this point.

The impedance of the equivalent circuit is therefore:

$$\frac{V}{I} = K \frac{j}{1 + j S G} \quad \dots 2.39$$

$$\text{where } K = \frac{\beta g}{\mu_0} \frac{K_1}{K_2}$$

The equivalent circuit is as shown in Fig. 2.3.

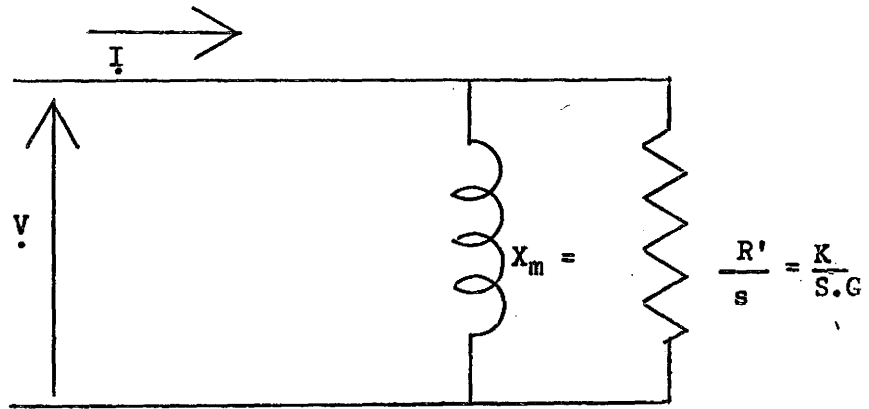


FIG. 2.3 : Equivalent circuit for 'ideal machine'

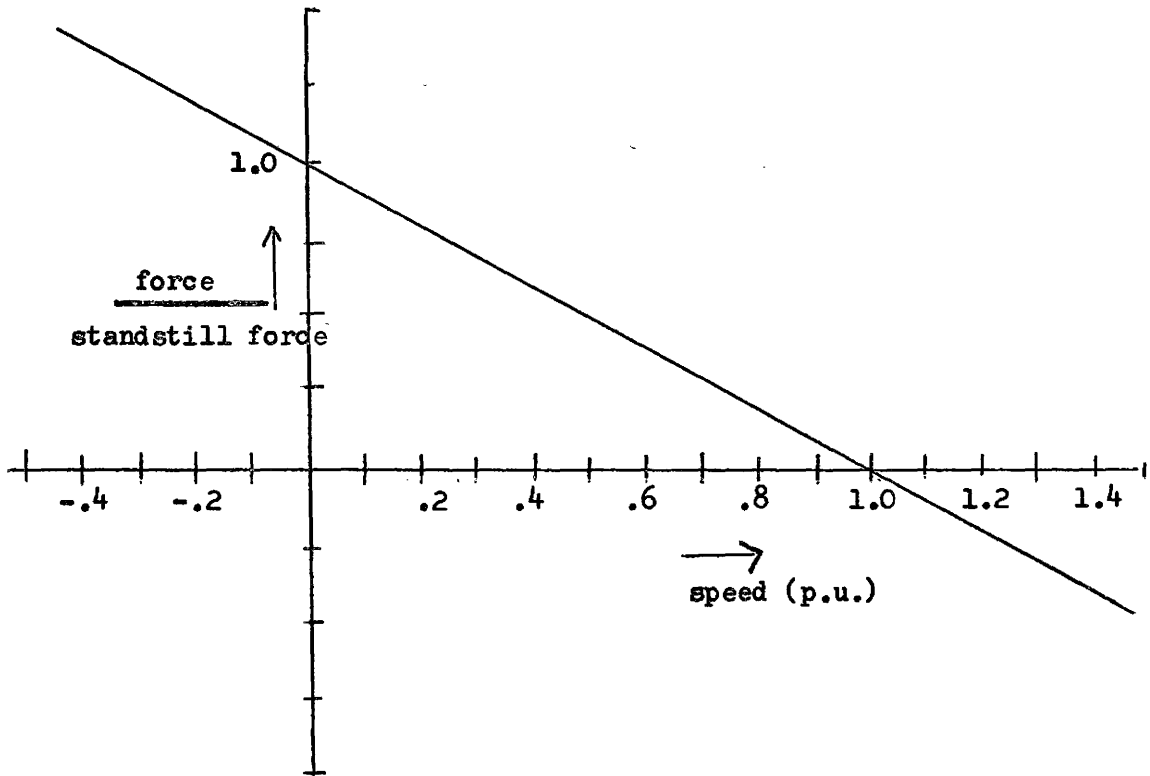


FIG. 2.4 : 'Ideal machine's' force-speed characteristic

This circuit represents the basic induction principle having the properties

1.  $(1 - S)$  of the input power appears as mechanical output. This also represents the efficiency.
2. The force developed is the input power divided by the synchronous velocity.

The force-speed characteristic is shown in Fig. 2.4. The Laithwaite Goodness factor (7), (9), (10) etc. is a measure of the machine's ability to convert volt-amperes to mechanical power. The better the machine the greater the proportion of the current flowing in the "load" circuit to that in the magnetising branch.

The difference between the Laithwaite Goodness factor and the Magnetic Reynolds number is that the latter is a parameter resulting from carrying out an inspectional analysis on the magnetic transport equation. Different materials within a magnetic field would have different Magnetic Reynolds numbers.

The Goodness factor on the other hand expresses an overall effect. Individual Reynolds numbers, dimensions and simplifying assumptions must be used in determining the Goodness factor. It is interesting to note that the Goodness factor as defined by Laithwaite is the inverse of the Quality of the circuit (as defined in traditional circuit theory).

The Goodness factor is of fundamental importance in determining the characteristics of induction machines. For example, following the development in (9) we get the relationship between maximum efficiency and primary/secondary resistance ratio for different values of  $G$ .

The slip at the maximum efficiency is given by the quadratic:

$$S^2(1 + t) + \frac{2t}{G^2} S - \frac{t}{G^2} = 0$$

The efficiency is:

$$\eta = \frac{1 - S}{1 + (S + \frac{1}{S G^2})t}$$

where S is the slip

t is ratio of primary to referred secondary resistance

G is the Goodness factor.

Typical curves are shown in Fig. 2.5.

Another parameter relating to the effectiveness of induction machines is the "demagnetising coefficient" or "coefficient of secondary current reaction".

This was introduced by Okhremenko (22 ).

$$k_r = \frac{B_{.2} z_{avg}}{B_{.20}} \Big|_{h_3} \text{ constant} = k_r e^{j\theta} \dots\dots\dots 2.40$$

In the case of the ideal machine this is:

$$\frac{1}{1 + j S G} \dots\dots\dots 2.41$$

Actually Okhremenko did not use Laithwaite's Goodness number - but the

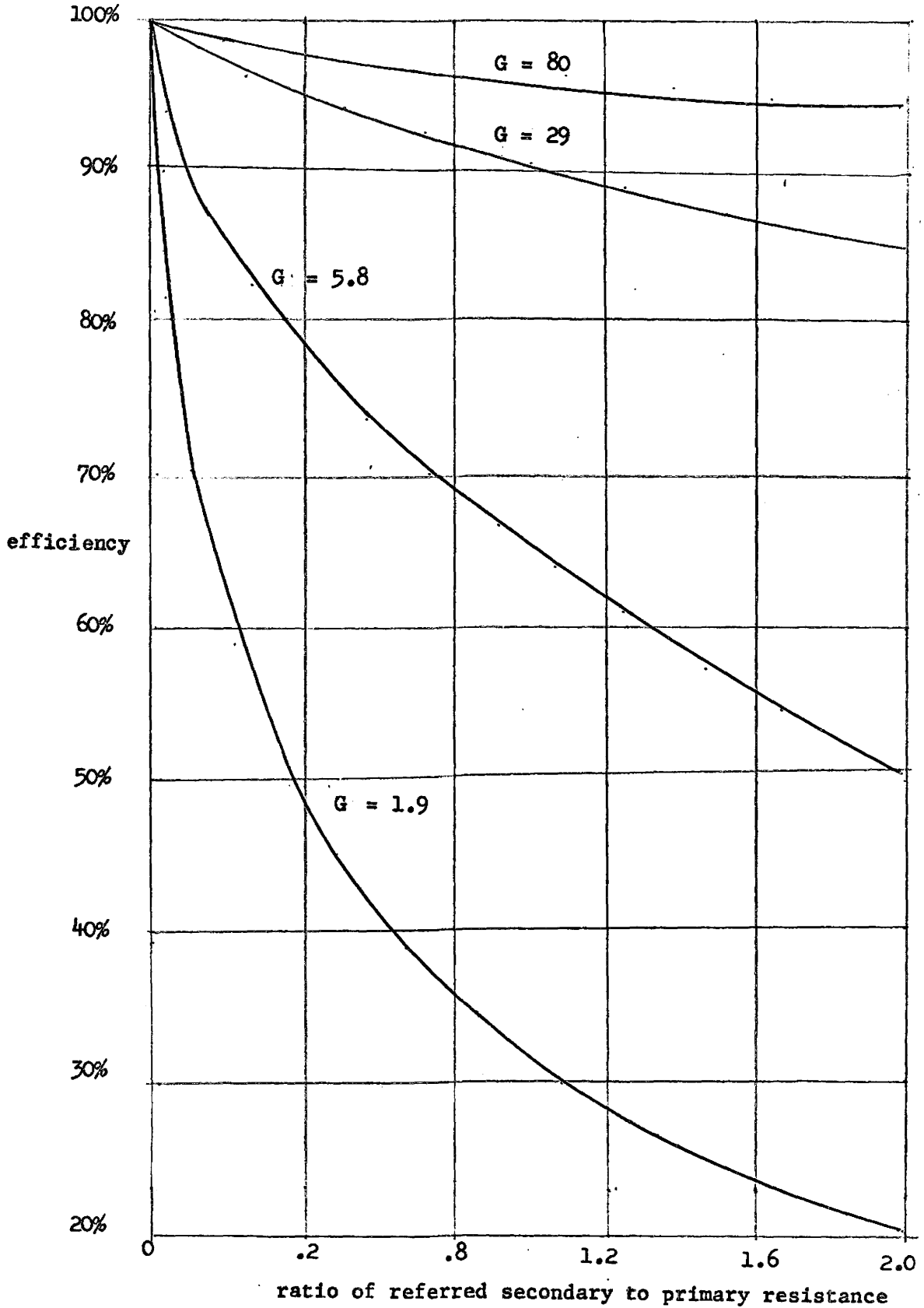


FIG. 2.5 : Maximum efficiency's dependence on Goodness

dimensionless parameter used was identical.

From the definition, the term "demagnetising coefficient" or "coefficient of secondary current reaction" is unfortunate. Actually the demagnetising field increases with decrease in demagnetising coefficient. The poor choice of nomenclature probably occurred in translation from the original Russian version.

A good appreciation for both the Goodness number and the demagnetising coefficient can be obtained by studying Fig. 2.6-a.

Now:

$$\underline{B}_a = \underline{B}_{20} + \underline{B}_{2i} \dots\dots\dots 2.42$$

where  $\underline{B}_{2i}$  is the induced field.

From (2.38) we have:

$$\underline{B}_{2i} = -j S G \underline{B}_2$$

The locus of the phasors  $\underline{B}_2$  and  $\underline{B}_{2i}$  are seen to lie on the circle shown.

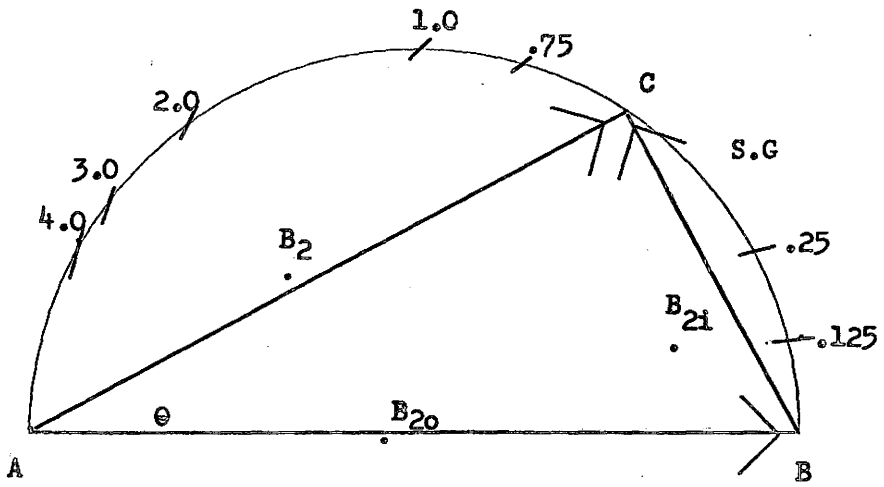
The demagnetising coefficient is  $AC/AB$  with an angle  $\theta$  shown.

The Goodness factor is the ratio  $BC/AC$  with  $S = 1$ .

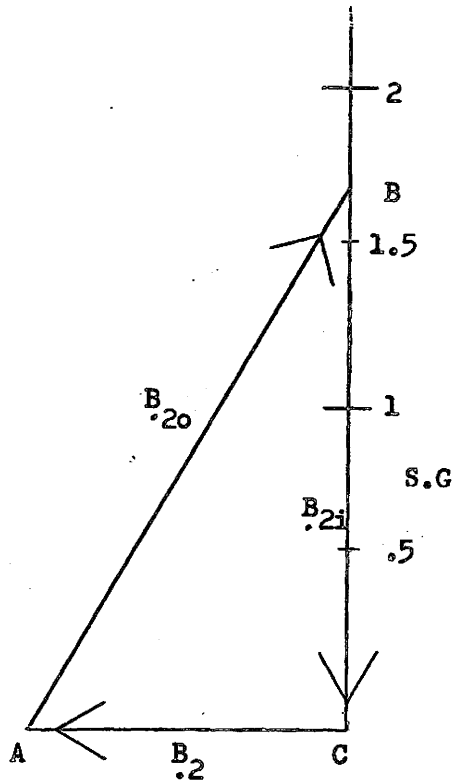
The power factor of the machine is  $BC/AB$ .

The circle diagram shown (Fig. 2.6-a) implies a constant current fed machine.

For a constant "air gap" voltage machine, the locus of the phasors is as shown in Fig.(2.6-b).



(a)  
Constant current.



(b)

Constant voltage

FIG. 2.6 : Phasor relationships in ideal machine

## 2.6 Finite Width Machine:

With reference to 2.37 there are 3 general conditions of interest

$$(a) \quad \Delta_1 = \Delta_2 = 0$$

In this case the solution reduces to

$$B_2 = \frac{B_{\sim 20}}{1 + j S G} \left\{ 1 + j S G \frac{\text{Cosh } \gamma_0 z}{\text{Cosh } \gamma_0 a} \right\} \quad \dots 2.43$$

This is in agreement with Okhremenko (22). Plots showing the lateral variation of  $B_2$  as a function of  $a/\lambda$  and  $G$  appear in Fig. 2.7 and Fig. 2.8 respectively. The non-uniform flux distribution results from the non-uniformity of the induced current. At the secondary centre ( $z=0$ ) the induced current is  $z$  directed. At  $z=\pm a$  the induced current density in the  $z$  direction is zero.

The expressions for the induced current densities can be obtained from 2.43 by applying equations 2.5 and 2.6

The resulting expressions are:

$$J_{\sim 1} = -j \gamma_0 \frac{S G}{1 + j S G} B_{\sim 20} \frac{\text{Sinh } \gamma_0 z}{\text{Cosh } \gamma_0 a} e^{j(\omega t - \beta x)} \quad \dots 2.44-a$$

$$J_{\sim 3} = \beta \frac{S G}{1 + j S G} B_{\sim 20} \left[ \frac{\text{Cosh } \gamma_0 z}{\text{Cosh } \gamma_0 a} - 1 \right] e^{j(\omega t - \beta x)} \quad \dots 2.44-b$$

The appropriate stream function describing the flow is:

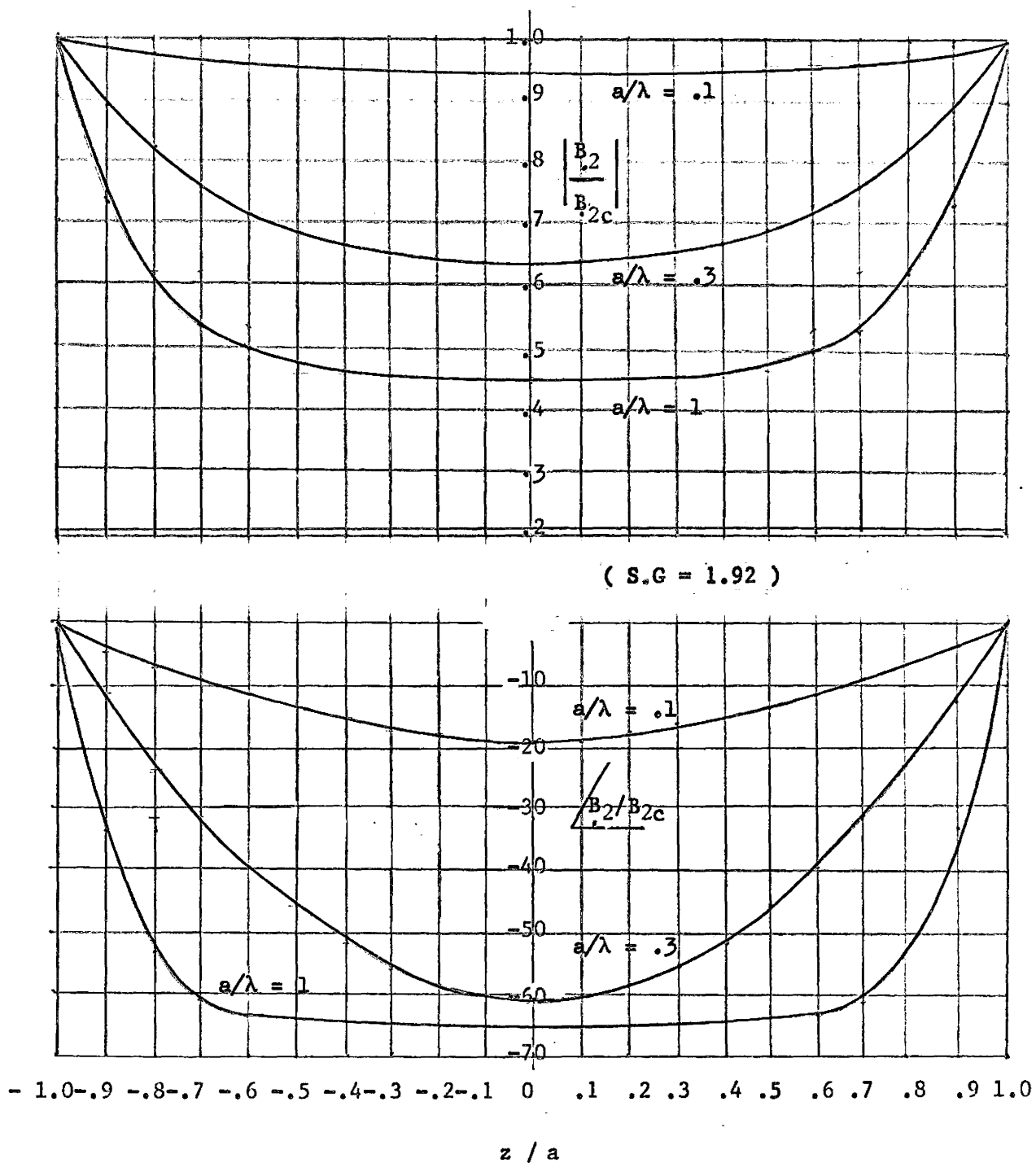


FIG. 2.7 : Dependence of lateral variation of flux density on  $a / \lambda$

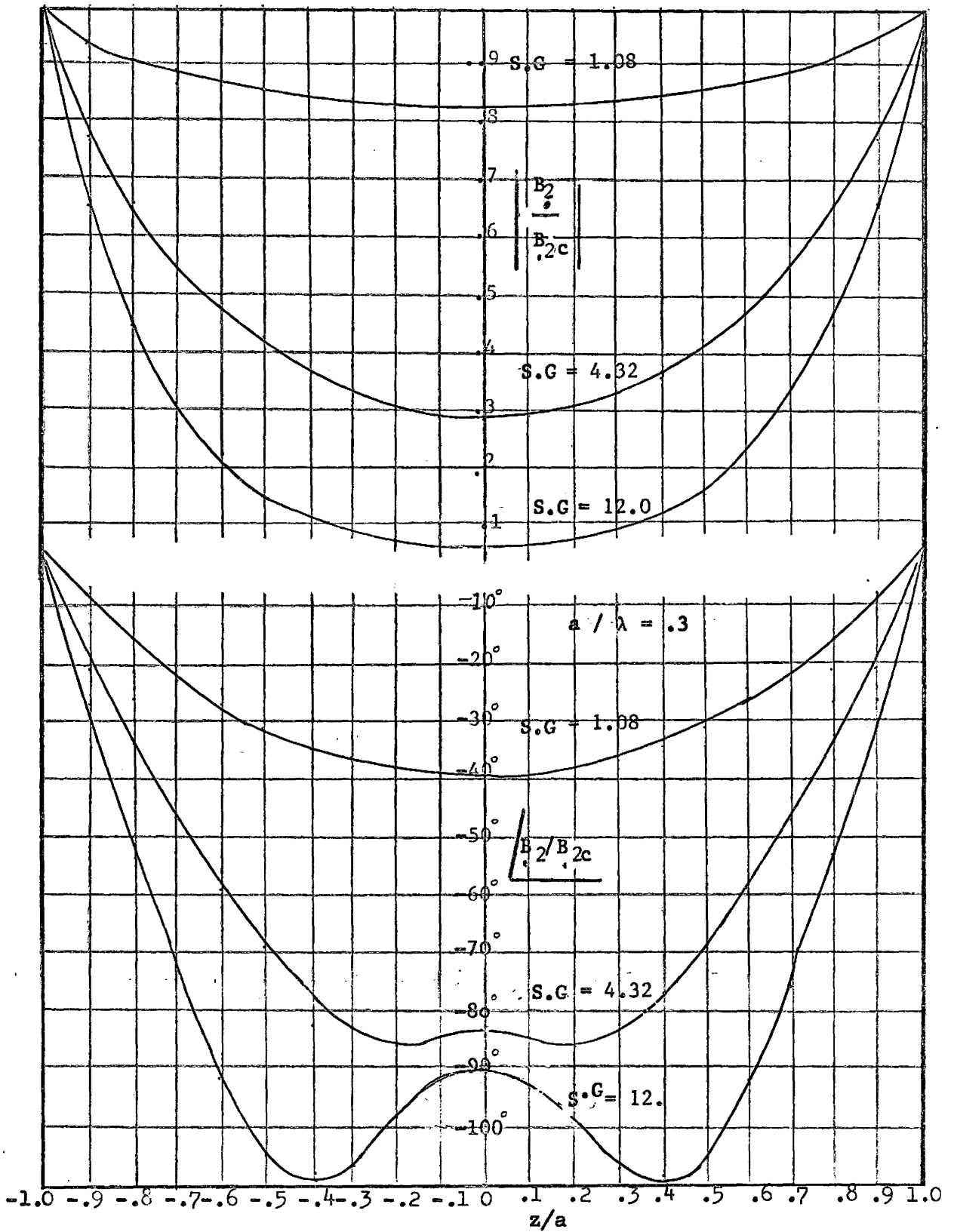


FIG. 2.8 : Dependence of lateral variation of flux density with S.G

$$\psi(x, z, t) = \operatorname{Re}\{\psi(x, z, t)\}$$

where

$$\psi(x, z, t) = \frac{\left[ \frac{\cosh \gamma_0 z}{\cosh \gamma_0 a} - 1 \right]}{\left| \frac{1}{\cosh \gamma_0 a} - 1 \right|} e^{j(\omega t - \beta x)} \quad \dots 2.45$$

The current stream lines are shown in Fig. 2.9-a, -b and -c. Fig. 2.9-a is for a low Laithwaite Goodness number. ( S.G = .1 ). The induced current paths are roughly elliptical as described in (1). The contours in Fig. 2.9-b are for a higher value of Laithwaite Goodness number. In this case there is a distortion in the paths as shown. This results from the larger phase shift in the z direction due to the increase in the imaginary component of  $\gamma_0$ . Finally, Fig. 2.9-c which corresponds to  $a/\lambda=1$  shows the justifiability of the infinite width assumption. In this case over most of the width the induced current is z directed. The "demagnetising coefficient" (expression 2.40) in this case is:

$$K_r = \frac{1}{1 + j S G} \left\{ 1 + j S G \frac{\tanh \gamma_0 a}{\gamma_0 a} \right\} \quad \dots 2.46$$

The demagnetising coefficient is plotted in Fig. 2.10. Again the justification of using the 'infinite width' approximation is shown for values of  $a/\lambda > 1$ .

A convenient parameter in the evaluation of the finite width effect is the ratio of output power of the finite width machine to the output power available from the same width of an infinitely wide

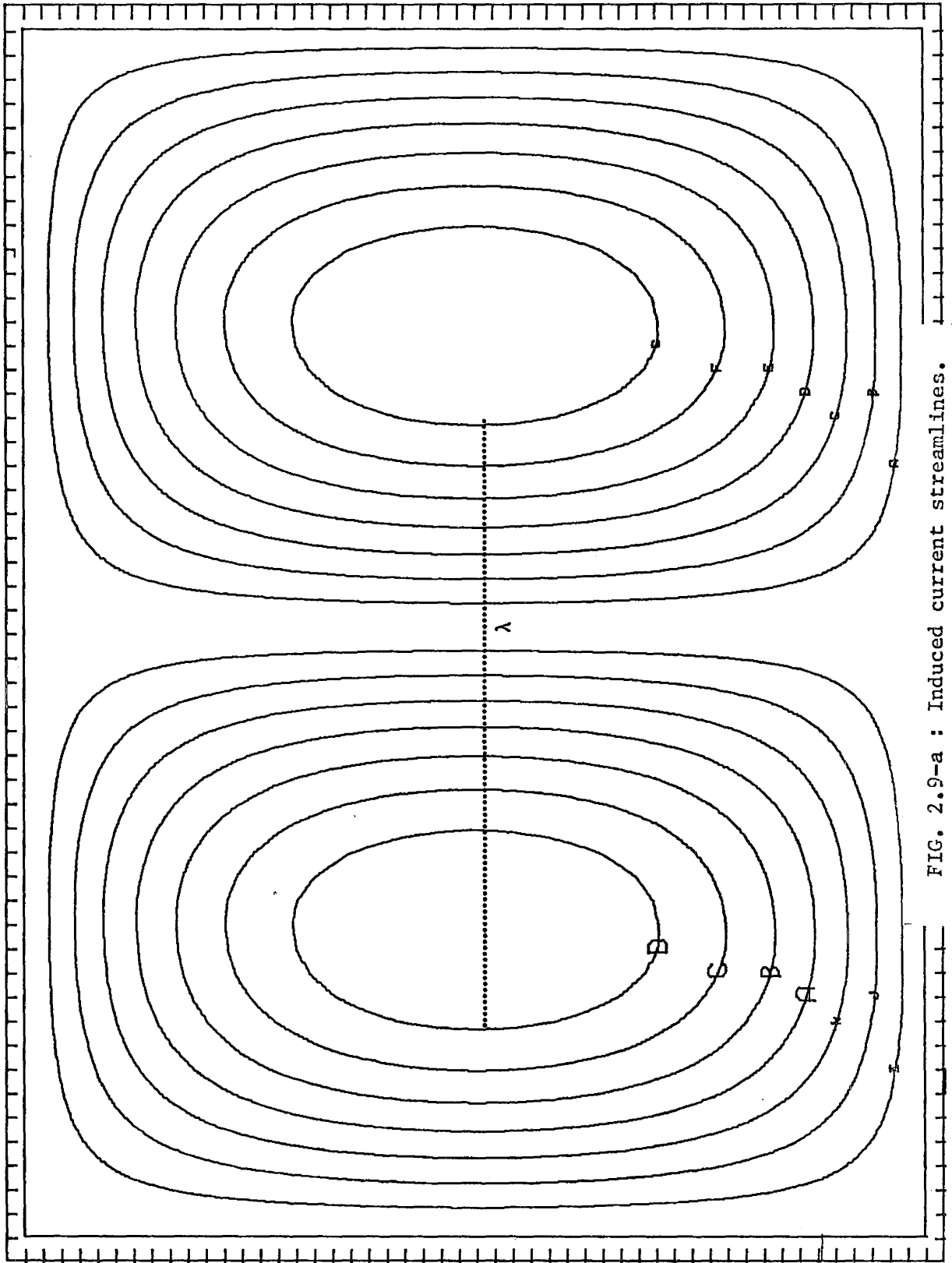


FIG. 2.9-a : Induced current streamlines.

( S.G = .1 , a / lambda = .3 )

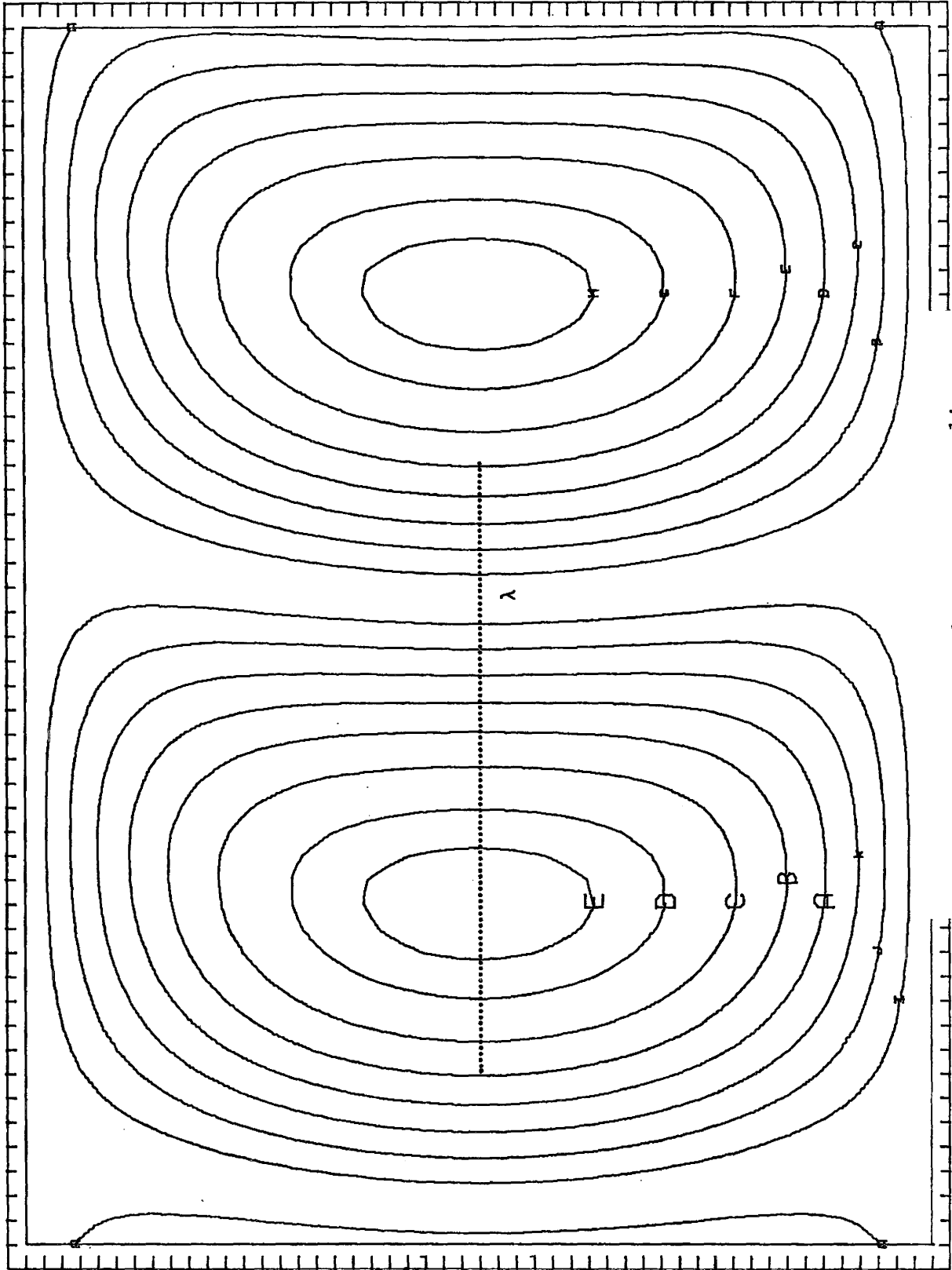


FIG. 2.9-b : Induced current streamlines.

( S.G = 1.92 ,  $a / \lambda = .3$  )

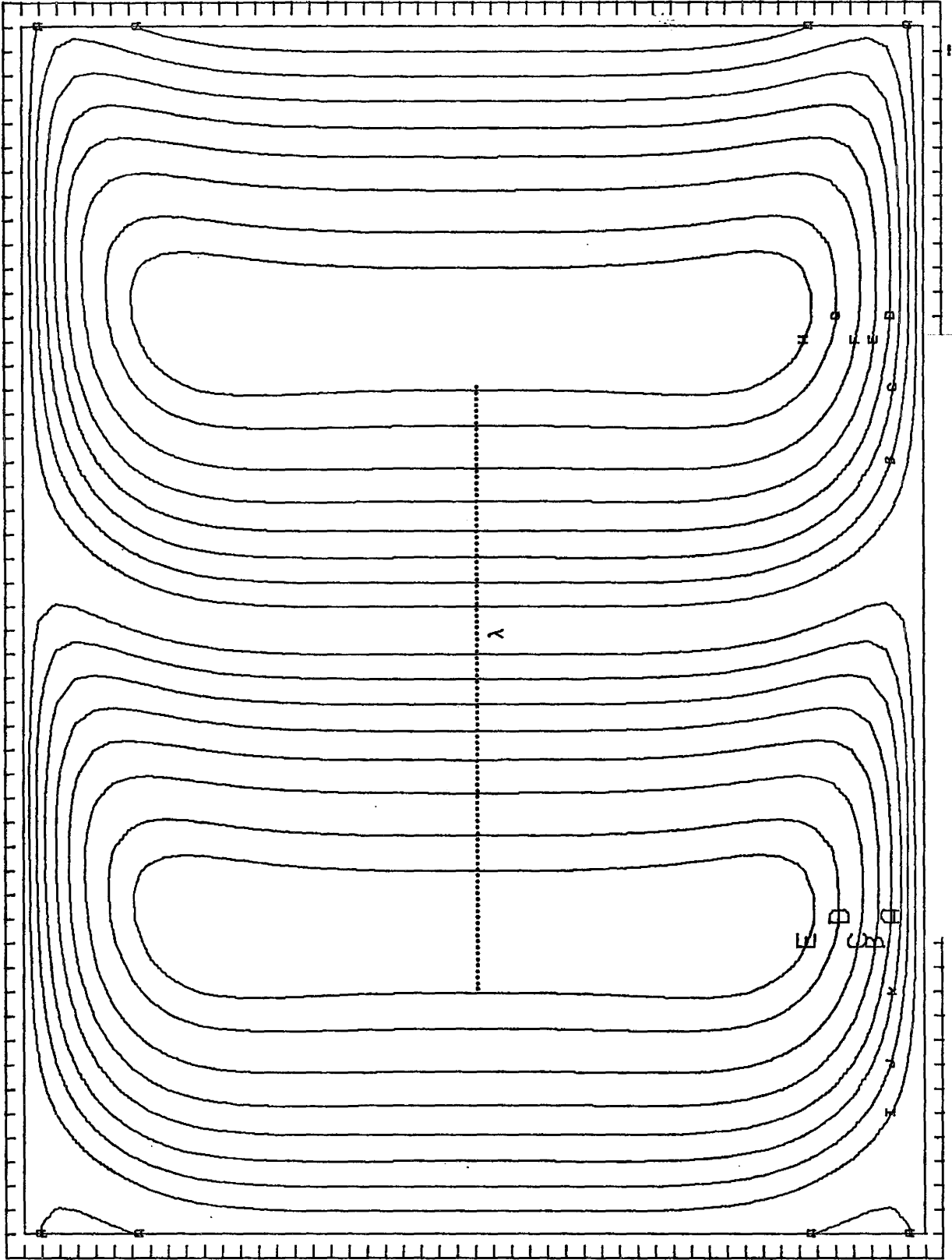
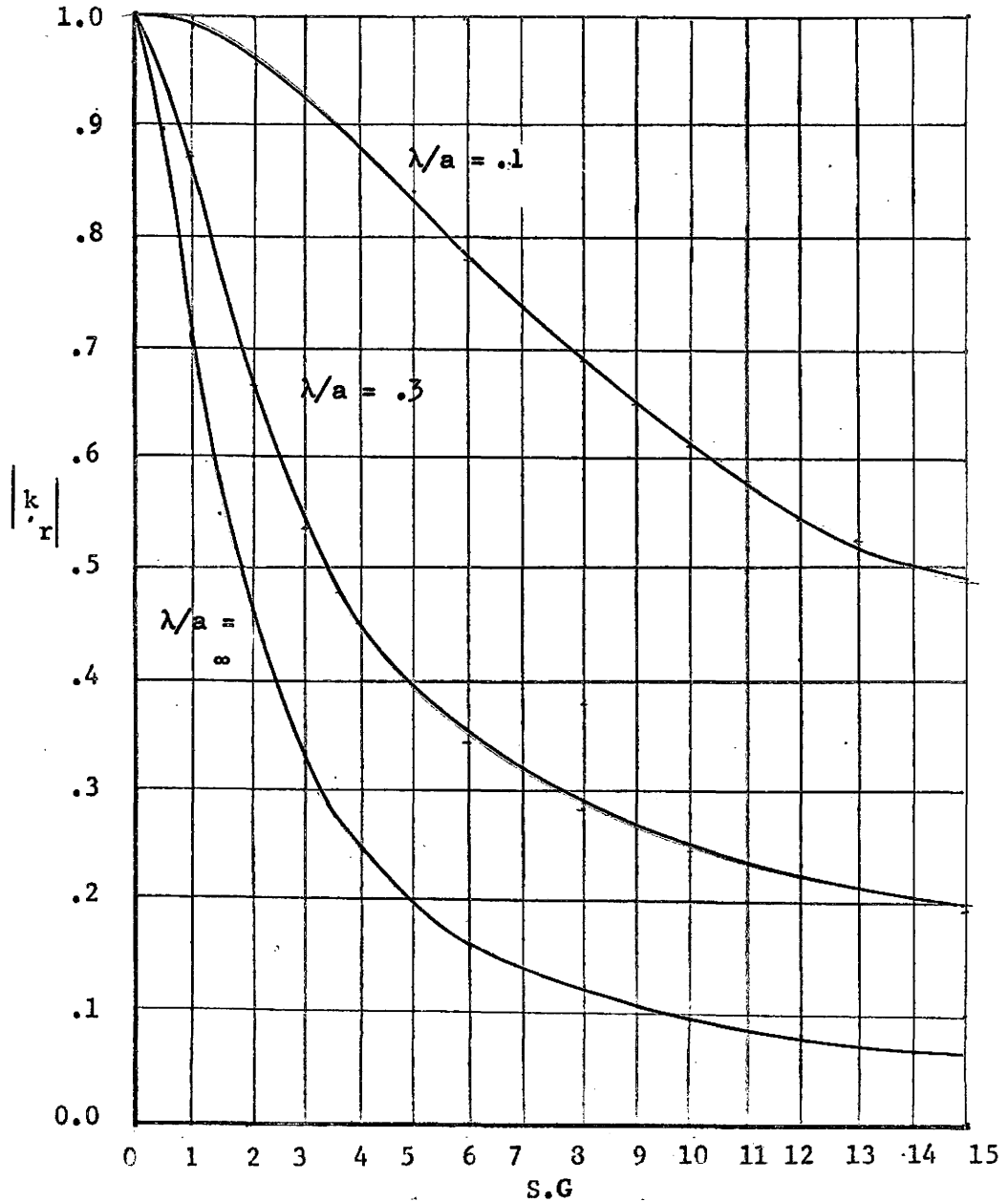


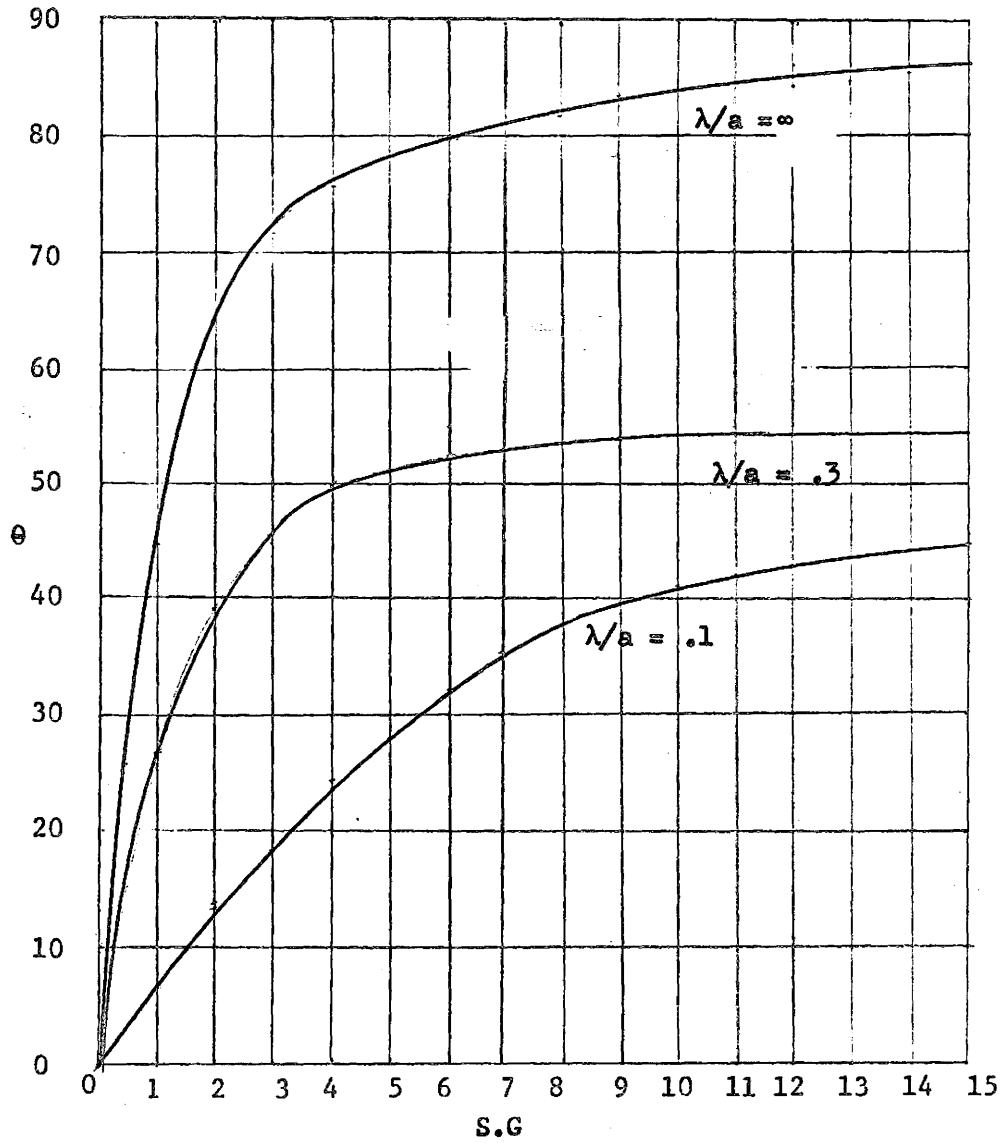
FIG. 2.9-c : Induced current streamlines .

( S.C = 1.92, a / λ = 1.0 )



( a ) Modulus of  
Demagnetising coefficient

FIG. 2.10 : Dependence of Demagnetising Coefficient  
on  $\lambda / a$  and S.G .



( b ) Argument of Demagnetising Coefficient

FIG. 2.10 (contd.)

machine. In the latter case the induced currents will be  $z$  directed over the entire width.

The force density is given:-

$$f = -\frac{1}{2} \operatorname{Re}\{J_3 B_2^*\}$$

Substituting from 2.43 and 2.44-b we obtain:

$$f = -\frac{1}{2} \operatorname{Re} \left[ \left\{ \left( \frac{\beta S G}{1 + j S G} \right) B_{20} \left( \frac{\cosh \gamma_0 z}{\cosh \gamma_0 a} - 1 \right) \right. \right. \\ \left. \left. \left\{ \frac{B_{20}^*}{(1 - j S G)} \left( 1 + j S G \frac{\cosh \gamma_0 z}{\cosh \gamma_0 a} \right)^* \right\} \right\} \right] \quad \dots 2.47$$

This can be re-arranged as

$$\frac{1}{2} \beta \frac{S G}{1 + S^2 G^2} |B_{20}|^2 \operatorname{Re} \left\{ \left( \frac{\cosh \gamma_0 z}{\cosh \gamma_0 a} - 1 \right) \right. \\ \left. \left( 1 + j S G \frac{\cosh \gamma_0 z}{\cosh \gamma_0 a} \right)^* \right\} \quad \dots 2.48$$

The expression for the force density in the infinitely wide machine. can be obtained from 2.47 by setting  $\gamma_0 a \gg \gamma_0 z$ . In this case  $\cosh \gamma_0 a \gg \cosh \gamma_0 z$  and the expression for the force density reduces to:-

$$\frac{1}{2} \beta \frac{S G}{1 + S^2 G^2} |B_{20}|^2 \quad \dots 2.49$$

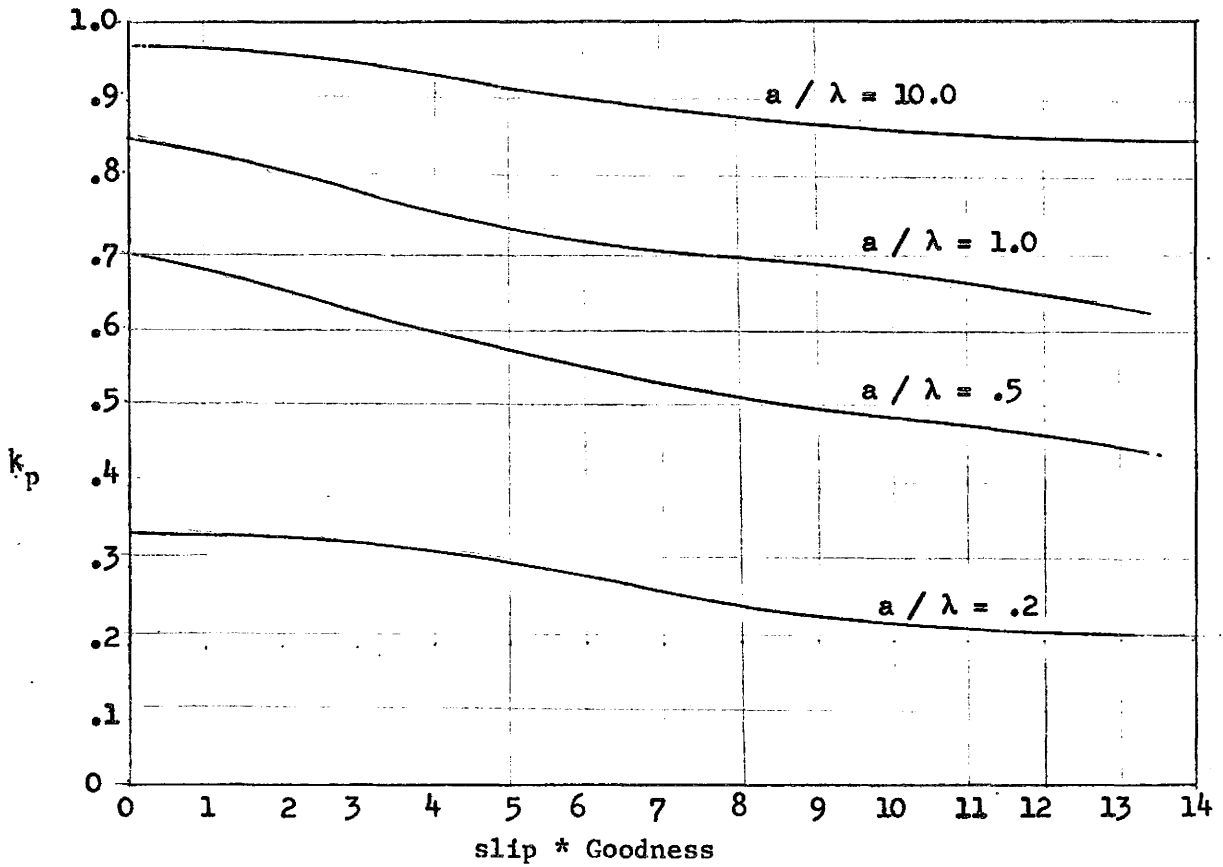


FIG. 2.11 : Force attenuation factor due to finite width effect .

The ratio of the average force densities is then

$$- \operatorname{Re} \int_{z=0}^{z=a} \left\{ \left( \frac{\cosh \gamma_0 z}{\cosh \gamma_0 a} - 1 \right) (1 + j S G \frac{\cosh \gamma_0 z}{\cosh \gamma_0 a})^* \right\} dz \quad \dots 2.50$$

Typical values of the finite width force attenuation factor appear in Fig. 2.11.

(b)  $\Delta_1 = \Delta_2$

Under the above general category is the sheet secondary machine with a wider secondary than primary and the liquid metal pump with short circuiting side conductors at  $z = \pm a$ . Referring to 2.37 it is seen that the flux distribution is determined by the dimensionless parameters  $a/\lambda$ ,  $S.G$ ,  $\rho/\rho'$  and  $\Delta/\lambda$ . Sample curves are shown in Fig. 2.12. In this case the variation of flux density over the width for different side conductor resistances is shown. As the relative conductivity of the side conductors increases the machine becomes "ideal".

(c)  $\Delta_1 \neq \Delta_2$ .

This case describes a laterally asymmetric secondary. This was first investigated by Bolton.<sup>(30)</sup> It can be shown that when  $\Delta_1 > \Delta_2$ ,  $|B_{\nu+}| > |B_{\nu-}|$  in which case there is a net travelling field in the  $+z$  direction. By normal induction motor action in the  $z$  direction a force exists which increases the eccentricity.

A plot of the flux density under this condition is shown in Fig. 2.13. Observe the presence of the basic requirement for "shaded pole action", that is the decentralised phase lag.

The stability of such systems has been considered by Laithwaite.

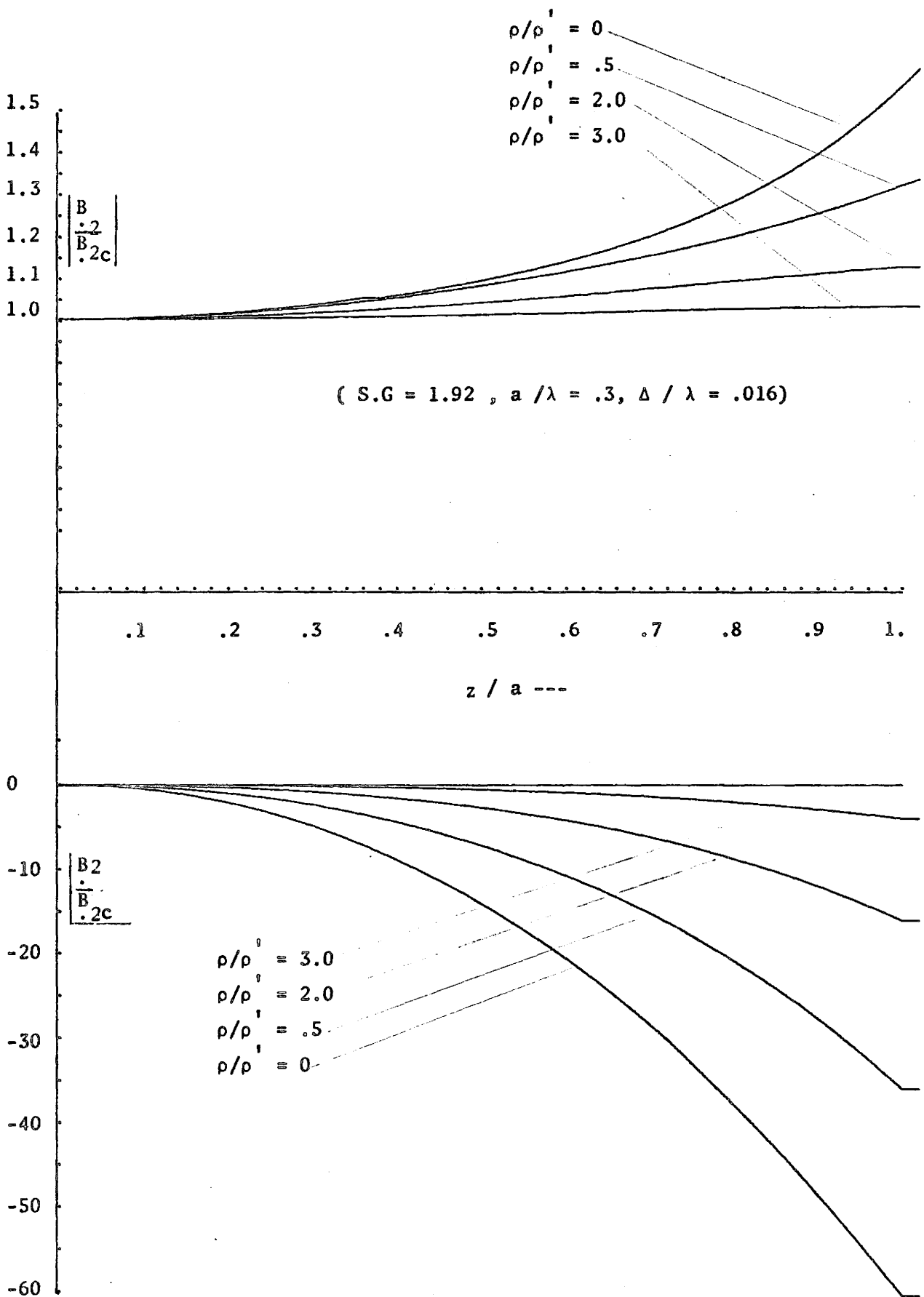
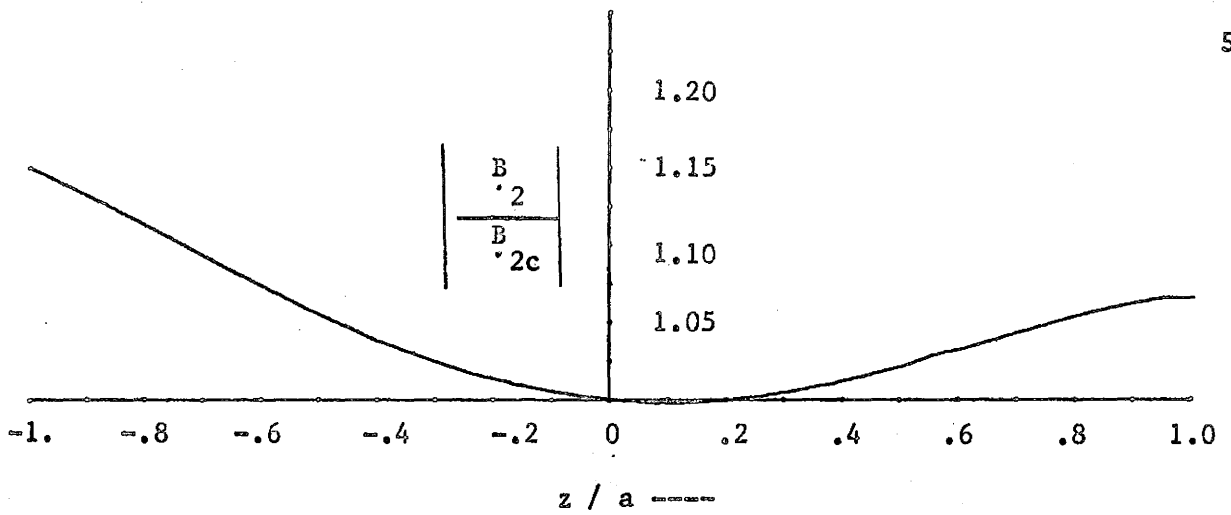


FIG. 2.2 : Lateral variation of flux density in induction pump with side conductors.



(  $a / \lambda = .3$  ,  $S.G = 1.92$  ,  $\Delta_1 / \lambda = .024$  ,  $\Delta_2 / \lambda = .04$  )

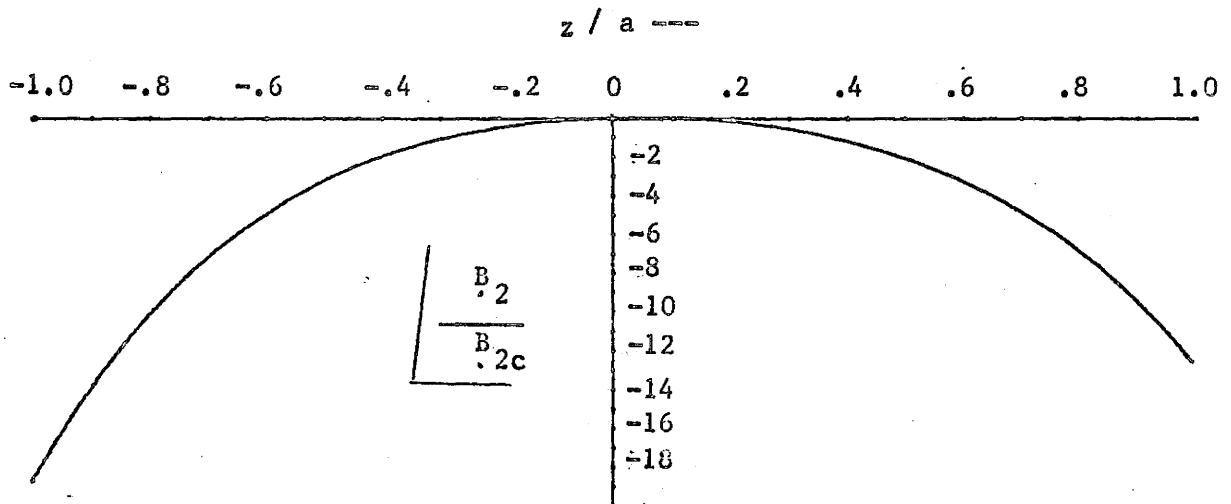


FIG. 2.13 : Lateral variation of flux density in machine with laterally asymmetric secondary.

## CHAPTER III

### ANALYSIS UNDER THE INFINITE WIDTH ASSUMPTION

#### 3.1 Introduction

From the last chapter it follows that if the width of the secondary is comparable with the wavelength the infinite width approximation is valid. Using this assumption we now consider flux penetration effects.

In this chapter the solution of the field equations is found for the case where lateral variation is neglected. Due to penetration effects the field quantities in this case will be non-uniform over the depth. It is desirable that the actual distributions and their effect on performance be determined. We also wish to find the criteria under which the ideal machine's performance is obtained.

As mentioned in Chapter I , a normal or levitation force may be present in linear induction machines. It is important that this force be evaluated so that the phenomenon be more fully understood.

#### 3.2 Skin Effect in the Travelling Wave Case.

The usual "yardstick" employed in analysing penetration effects is the "skin depth". This is defined as the depth penetrated when a certain value of attenuation is reached. It is usually defined in terms of the infinite plane geometry shown in Fig.3.1.

From Maxwell's equations we have:

$$\nabla \times E = - \frac{\partial B}{\partial t}$$

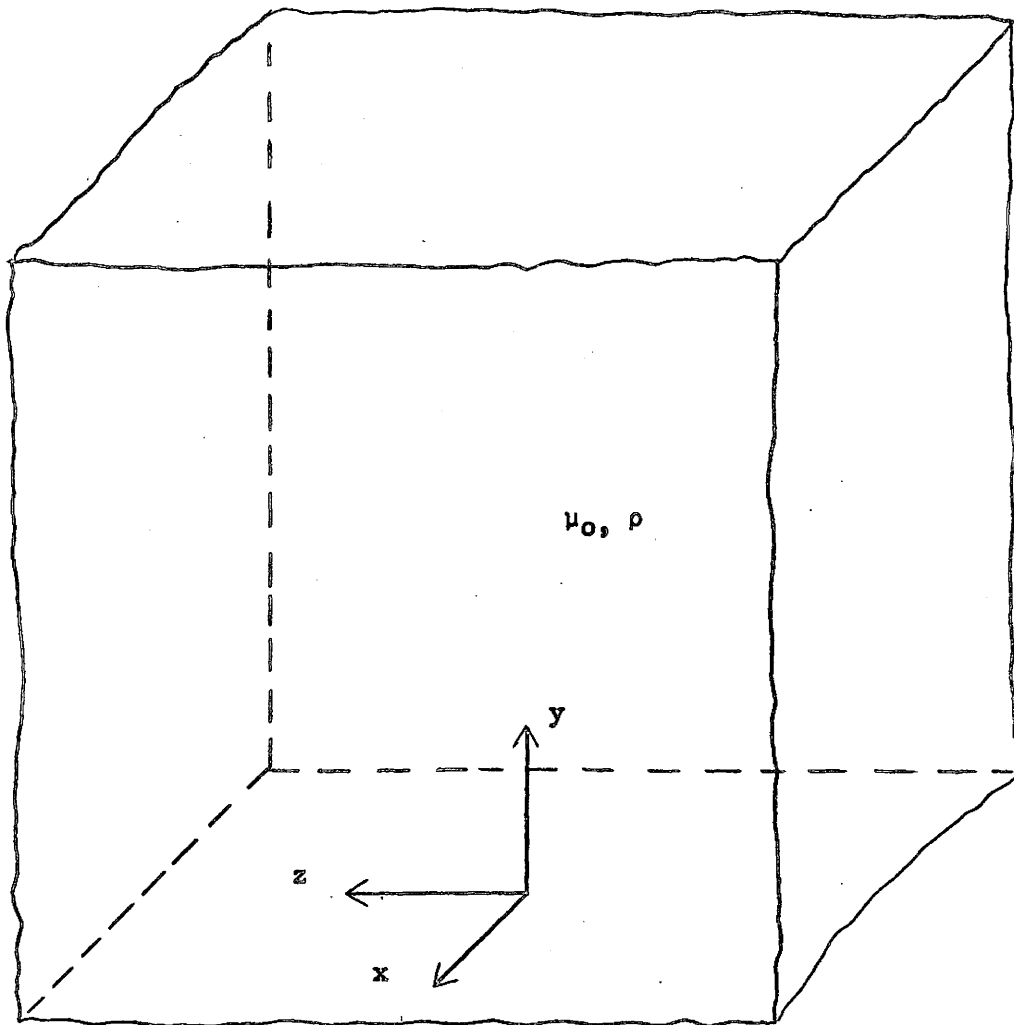


FIG. 3.1 : Co-ordinate system for analysis of skin effect.

taking the curl we obtain:

$$\begin{aligned}\nabla \times \nabla \times \mathbf{E} &= -\mu_0 \frac{\partial}{\partial t} (\nabla \times \mathbf{H}) = -\mu_0 \frac{\partial}{\partial t} \mathbf{J} \\ &= -\mu_0 \sigma \frac{\partial}{\partial t} \mathbf{E} .\end{aligned}$$

Since  $\nabla \times \nabla \times \mathbf{E} = -\nabla^2 \mathbf{E} + \nabla(\nabla \cdot \mathbf{E})$  and  $\nabla \cdot \mathbf{E} = 0$  we obtain

$$\nabla^2 \mathbf{E} = \mu_0 \sigma \frac{\partial}{\partial t} \mathbf{E} \quad \dots 3.1$$

Let us consider the penetration of an electric field whose surface value is represented by the complex number

$$E_{y=0} = E_{.30} e^{j(\omega t - \beta x)} \quad \dots 1z$$

Since we are assuming infinite width in the z direction we get:

$$\left( \frac{\partial^2}{\partial x^2} + \frac{\partial^2}{\partial y^2} \right) E_{.3} = j \omega \mu_0 \sigma E_{.3} \quad \dots 3.2$$

Replacing  $\frac{\partial^2}{\partial x^2}$  by  $-\beta^2$  and multiplying by  $e^{-j(\omega t - \beta x)}$  we obtain:

$$\frac{\partial^2 E_{.3}}{\partial y^2} = \kappa^2 E_{.3} \quad \dots 3.3$$

where  $\kappa^2 = \beta^2 (1 + j R)$

R is the Magnetic Reynolds number  $= \frac{\omega \mu_0 \sigma}{\beta^2}$

The solution to 3.3 is:

$$\begin{aligned}E_{.3} &= E_{.30} e^{-\kappa y} \\ &= E_{.30} e^{-\frac{\kappa y}{\beta}} e^{-j \frac{\kappa y}{\beta}}\end{aligned} \quad \dots 3.4$$

where  $\kappa = \kappa_r + j\kappa_i$

$$\kappa_{r,i} = \beta \sqrt{\frac{\sqrt{1 + R^2} \pm 1}{2}} \quad \dots 3.5$$

Consequently:

$$E_3 = E_{30} e^{-\kappa_r y} e^{j(\omega t - \beta x - \kappa_i y)} \quad \dots 3.6$$

Thus for any x value there is a phase shift in the y direction. The maximum electric field intensity is fixed by the  $e^{-\kappa_r y}$  envelope but the phase shift is such that we get a travelling field in the y direction. Following an analogous definition for skin depth as in the standing wave case we obtain:

$$\delta_S = \frac{1}{\kappa_r} = \frac{1}{\beta} \sqrt{\frac{2}{\sqrt{1 + R^2} + 1}} \quad \dots 3.7$$

Typical values appear in table 3.1.

The frequency dependence is shown in Fig. 3.2.

In the travelling wave case besides decreasing with increasing conductivity, frequency ( $R = \frac{\mu_0 \sigma \omega}{\beta^2}$ ), we also have decrease with increasing  $\beta$ . This means a decrease with decreasing wavelength.

If  $\beta \rightarrow 0$ , i.e. the wavelength becomes infinite and the travelling wave skin depth becomes:

$$\sqrt{\frac{2}{\mu_0 \sigma \omega}} \quad \dots 3.8$$

which is the standing wave value.

Even at zero frequency or in a non-conductor there is a penetration depth of a travelling wave. This is obviously due to the non-uniformity of the excitation in the x direction.

metal	frequency (hertz)	skin depth in cms.			
		wavelength			
		.1m	.2m	.4m	1.0m
liquid iron	25	1.59	3.19	6.26	11.9
	60	1.59	3.16	5.85	8.60
	400	1.56	2.67	3.35	3.59
mercury	25	1.59	3.17	5.96	9.11
	60	1.59	3.10	5.06	6.23
	400	1.49	2.16	2.42	2.50
sodium	25	1.54	2.47	2.94	3.09
	60	1.39	1.82	1.97	2.00
	400	.735	.768	.777	.780
aluminium	25	1.29	1.57	1.66	1.69
	60	.972	1.06	1.08	1.09
	400	.416	.421	.423	.423
copper	25	1.12	1.27	1.31	1.32
	60	.794	.839	.851	.852
	125	.327	.329	.330	.330

( the corresponding magnetic Reynold's numbers appear in Table 1.1)

TABLE 3.1 : Travelling wave skin depth

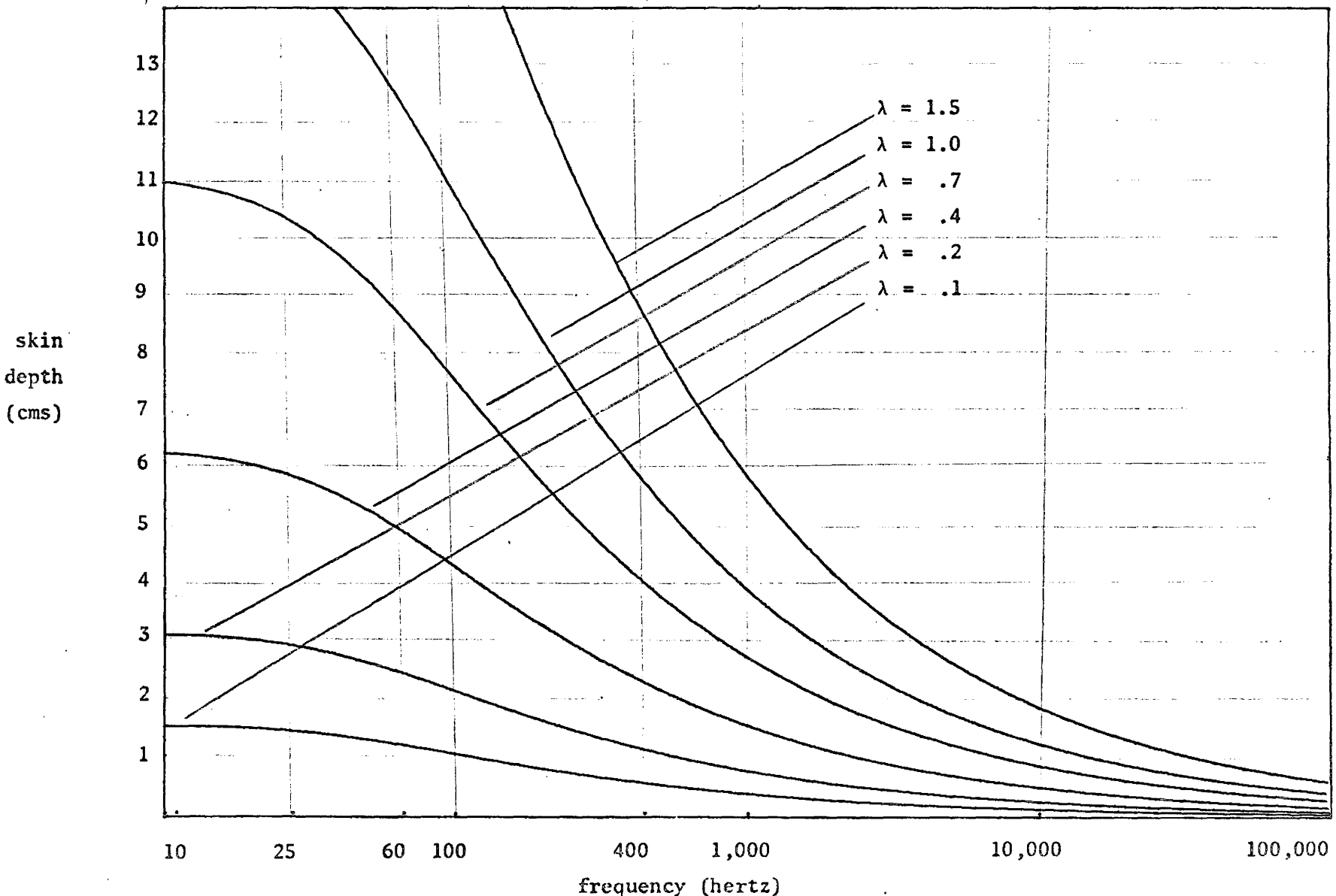


FIG. 3.2 : Frequency dependence of travelling wave skin depth.

The penetration in this case is :

$$\delta_s = 1/\beta$$

The effect of the conducting medium is to reduce the skin depth by the factor :

$$\sqrt{\frac{\sqrt{1 + R^2} + 1}{2}}$$

A good appreciation can be gained by considering the plots in Figs. 3.3 and 3.4. These represent the magnetic vector potential (A) over a single sided machine which has an excitation current sheet  $\vec{h}_3 = \text{Re } h_3 e^{j(\omega t - \beta x)}$ . The vector potential is defined:

$$\mathbf{B} = \nabla \times \mathbf{A}$$

and

$$\nabla \cdot \mathbf{A} = 0.$$

The solution for A over a single sided machine has the same form as that shown for E in expression 3.6. The physical significance of the results in Fig. 3.3 and 3.4 is as follows:- the value of A represents the fraction of the total flux  $\{\phi t\}$  which is cut by a plane whose edges are the z axis and a parallel line through x,y. The plane has unit length in the z direction.  $\phi t$  is the flux between  $x=0$  and  $x=\tau/2$  at  $y=0$ . This property of the vector potential follows from Stokes theorem (Ch. 1. section 4.1).

In Fig. 3.3 the magnetic Reynolds number is zero. 63% of the total flux,  $\phi t$ , is contained below a height  $\tau/\pi$  which is the skin depth. In Fig. 3.4,  $SR = 1.92$  and 63% of the total flux only reaches  $.8\tau/\pi$ . Besides more severe attenuation there is also distortion of the field in the x direction. This inherent distortion is a consequence of the phase

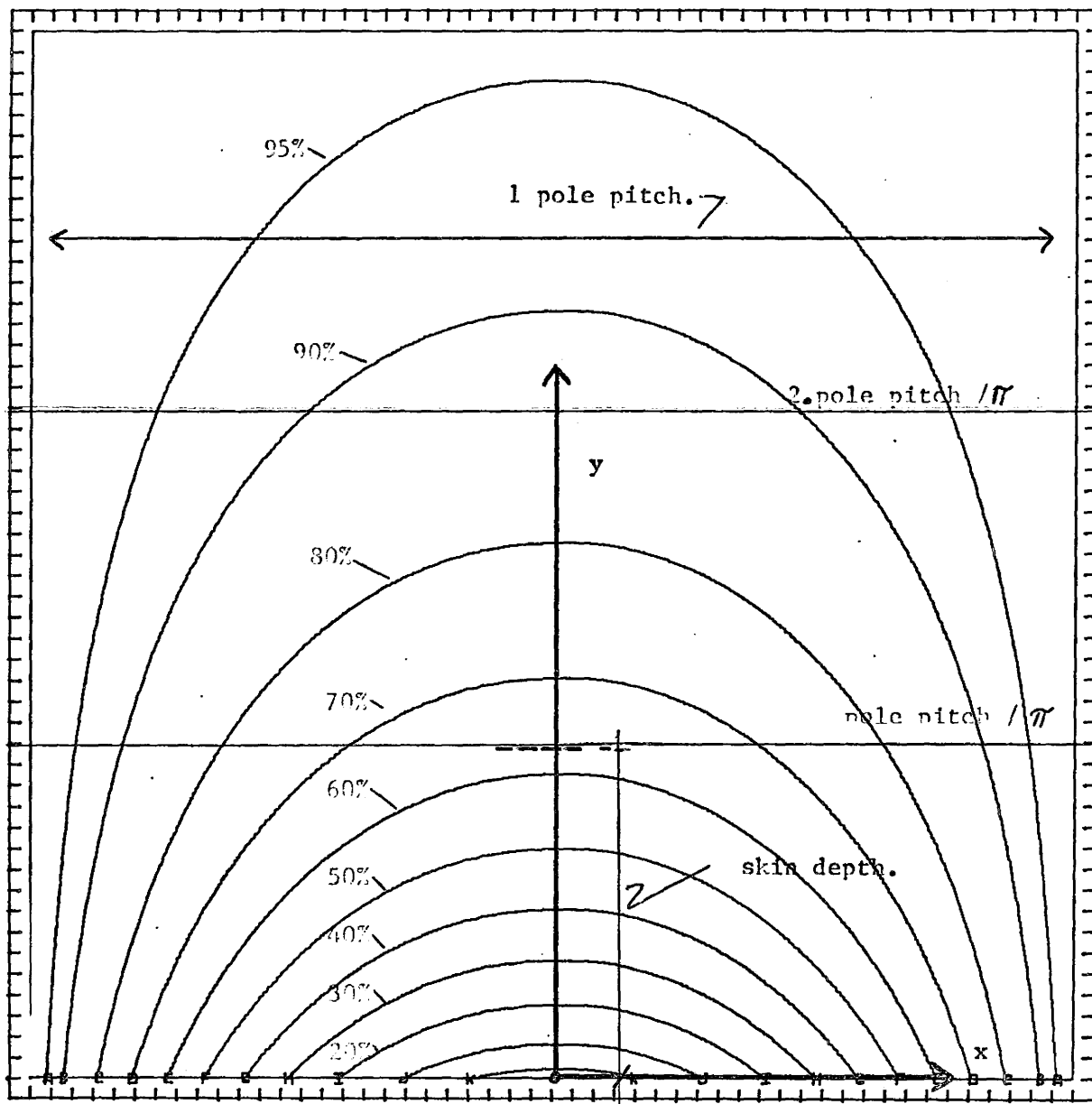


FIG. 3.3 : Flux distribution in open sided machine

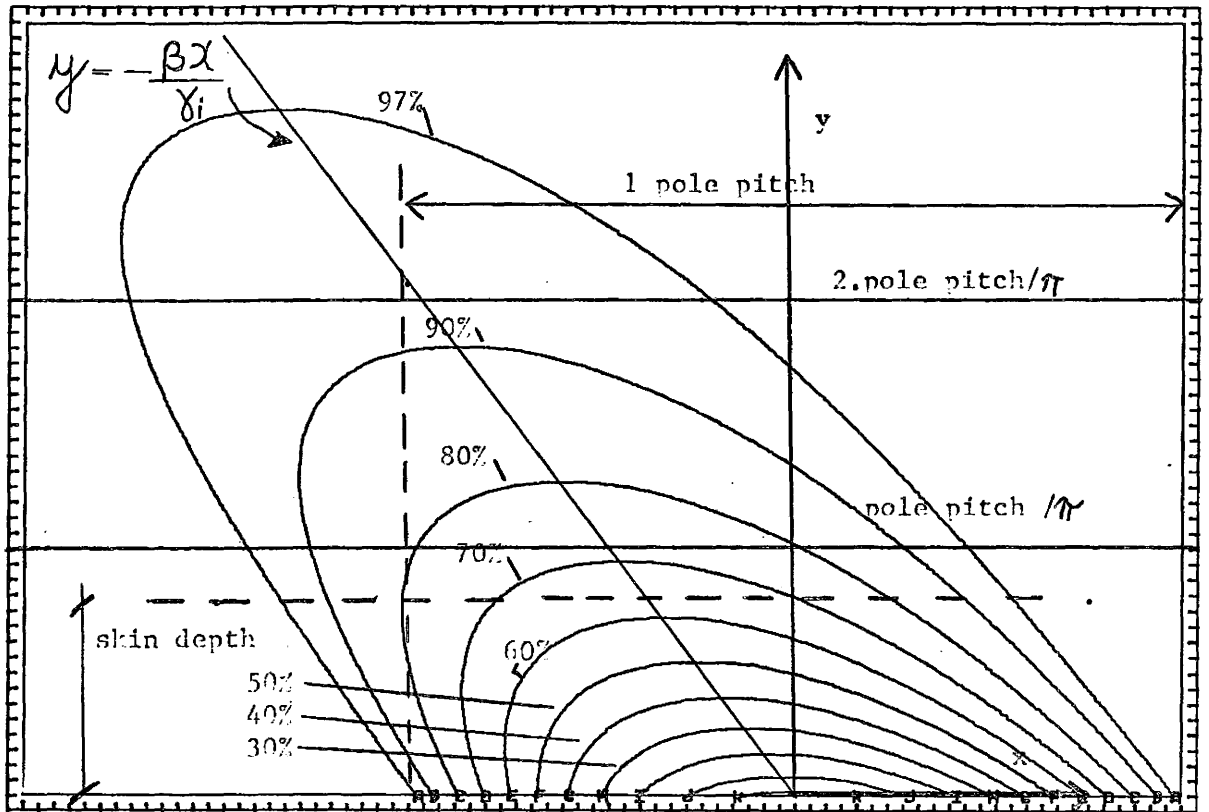


FIG. 3.4 : Flux distribution in open sided machine

with conducting medium ( S.R = 1.92 )

shift in the y direction. As shown in Fig. 3.4, for any y value the vector potential is an even function of x about the origin  $x = (-\gamma/\beta)y$

### 3.3 Normal Forces Due to Skin Effect:

From section 3.2 we have the solution for  $E_3$ :

$$\underline{E}_3 = E_{30} e^{-\kappa_1 y} e^{j(\omega t - \beta x - \kappa_1 y)}$$

We see from the above that besides the travelling field in the x direction, there is also a travelling field in the y direction. Even in the absence of the travelling field in the x direction ( $\beta \rightarrow 0$ , i.e.  $\lambda \rightarrow \infty$ ) there is a travelling field away from the stator surface.

We now consider the normal force due to the interaction of the induced current with the field.

Since  $\nabla \times E = -\frac{\partial B}{\partial t}$ , we obtain:

$$\underline{B}_1 = \frac{j}{\omega} \frac{\partial \underline{E}_3}{\partial y} \quad \dots 3.9$$

$$= -\frac{j\kappa}{\omega} \underline{E}_3 \quad \dots 3.10$$

Since  $\underline{J}_3 = \sigma \underline{E}_3$  and  $f_2 = \frac{1}{2} \text{Re}\{J_3 B_1^*\}$  ( $f_2$  is the average force density in the y direction and the asterisk denotes 'complex conjugate') we obtain:

$$f_2 = \frac{\sigma}{2\omega} \text{Re} \{ j \kappa \underline{E}_3 \underline{E}_3^* \} \quad \dots 3.11$$

$$= \frac{1}{2} \frac{\sigma}{\omega} \kappa_1 |E_{30}|^2 e^{-2\kappa_1 y} \quad \dots 3.12$$

The total normal force per unit area in the xz plane is given:

$$f_{sy} = \int_0^{\infty} f_2 dy \quad \dots 3.13$$

Thus

$$f_{sy} = \frac{1}{4} \frac{\sigma}{\omega} \frac{\kappa_1}{\kappa_T} |E_{30}|^2 \quad \dots 3.14$$

This can be more easily interpreted if we recall the definition of  $\kappa$ :

$$\kappa^2 = (\kappa_T + j \kappa_1)^2 = \beta^2 (1 + j R)$$

Consequently:

$$\kappa_T = \frac{\beta^2 R}{2 \kappa_1} \quad \dots 3.15$$

Substituting for  $\kappa_T$  and R in 3.19 we obtain:

$$f_{sy} = \frac{1}{2} \frac{1}{\omega^2 \mu_0} \kappa_1^2 |E_{20}|^2 \quad \dots 3.16$$

substituting from 3.5 for  $\kappa_1$  we obtain:

$$f_{sy} = \frac{1}{4} \frac{\beta^2}{\omega^2 \mu_0} |E_{20}|^2 \{ \sqrt{1 + R^2} - 1 \} \quad \dots 3.17$$

The above expression is in agreement with the results in (9).

It is interesting to compare the above surface force density with the power density.

From (3.14) we have:

$$H_{z1} = -j \frac{\kappa}{\mu_0 \omega} E_{z3} \quad \dots 3.18$$

The power density is:

$$\frac{1}{2} \operatorname{Re}\{E_{z3} H_{z1}^*\} \quad \dots 3.19$$

$$= \frac{1}{2} \operatorname{Re}\left\{j \frac{\kappa}{\mu_0 \omega} E_{z3} E_{z3}^*\right\} \dots 3.20$$

Consequently, the power density at the stator surface is:

$$P_2 = \frac{1}{2} \frac{\kappa_1}{\mu_0 \omega} |E_{z30}|^2 \quad \dots 3.21$$

It follows from above that:

$$\frac{P_2}{F_{sy}} = \frac{\omega}{\kappa_1} \quad \dots 3.22$$

Upon examining 3.6 it is seen that  $\omega/\kappa_1$  is the phase velocity of the travelling field. The mechanisms involved in setting up the travelling fields in the direction of motion and in the normal direction are different. However, in both cases, the force is given by the power divided by the wave velocity.

### 3.4 Model and Assumptions:

The model being considered is shown in Fig. 3.4. The following are the main assumptions:

1. The lateral edge effect is neglected - consequently the induced current

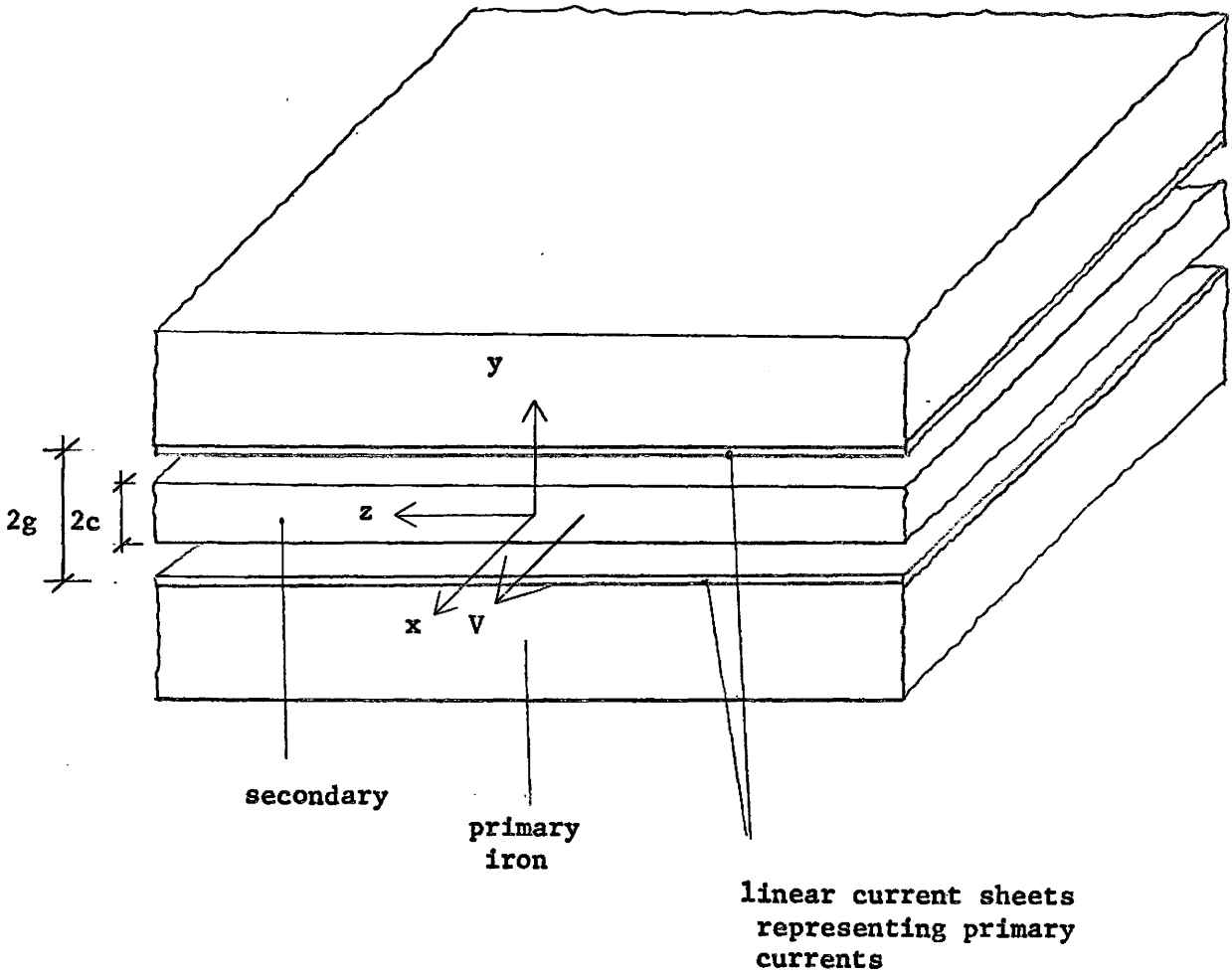


FIG. 3.5 : Model for analysis under infinite width approximation

is z directed.

2. The machine being analysed is infinitely long so the "finite length" effect is neglected.

3. The primary winding can be replaced by a continuous current sheet backing a smooth iron surface. The permeability of the core is infinite. Only the fundamental of the primary current sheet is considered in the analysis.

4. In the case of a liquid metal pump a flat velocity profile is assumed.

### 3.5 Equations and General Solution:

The magnetic transport equation ( Section 1.3 ) describes the field distribution in both the air gap and secondary region.

In general:

$$\nabla^2 \bar{B} = \mu_0 \sigma \left\{ \frac{\partial \bar{B}}{\partial t} - \nabla \times \bar{V} \times \bar{B} \right\} \quad \dots 3.23$$

In the air gap, where  $\sigma = 0$ , the above reduces to Laplaces' equation:

$$\nabla^2 \bar{B} = 0 \quad \dots 3.24$$

Since  $\bar{V} \times \bar{B} = (V \hat{1}_x) \times (B_1 \hat{1}_x + B_2 \hat{1}_y)$

$$= V B_2 \hat{1}_z$$

therefore  $\nabla \times \bar{V} \times \bar{B} = V \frac{\partial B_2}{\partial y} \hat{1}_x - V \frac{\partial B_2}{\partial x} \hat{1}_y$

Using the property  $\nabla \cdot \bar{B} = 0$ , this reduces to give:

$$\nabla \times \bar{V} \times \bar{B} = -V \frac{\partial B_1}{\partial x} \hat{1}_x - V \frac{\partial B_2}{\partial x} \hat{1}_y \quad \dots 3.25$$

Consequently, we get two scalar equations:

$$\nabla^2 B_1 = \mu_0 \sigma \left\{ \frac{\partial B_1}{\partial t} + V \frac{\partial B_1}{\partial x} \right\} \quad \dots 3.26$$

$$\nabla^2 B_2 = \mu_0 \sigma \left\{ \frac{\partial B_2}{\partial t} + V \frac{\partial B_2}{\partial x} \right\}$$

Since we are neglecting lateral variation  $\frac{\partial^2}{\partial y^2} = 0$ .

Consequently, using phasor notation we obtain:

$$\left\{ -\beta^2 + \frac{\partial^2}{\partial y^2} \right\} \underline{B}_1 = j S \mu_0 \sigma \omega \underline{B}_1 \quad \dots 3.27$$

$$\left\{ -\beta^2 + \frac{\partial^2}{\partial y^2} \right\} \underline{B}_2 = j S \mu_0 \sigma \omega \underline{B}_2$$

where S is the slip:

$$= 1 - \frac{V}{u_s}$$

$u_s$  is the synchronous speed =  $\omega/\beta$ .

Consequently we obtain, upon rearranging and multiplying by  $e^{-j(\omega t - \beta x)}$

$$\frac{\partial^2 \underline{B}_1}{\partial y^2} = \gamma_0^2 \underline{B}_1$$

... 3.28

$$\frac{\partial^2 \underline{B}_2}{\partial y^2} = \gamma_0^2 \underline{B}_2$$

where  $\gamma_0^2 = \beta^2 (1 + j S R)$

R being the Magnetic Reynolds number as defined previously.

In the air gap, Laplaces' equation reduces to:

$$\frac{\partial^2 B_1}{\partial y^2} = \beta^2 B_1$$

...3.29

$$\frac{\partial^2 B_2}{\partial y^2} = \beta^2 B_2$$

The general solution for the secondary region is:

$$B_2 = C \cosh \gamma_0 y + D \sinh \gamma_0 y$$

...3.30

$$B_1 = -j \frac{\gamma_0}{\beta} C \sinh \gamma_0 y - j \frac{\gamma_0}{\beta} D \cosh \gamma_0 y$$

(The solution for  $B_1$  is obtained by applying the divergence theorem)

In the air gap region the solution takes the form:

$$B_2 = E \cosh \beta y + F \sinh \beta y$$

...3.31

$$B_1 = -j E \sinh \beta y - j F \cosh \beta y$$

C, D, E, and F are arbitrary constants.

The boundary conditions to be satisfied are:

(a) At the secondary - air gap interface.

1. Continuity of  $B_2$
2. Continuity of  $H_1$ .

(b) At the stator surface

$$1. \quad \underline{B}_2 = \underline{C}_1 V$$

$$2. \quad \underline{H}_1 = \underline{C}_2 I$$

where  $V$  and  $I$  are the phase voltage and current respectively.  $\underline{C}_1$  and  $\underline{C}_2$  are complex constants depending on the co-ordinate system origin relative to the machine poles and the winding arrangement. (appendix 1)

Generally, corresponding top and bottom windings will carry in-phase currents. In this case the  $x$  component of flux density is zero at the channel centre.

In this case we get the solution:

In the secondary:

$$\underline{B}_2 = \frac{\text{Cosh } \gamma_0 y}{\text{Cosh } \gamma_0 c} \underline{B}_{2c}$$

...3.32

$$\underline{B}_1 = -j \frac{\gamma_0}{\beta} \frac{\text{Sinh } \gamma_0 y}{\text{Cosh } \gamma_0 c} \underline{B}_{2c}$$

$\underline{B}_{2c}$  is the phasor representing the induction at  $y = c$ .

In the air gap:

$$\underline{B}_2 = \underline{B}_{2c} \left\{ \text{Cosh } \beta y' + \frac{\gamma_0}{\beta} \tanh \gamma_0 c \text{ Sinh } \beta y' \right\}$$

...3.33

$$\underline{B}_1 = -j \underline{B}_{2c} \left\{ \text{Sinh } \beta y' + \frac{\gamma_0}{\beta} \tanh \gamma_0 c \text{ Cosh } \beta y' \right\}$$

In the case of the transverse flux machine the normal component of induction is zero at  $y = 0$ .

Consequently we obtain:

In the secondary:

$$B_{.1} = \frac{\text{Cosh } \gamma_0 y}{\text{Cosh } \gamma_0 c} B_{.1c} \quad \dots 3.34$$

$$B_{.2} = j \frac{\beta}{\gamma_0} \frac{\text{Sinh } \gamma_0 y}{\text{Cosh } \gamma_0 c} B_{.1c}$$

$B_{.1c}$  is the tangential component of induction at  $y =$

In the air gap:

$$B_{.1} = B_{.1c} \left\{ \text{Cosh } \beta y' + \frac{\beta}{\gamma_0} \text{Sinh } \beta y' \right\} \quad \dots 3.35$$

$$B_{.2} = j B_{.1c} \left\{ \text{Sinh } \beta y' + \frac{\beta}{\gamma_0} \tanh \gamma_0 c \text{Cosh } \beta y' \right\}$$

### 3.6 Magnetic Field and Current Density Distribution:

From  $\nabla \times E = - \frac{\partial B}{\partial t}$  since the only electric field in the infinite width analysis is  $z$  directed we obtain:

$$- \frac{\partial E_{\sqrt{3}}}{\partial x} = - \frac{\partial B_{\sqrt{2}}}{\partial t} \quad \dots 3.36$$

Since  $\frac{\partial}{\partial x} = -j\beta$  and  $\frac{\partial}{\partial t} = j\omega$  we obtain in phasor notation

$$E_{\sqrt{3}} = - \frac{u_s B_{\sqrt{2}}}{S_{\sqrt{2}}} \quad \dots 3.37$$

where  $u_s = \omega/\beta$  the synchronous speed.

Ohm's law then gives:

$$\begin{aligned} J_3 &= \sigma(-u_S B_2 + V B_2) \\ &= -Su_S \sigma B_2 \end{aligned}$$

where  $S$  is the slip as previously defined.

Thus the current density distribution is identical with that of the normal component of flux density.

The normal flux density in the through flux machine has the same distribution as the tangential flux density in the transverse flux machine. Consequently, it follows that the distributions are determined by the following functions:

$$\begin{aligned} \Gamma_1 &= \frac{\text{Sinh } \gamma_0 z}{\text{Sinh } \gamma_0 c} \\ \Gamma_2 &= \frac{\text{Cosh } \gamma_0 z}{\text{Cosh } \gamma_0 c} \end{aligned} \quad \dots 3.38$$

Upon examination of the above it follows that the arguments can be conveniently expressed in terms of the dimensionless quantities  $S.R$ ,  $c / \lambda$  and  $z/c$ :

$$\gamma_0 z = (\gamma_0 / \beta) (\beta c) (z/c)$$

Since

$$\gamma_0 / \beta = \sqrt{1 + j S R}$$

and

$$\beta = 2\pi / \lambda .$$

In Figs. 3.5 and 3.6 the magnitude and phase of the above functions are given.

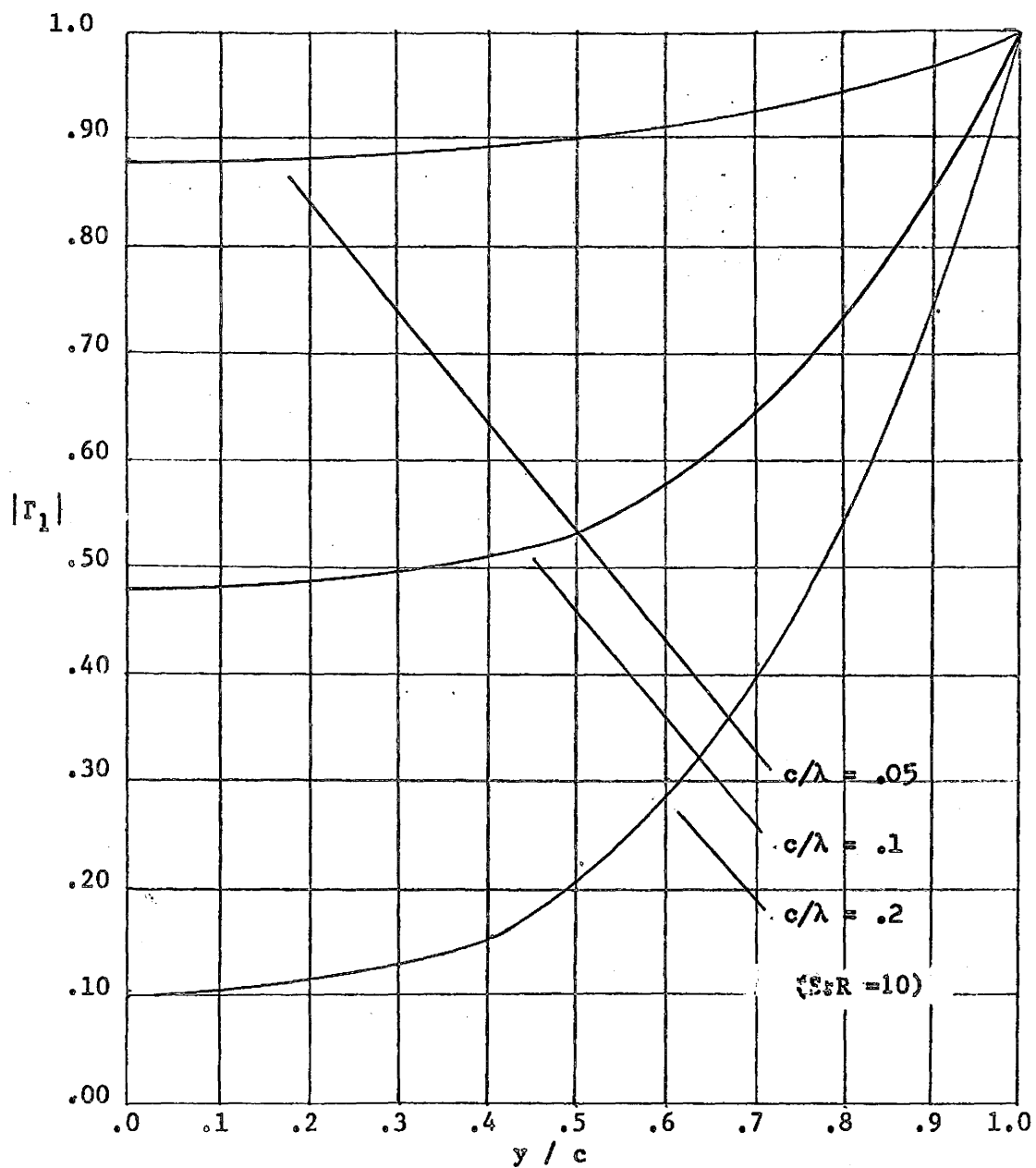


FIG. 3.6 : Distribution of  $r_1$  for different  $c/\lambda$  values

(a) Modulus

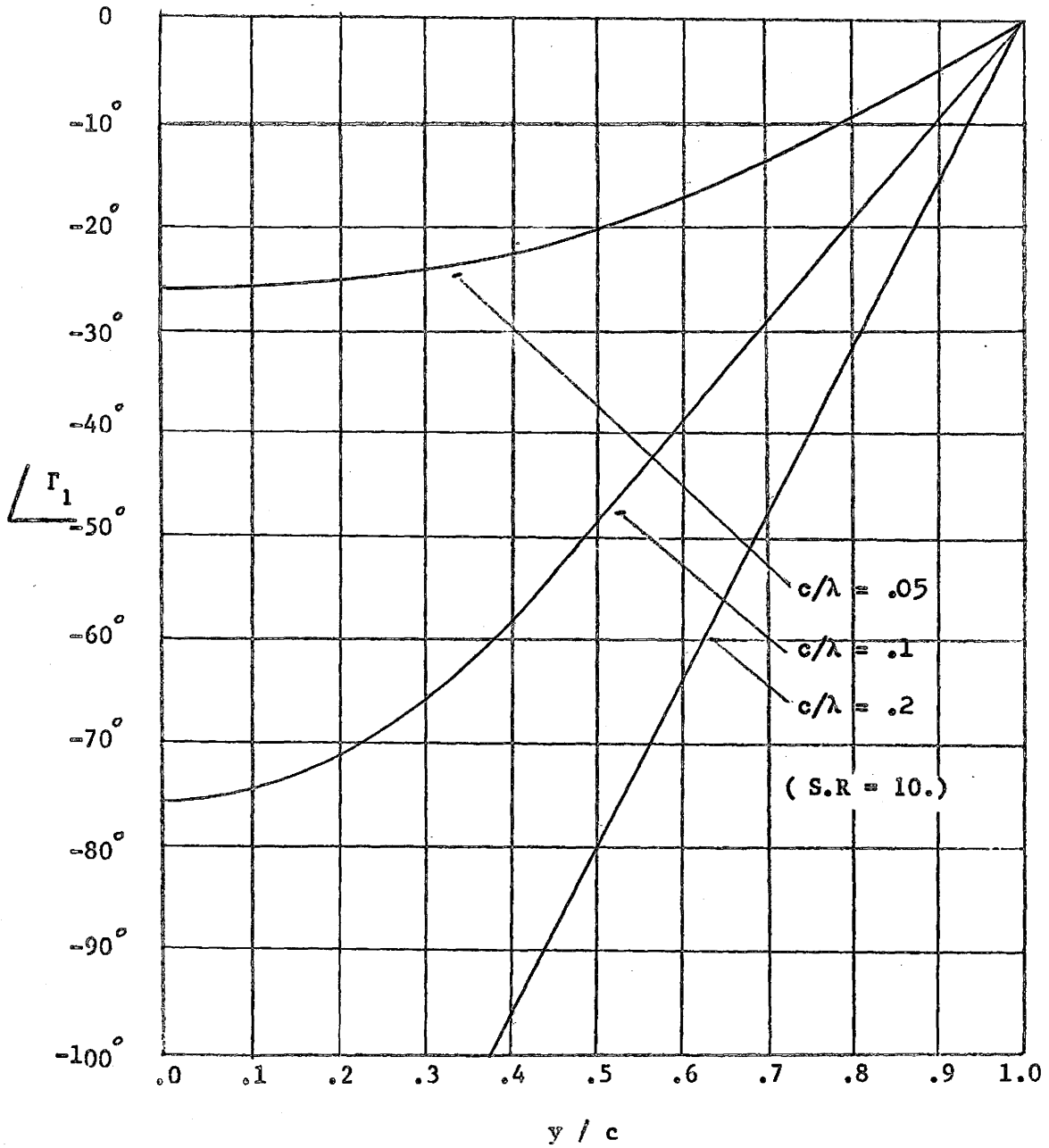


FIG. 3.6. contd. (b) argument

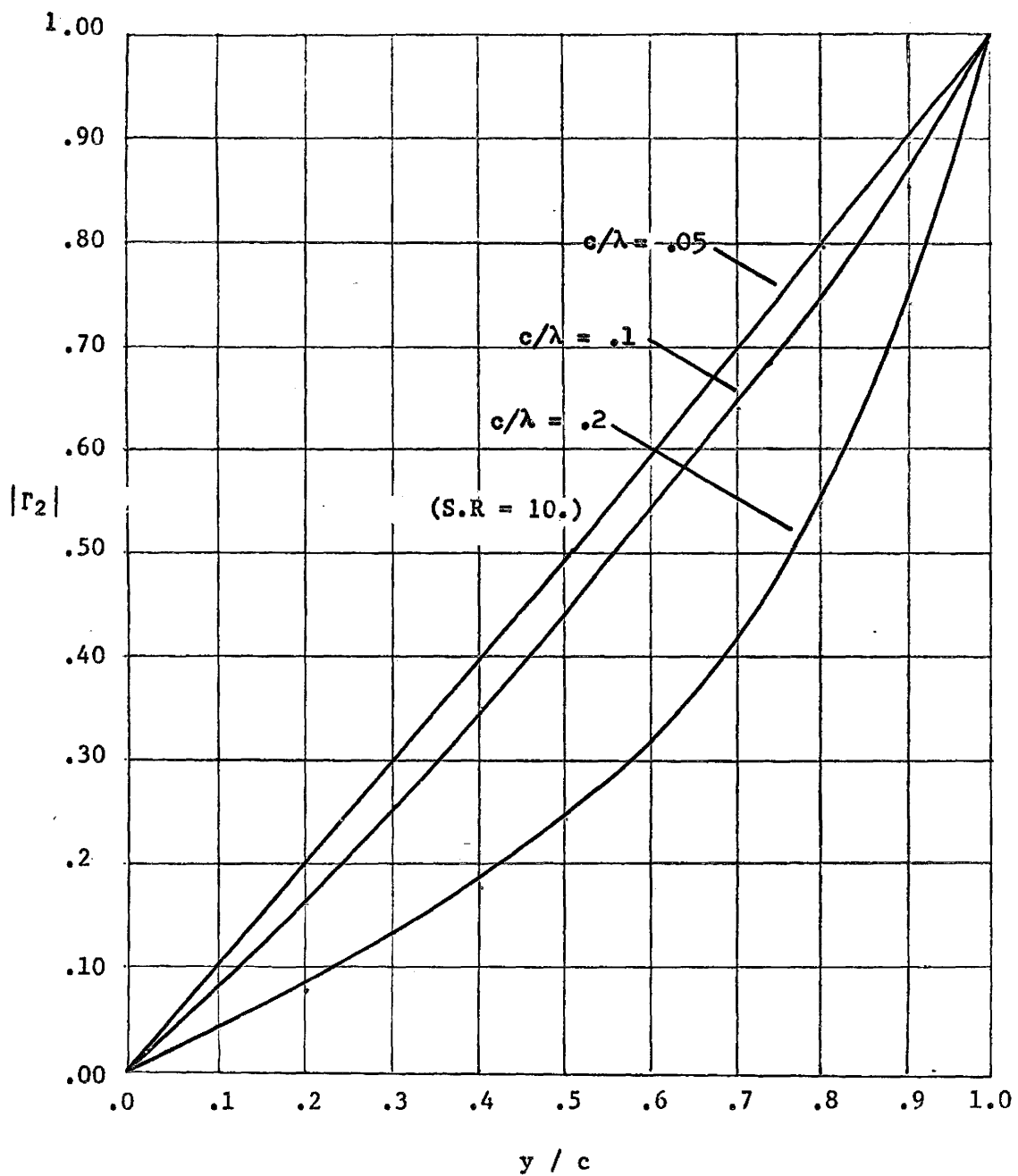


FIG. 3.7 : Distribution of  $\Gamma_2$   
for different  $c/\lambda$  values

(a) Modulus

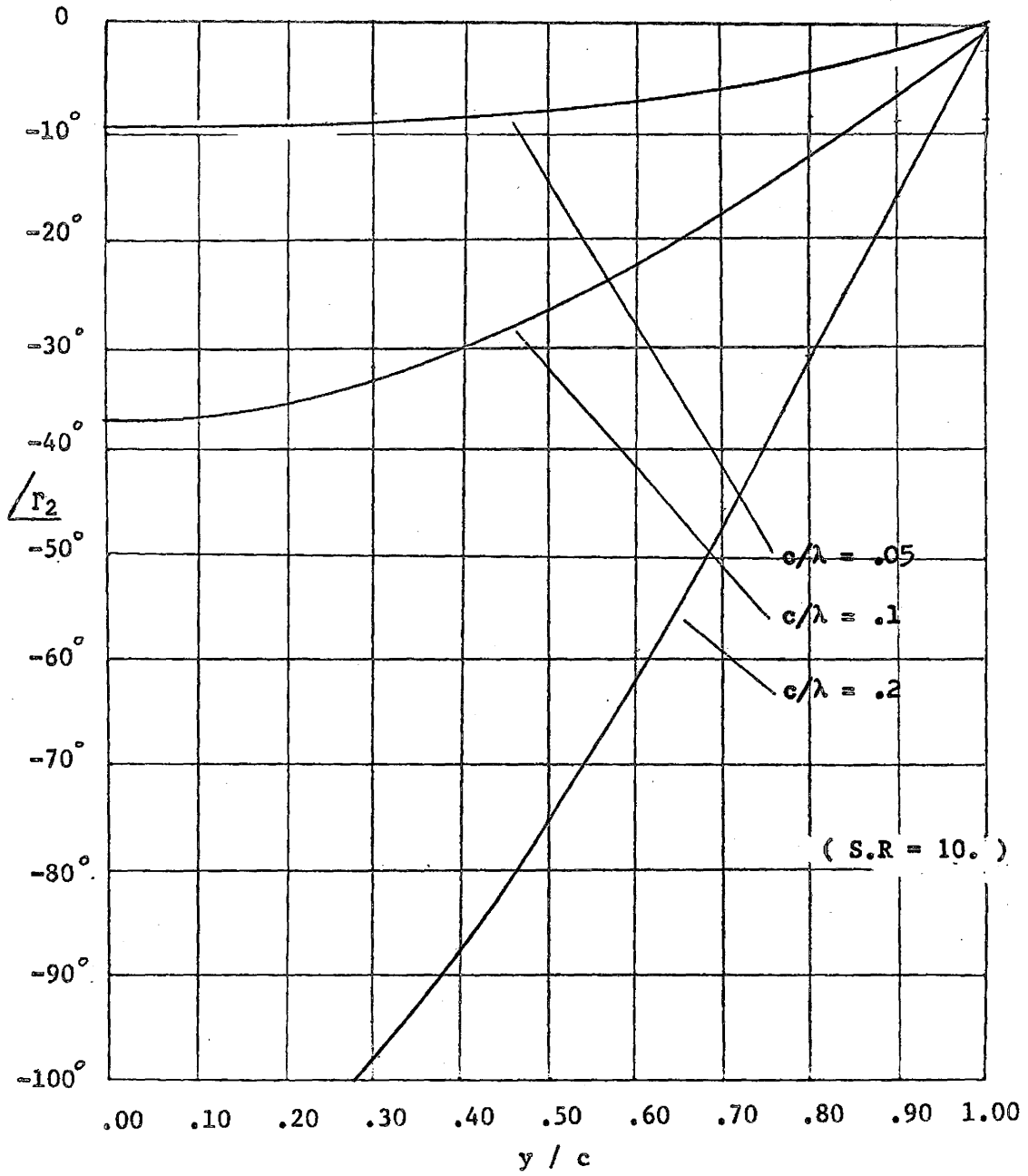


FIG. 3.7.contd. (b) argument

### 3.7 Performance of the Through Flux Machine:

We now compare the performance of the through flux machine with the ideal induction machine discussed in (Sect. 2.5). It is apparent from Fig. 3.5 that except when  $c/\lambda \ll 1$  the flux density decays significantly over the secondary depth.

We had in 3.6:

$$\underline{J}_3 = - S \mu_0 \sigma \underline{B}_2$$

The Lorentz force is given:

$$f_1 = \frac{1}{2} \text{Re}\{- \underline{J}_3 \underline{B}_2^*\} \quad \dots 3.39$$

It follows from the above that the ratio of average force density in the actual machine to that in the ideal machine is given:

$$k_a = \frac{\frac{1}{c} \int_0^c |\underline{B}_2|^2 dy}{|\underline{B}_{2c}|^2} \quad \dots 3.40$$

$k_a$  is defined as a force or pressure attenuation factor. Plots of this factor appear in Fig. 3.7. Again the justification of using the "ideal machine equations" is shown at low values of  $c/\lambda$ .

To determine the power factor we must compute the "demagnetisation coefficient" or Goodness factor. This information allows us to determine an equivalent circuit of the form shown in Fig. 2.3.

Following the definition in (Section 2.5) the demagnetisation coefficient is obtained:

$$k_r = \frac{B_2}{B_{20}} \Big|_{h_3 \text{ constant}} \quad \dots 3.41$$

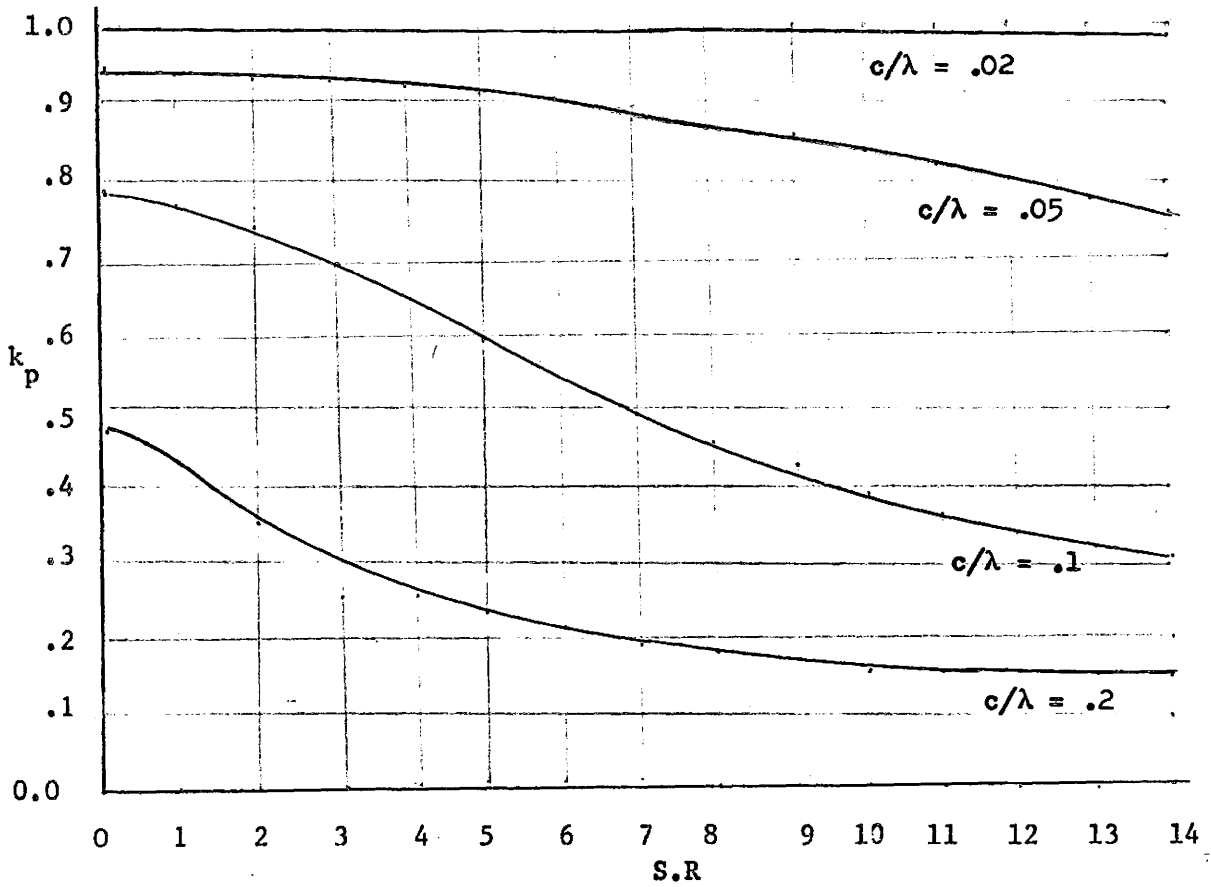


FIG. 3.8 : Force attenuation factor due to flux penetration effect.

If the linear current sheet is kept constant as we go from no load to full load then  $B_{1c}$  is constant. [ $B_{1c} = \mu h_3$ ]. Consequently by expressing  $B_{20}$  and  $B_{20}$  in terms of  $B_{1c}$  the demagnetising coefficient can be determined.

Constant  $B_{1c}$  is equivalent to constant  $h_3$ . Hence from 2.40,

$$k_r = \frac{j \frac{\beta}{\gamma} \frac{B_{1c}}{\sinh \gamma c}}{j \frac{B_{1c}}{\sinh \beta c}} = \frac{\beta \sinh \beta c}{\gamma \sinh \gamma c} \quad \dots 3.42$$

For the case of  $\gamma c \ll 1$  we can replace the hyperbolic functions by the first term of their Taylor series expansions:

In this case:

$$k_r \rightarrow \frac{1}{1 + S R} \quad \dots 3.43$$

which is the result obtained in (2.41).

The "demagnetising coefficient" is plotted in Fig. 3.10. Note that for all cases the "demagnetisation coefficient" is greater than that in the ideal machine. The values in Fig. 3.10 permit the modified phasor diagrams in Fig. 3.11 to be drawn. The overall result is that the output power is less than that of the "ideal machine".

In the above, the analysis has been based on the assumption that the air gap region is absent.

The effect of the air gap is to introduce a leakage and additional magnetising reactance into the circuit.

The effect of air gap can best be appreciated by writing Eqn. 3.31 in the following matrix form:

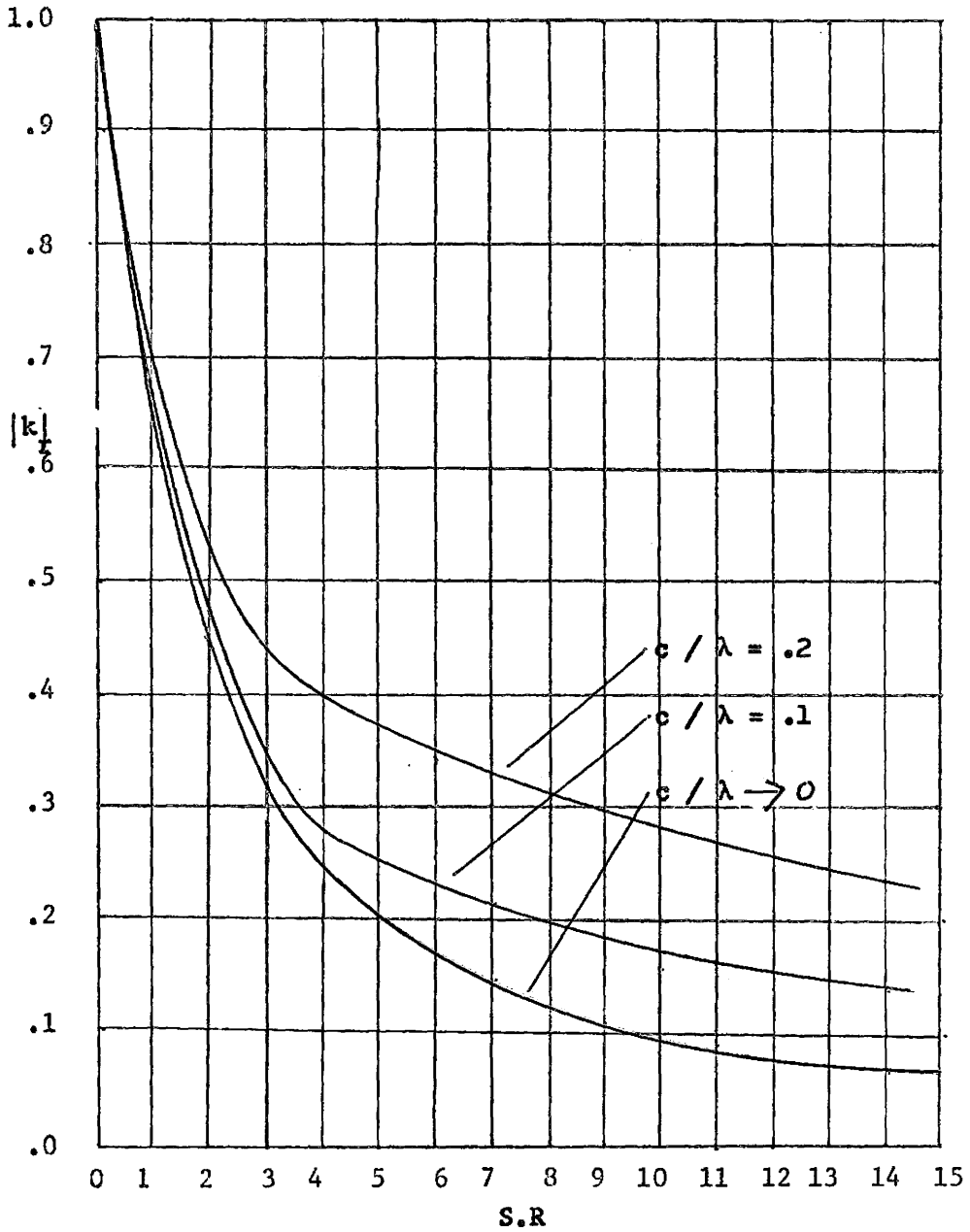


FIG. 3.9 : Dependence of Demagnetising Coefficient on S.R. and  $c / \lambda$

(a) modulus

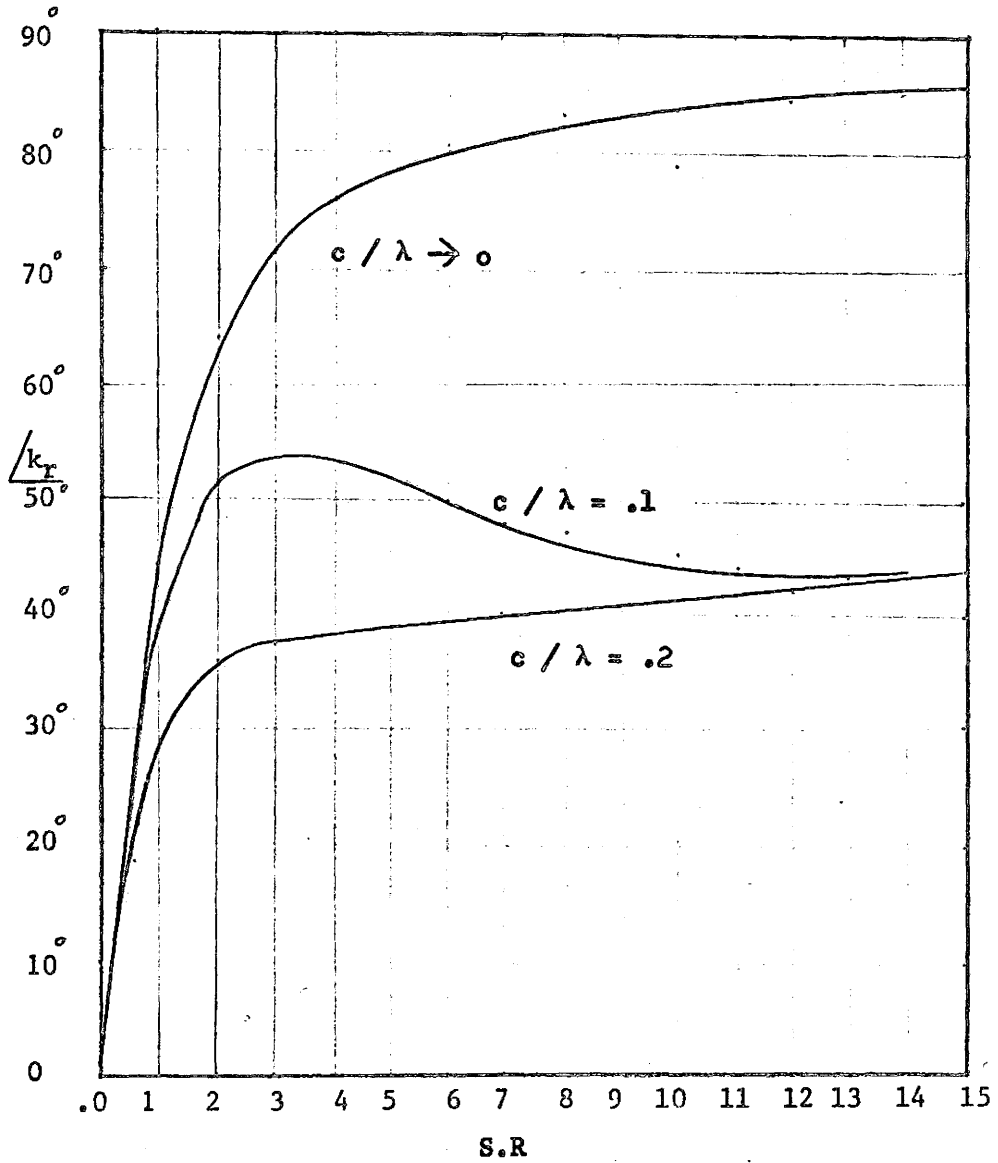
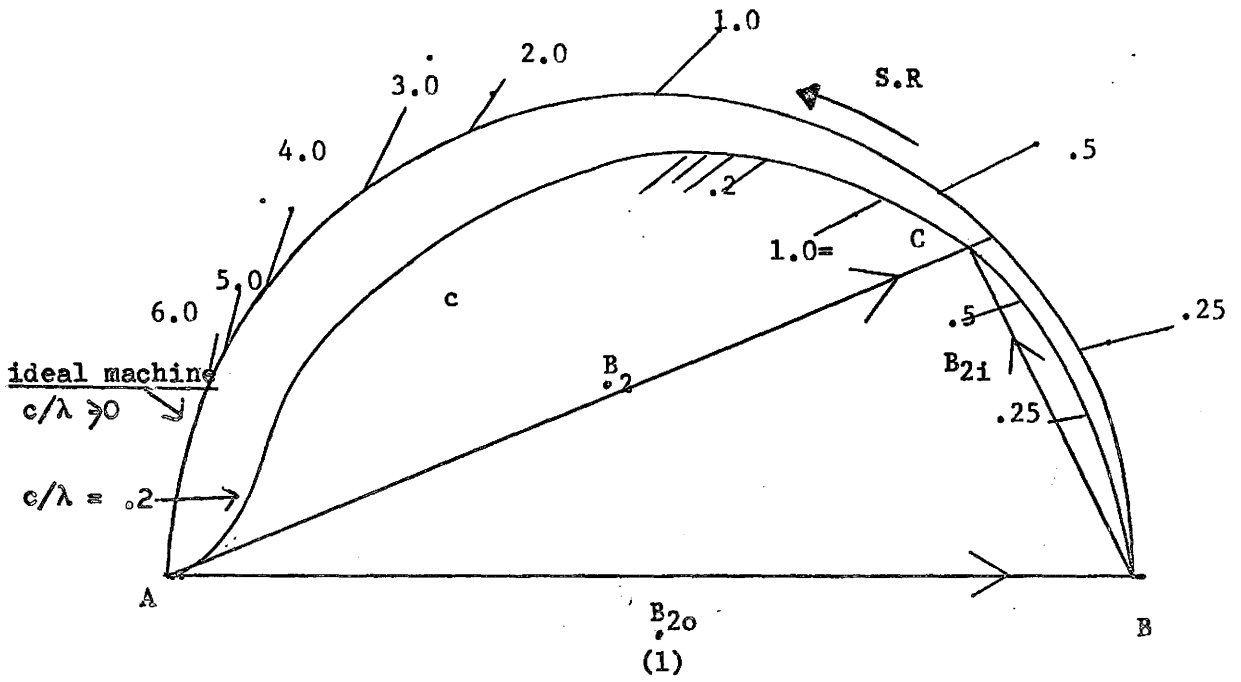
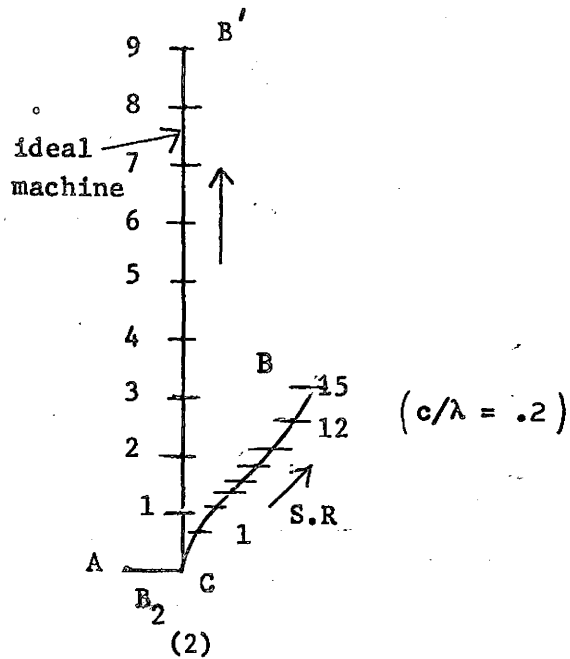


FIG. 3.9. contd. (b) argument



Locus of phasors - constant current case.



Locus of phasors - constant voltage case.

FIG. 3.10 : Phasor diagrams for machine in presence of flux penetration effect

$$\begin{vmatrix} B_2 \\ B_1 \end{vmatrix}_g = \begin{vmatrix} \text{Cosh } \beta(g-c) & j \text{ Sinh } \beta(g-c) \\ -j \text{ Sinh } \beta(g-c) & \text{Cosh } \beta(g-c) \end{vmatrix} \begin{vmatrix} B_2 \\ B_1 \end{vmatrix}_c \quad \dots 3.44$$

The subscripts  $g$  and  $c$  refer to the evaluation at the boundaries  $y=g$  and  $y=c$  respectively.

The leakage and magnetising reactances cannot be separated into two lumped parameter values. In general a T or  $\pi$  circuit is necessary to represent leakage and magnetising reactance of a large air gap. This will be investigated further in Chapter 4.

## CHAPTER IV

### GENERALISED ANALYSIS OF THE FLAT LINEAR INDUCTION MACHINE

#### USING AN ANALOGUE CIRCUIT

##### 4.1 Introduction:

To date there has been no common theory on linear travelling field induction machines. The various problems pertaining to double-sided, single-sided, composite secondary etc, etc, have been treated quite independently.

Two very striking observations emerge from a study of the literature. The first is the virtual intractability of the algebra involved in solving the field equations even in highly idealized configurations. The second is the great deal of duplication - since really the only equation used is that of magnetic transport. The problem is not confined to linear machines - due to the formidability of the mathematics, even under very simplifying assumptions, nearly all electrical machines are analysed from a circuit theory viewpoint rather than by direct solution of Maxwells' equations.

The most note-worthy attempt to use the latter approach was made by Mishkin (39). In this work the stator and rotor of a squirrel cage induction machine were replaced by anisotropic magnetic media. Though the assumptions render the model approximate, the results are exceedingly complicated and not easily physically interpretable. A transmission line analogy was suggested by Cullen and Barton (40) for the same problem. The first paper generalizing the procedure in-

volved in the calculation of travelling fields in machines represented by homogeneous isotropic laminar regions is by Greig and Freeman (37). The application of these ideas in the area of linear machines was suggested. Anisotropy was taken into account by Freeman (38).

In this chapter is given a more complete treatment of the subject of travelling fields with reference to flat linear induction machines. The transmission line analogy is investigated and equivalent circuits obtained. A clear physical appreciation follows - induced current reaction, magnetising and leakage effects are isolated. Unlike previous work, a solution for the field quantities in the region of the stator teeth is found. This means that the usual assumption of replacing the slotted stator by a linear current sheet can be waived.

#### 4.2 Model and Assumptions:

The machine is considered as consisting of a number of planar regions stacked together as shown in Fig. 4.1. These regions generally represent stator(s), air gaps, conducting secondaries and iron segments. In general at least one of these regions will have velocity. Due to slotting, slitting of secondaries, inclusion of ferromagnetic slugs etc, these regions will generally be inhomogeneous. The regions will generally be considered to be stratified in the direction of motion (  $x$  direction) as shown in Fig. 4.2. The permeability and conductivity will then be periodic functions in  $x$ . To avoid having to solve differential equations with periodically varying coefficients

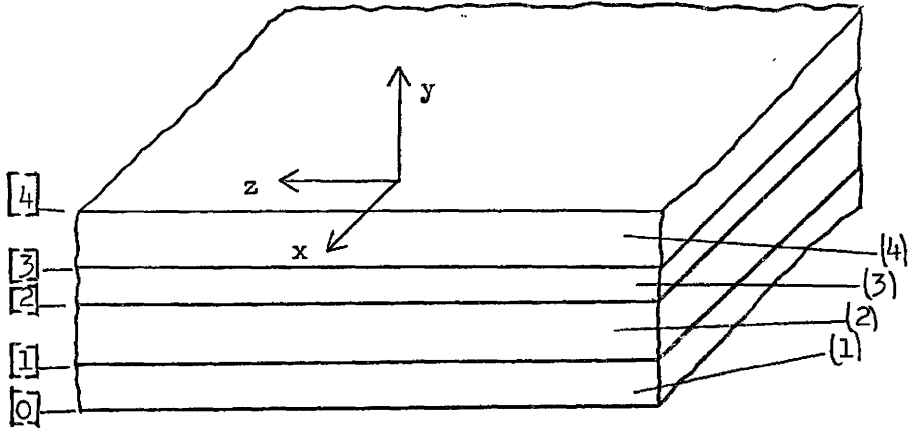


Fig 4.1: General multiregion representation of linear machine under the infinite width assumption

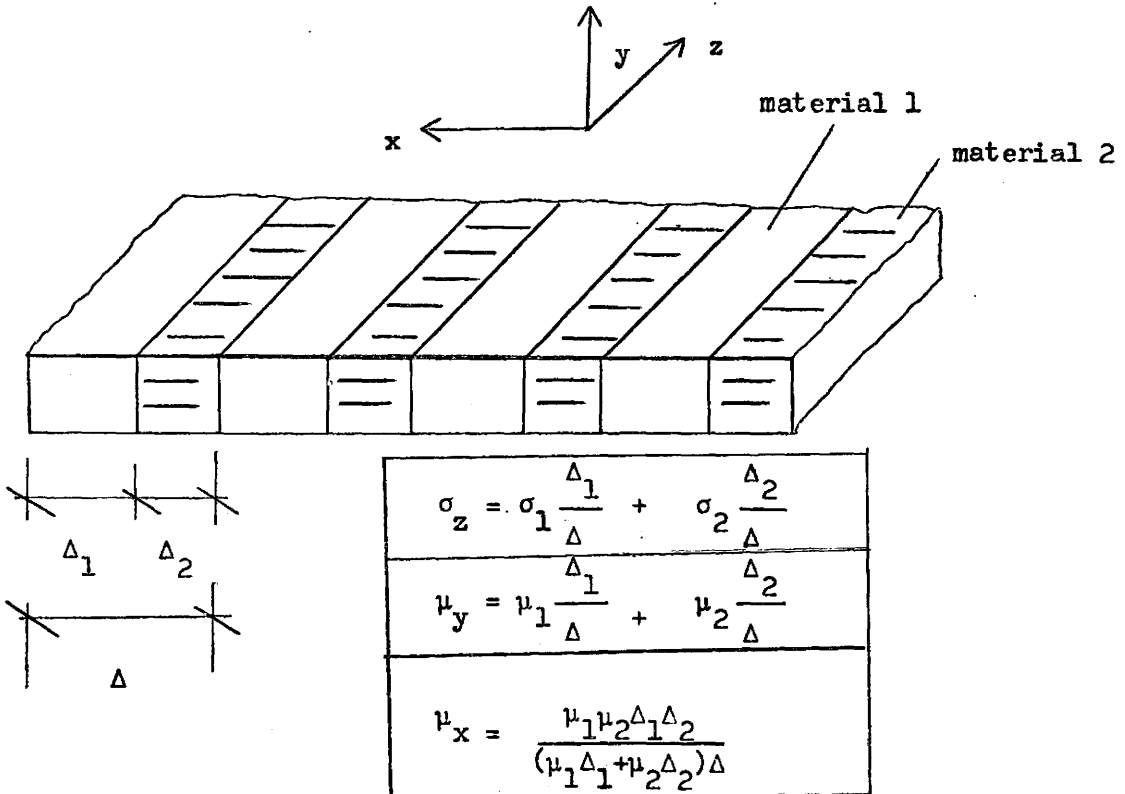


Fig 4.2 : Equivalent anisotropic medium properties.

we make the simplifying assumption employed previously in (38), (39), (40). This is that the solution for the fundamental component of the field quantities can be obtained by considering only the average values of permeability and conductivity. The stratified structure is then replaced by a homogeneous anisotropic structure.

The above representation of anisotropy becomes invalid when the wavelengths of the space harmonics are comparable with the slot pitch. The postulate of Mishkin and Ollendorf (39) regarding the homogeneous anisotropic medium shall be used. It states that the equivalence is such that the resistance and reluctance of a circuit made of the original structure and the anisotropic medium are the same. Consequently it is possible to draw up the table shown in Fig. 4.2 which gives the appropriate conductivity and permeability for different configurations.

Lateral edge effects are neglected and consequently there is no variation in the  $z$  direction and all induced currents flow in this direction. As was seen in chapter II this approximation is very often appropriate.

#### 4.3 Field Equations and Analogue Circuit:

Consider the infinitesimal section shown in Fig. 4.3. From Maxwells' equations we have:

$$\nabla \times E = - \frac{\partial B}{\partial t}$$

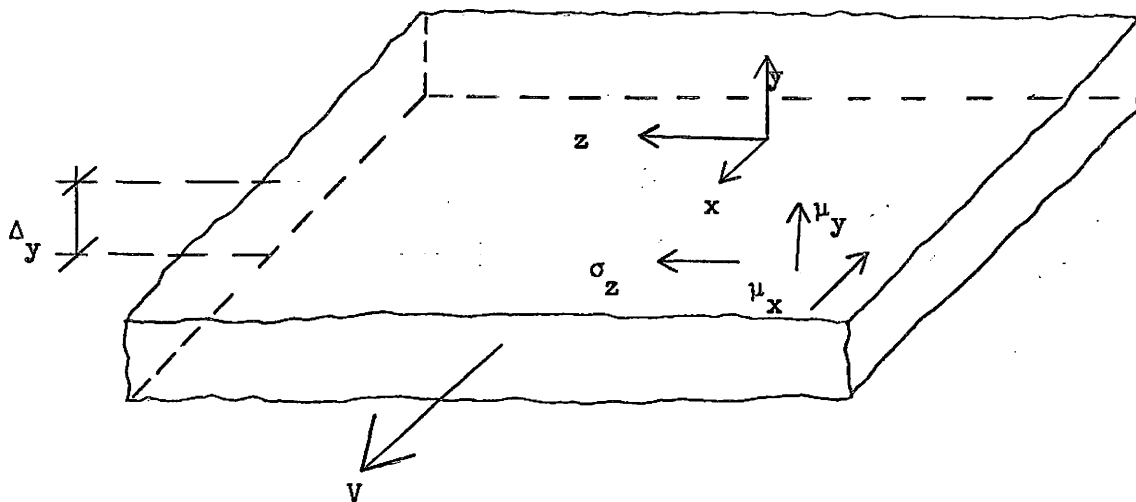


Fig 4.3 : Infinitesimal section used in formulation of equations.

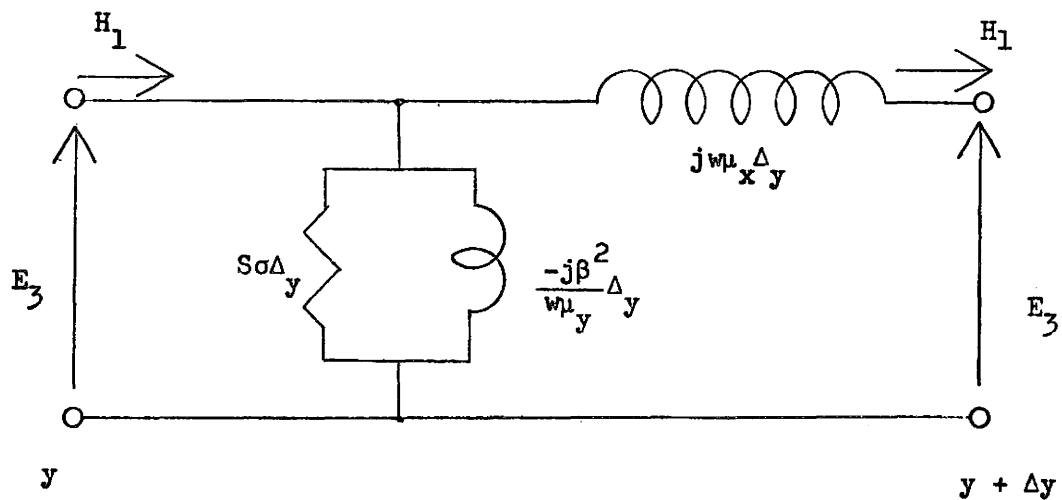


Fig 4.4 : Analogue circuit for infinitesimal section.

Since there is no variation in the  $z$  direction and  $\frac{\partial}{\partial t} = -j\omega$

we obtain:

$$\frac{\partial E_{\tilde{z}_3}}{\partial x} = -j\omega B_{\tilde{z}_2} \quad \dots 4.1$$

(the laboratory rest frame is chosen for all quantities). Using Ohm's law we obtain:

$$J_{\tilde{z}_3} = \sigma_z \{E_{\tilde{z}_3} + v B_{\tilde{z}_2}\} \quad \dots 4.2$$

Since  $\frac{\partial E_{\tilde{z}_3}}{\partial x} = -j\beta E_{\tilde{z}_3}$  we have from 4.1

$$E_{\tilde{z}_3} = -\frac{\omega}{\beta} B_{\tilde{z}_2} \quad \dots 4.3$$

Consequently:

$$J_{\tilde{z}_3} = S \sigma_z E_{\tilde{z}_3} \quad \dots 4.4$$

where  $S$  is the slip as previously defined. Applying Maxwell's equation,  $\nabla \times H = J$  we obtain:

$$\frac{\partial H_{\tilde{z}_2}}{\partial x} - \frac{\partial H_{\tilde{z}_1}}{\partial y} = J_{\tilde{z}_3} \quad \dots 4.5$$

Substituting for  $J_{\tilde{z}_3}$  from 4.4 and using the property  $\frac{\partial}{\partial x} = -j\beta$  we obtain:

$$-\frac{\partial H_1}{\partial y} = E_3 S \sigma_z + j \beta \frac{H_2}{\nu_2} \quad \dots 4.6$$

From 4.3 and the constitutive relationship  $H_2 = B_2/\mu_y$ , 4.6 becomes

$$-\frac{\partial H_1}{\partial y} = E_3 \left\{ S \sigma_z - j \frac{\beta^2}{\omega \mu_y} \right\} \quad \dots 4.7-a$$

From  $\nabla \cdot B = 0$  and substituting for  $B_1$  and  $B_2$  from 4.3 and the constitutive relationship we obtain:

$$\frac{\partial E_3}{\partial y} = -j \omega \mu_x H_1 \quad \dots 4.7-b$$

By multiplying both 4.6 and 4.7 by  $e^{-j(\omega t - \beta x)}$  we can eliminate the  $x$ ,  $t$  variation and obtain phasor relationships. Since  $E_{\nu_3 y + \Delta y} \approx E_{\nu_3 y} + \Delta y \frac{\partial E_{\nu_3}}{\partial y}$  (Taylor series) it follows that the difference in electric field intensity between  $y$  and  $y + \Delta y$  is  $j \omega \mu_x \Delta y \frac{H_1}{\nu_1}$ .

Similarly from 4.7-a,  $H_{1y} - H_{1y + \Delta y} \approx E_3 \left\{ S \sigma - j \frac{\beta^2}{\omega \mu_y} \right\}$

The above very logically leads to the analogue circuit shown in Fig. 4.4. Cullen and Barton (40) first obtained this circuit by considering a transmission line analogy.

It is instructive to consider the origin of each element. The  $S \sigma \Delta y$  represents the "referred" load of an induction motor. Magnetising the leakage reactances are respectively represented by  $-j \frac{\beta^2}{\omega \mu_y}$  and  $j \omega \mu_x \Delta y$ . An open L circuit (i.e. having the leakage reactance on the other side of the admittance) would have been equally valid. Neither

circuit is exact for a finite thickness (y direction) region. To represent a finite thickness region 4.7-a and b must be combined to give a differential equation. It immediately follows that S per unit input energy represents joule heating, leaving 1-S per unit as the mechanical output and efficiency. Also the force, in the x direction, is the input power divided by the synchronous velocity. This is the basic induction process. Since there is no power loss across the leakage branch the above remarks apply to any number of such circuits in tandem and consequently to any thickness region.

The phasor form of Equations 4.6 and 4.7 can be combined to give the differential equations:

$$\frac{\partial^2 E_3}{\partial y^2} = \gamma_2^2 E_3 \quad \dots 4.8-a$$

$$\frac{\partial^2 H_1}{\partial y^2} = \gamma_2^2 H_1 \quad \dots 4.8-b$$

where:

$$\gamma_2^2 = \beta_2^2 (1 + jSR_2) \quad \dots 4.9-a$$

$$\beta_2^2 = \frac{\mu_x}{\mu_y} \beta^2 \quad \dots 4.9-b$$

$$R_2 = \frac{\mu_y \sigma_z \omega}{\beta^2} \quad \dots 4.9-c$$

$\gamma_2$  is the propagation constant in the y direction.  $\gamma_2$  in general has real and imaginary components - signifying attenuation of magnitude and phase retardation. In general:

$$\gamma_2 = \gamma_{2r} + j \gamma_{2i} \quad \dots 4.10-a$$

where

$$\gamma_{2r,i} = \beta_2 \sqrt{\frac{\sqrt{1 + SR^2} \pm 1}{2}} \quad \dots 4.10-b$$

Consider the solution to equations 4.8 in semi-infinite space.

The solution to 4.8-a is

$$E_{\tilde{z}} = A_{\tilde{z}} e^{-\gamma_2 y} \quad \dots 4.11-a$$

where  $A_{\tilde{z}}$  is an arbitrary constant.

It is interesting to compare the above solution with that obtained in Section 3.2. In that case a homogeneous medium was assumed. The solutions have the same general form except the rate at which the field decays in the  $y$  direction is different. Generally  $\mu_x \gg \mu_y$  in the case of the stratified structure so  $\beta_2 \ll \beta$ . This results in a less severe attenuation of the field in the  $y$  direction.

By applying 4.7 we obtain:

$$H_{\tilde{x}} = -j \frac{\gamma_2}{\omega \mu_x} A_{\tilde{z}} e^{-\gamma_2 y} \quad \dots 4.11-b$$

The ratio of  $E_{\tilde{z}}$  to  $H_{\tilde{x}}$  is defined as the characteristic wave impedance in accordance with the transmission line analogy:

$$\frac{E_{\tilde{z}}}{H_{\tilde{x}}} = Z_0 \quad \dots 4.12$$

where

$$Z_0 = j \frac{\omega \mu_x}{\gamma_2} \quad \dots 4.13-a$$

correspondingly

$$Y_0 = -j \frac{Y_2}{\omega \mu_x}, \quad \dots 4.13-b$$

where  $Y_0$  is the characteristic admittance.

#### 4.4 General Solution:

Consider the general region M. The solution for 4.8 under the constraint set by 4.7 is

$$E_{.3} = C_{.M} \text{Cosh } \gamma_{.2M} y_M + D_{.M} \text{Sinh } \gamma_{.2M} y_M \quad \dots 4.14-a$$

$$H_{.1} = -Y_{.0M} \{ C_{.M} \text{Sinh } \gamma_{.2M} y_M + D_{.M} \text{Cosh } \gamma_{.2M} y_M \} \quad \dots 4.14-b$$

where  $C_{.M}$  and  $D_{.M}$  are arbitrary constants.

Upon substituting the boundary conditions we obtain the solution in the following matrix notation:

$$\begin{bmatrix} E_{.3} \\ H_{.1} \end{bmatrix}_y = \begin{bmatrix} \text{Cosh } \gamma_{.2M} y_M & -Z_{.0M} \text{Sinh } \gamma_{.2M} y_M \\ -Y_{.0M} \text{Sinh } \gamma_{.2M} y_M & \text{Cosh } \gamma_{.2M} y_M \end{bmatrix} \begin{bmatrix} E_{.3} \\ H_{.1} \end{bmatrix}_{[M-1]} \quad \dots 4.15$$

(The square bracketed subscript denotes evaluation at the boundary)

The overall effect of the region M can now be expressed in terms of a transfer matrix (after Freeman and Greig 37)

$$\begin{bmatrix} E_3 \\ H_1 \end{bmatrix}_{[M]} = \begin{bmatrix} T_M \\ \cdot \\ \cdot \\ \cdot \end{bmatrix}_{[M-1]} \begin{bmatrix} E_3 \\ H_1 \end{bmatrix}_{[M-1]} \quad \dots 4.16-a$$

where

$$[T_M] = \begin{bmatrix} \text{Cosh } \gamma_{2M} \Delta_M & - Z_{0M} \text{ Sinh } \gamma_{2M} \Delta_M \\ - Y_{0M} \text{ Sinh } \gamma_{2M} \Delta_M & \text{Cosh } \gamma_{2M} \Delta_M \end{bmatrix} \quad \dots 4.16-b$$

where  $\Delta_M$  is the thickness of region M.

Note as defined here the matrix relates quantities at boundary [M] to those at [M-1]. Energy flow is from boundary M-1 to boundary M.

The T and  $\pi$  equivalent circuits for the general region M are shown in Fig. 4.5.

The boundary conditions to be satisfied at the interface between any two such regions are the continuity of the tangential components of magnetic and electric field intensities. Note that the latter also satisfies the continuity of normal component of flux density.

It follows from the above that any number of such regions can be accounted for by matrix multiplication. In terms of the equivalent circuit this implies tandem connection.

All least one of the extreme boundaries will have to contain source of excitation. The relation between the electric field intensity and the voltage as well as between the tangential magnetic

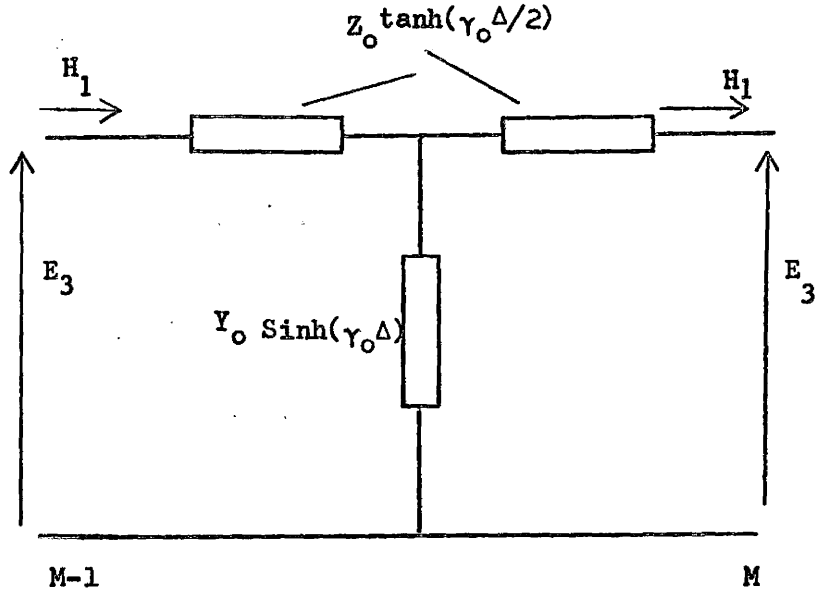
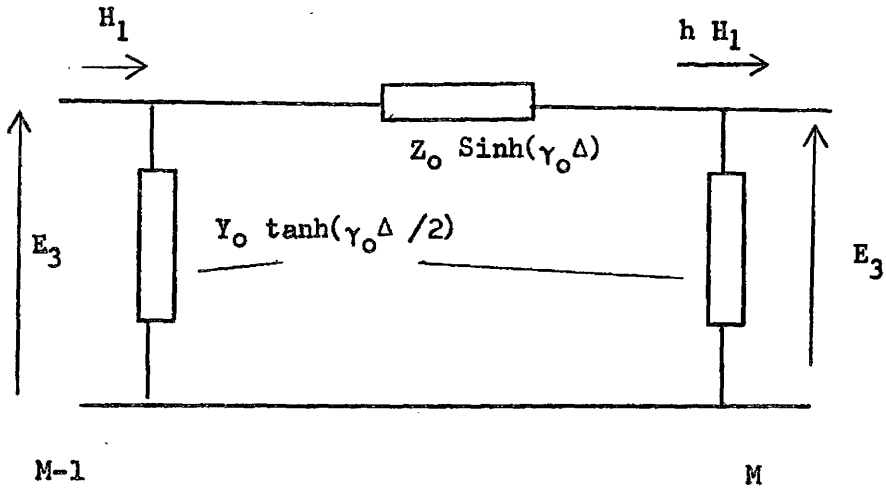


FIG 4.5:  $\pi$  and T analogue circuits.

field intensity and the stator currents is considered later. It is instructive to consider the circuit analogues of some configurations. An ideal ferromagnetic part, i.e. the backing iron in an electrically single-sided machine is represented by an open circuit. This results since it cannot accommodate any H field. A superconducting region would demand zero electric field intensity so a short circuit results. A semi-infinite half space, i.e. the air gap in a one sided machine has the characteristic wave impedance as its circuit element.

#### 4.5 Traction and Levitation Forces

The x direction force may be obtained by direct integration of the  $J \times B$  contributions in this direction over the volume. Because of the assumption of constant permeability in the x direction there is no x direction magnetic force.

The force in the y direction is more complicated. In this case the contributions of the interaction between both induced current and magnetic dipoles in the magnetic field has to be considered. Application of the principle of Maxwells' magnetic stresses is the most useful approach in this case (41), (44). The stress tensor is given in Section 1.4.

Consider the system depicted in Fig. 4.6-a. The total force on the control volume shown can be expressed as the surface integral of the stresses. Of the six sides of the control volume there is only a net contribution from the surfaces in the xz planes. This apparently results from the constancy of the time averaged field

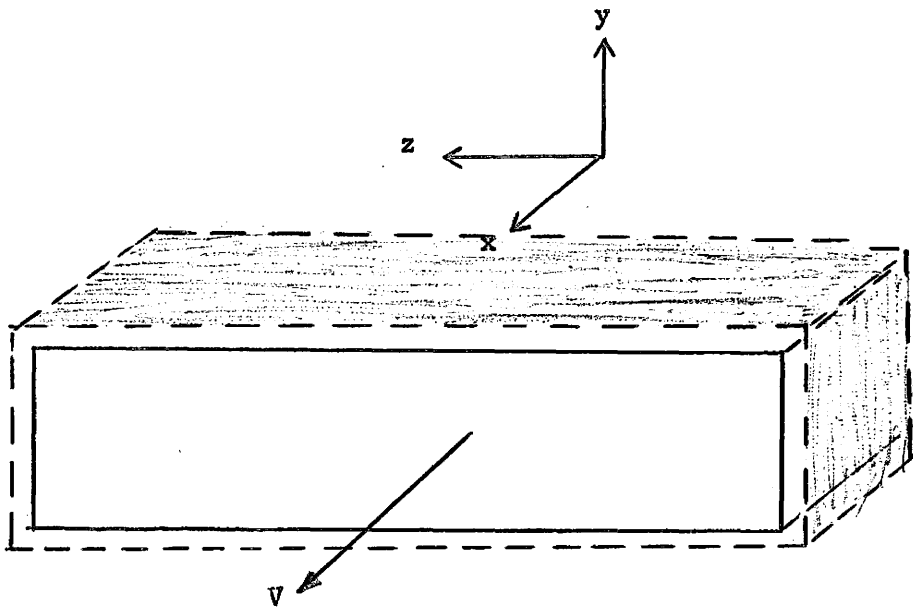


FIG 4.6-a : Control volume for force calculation.

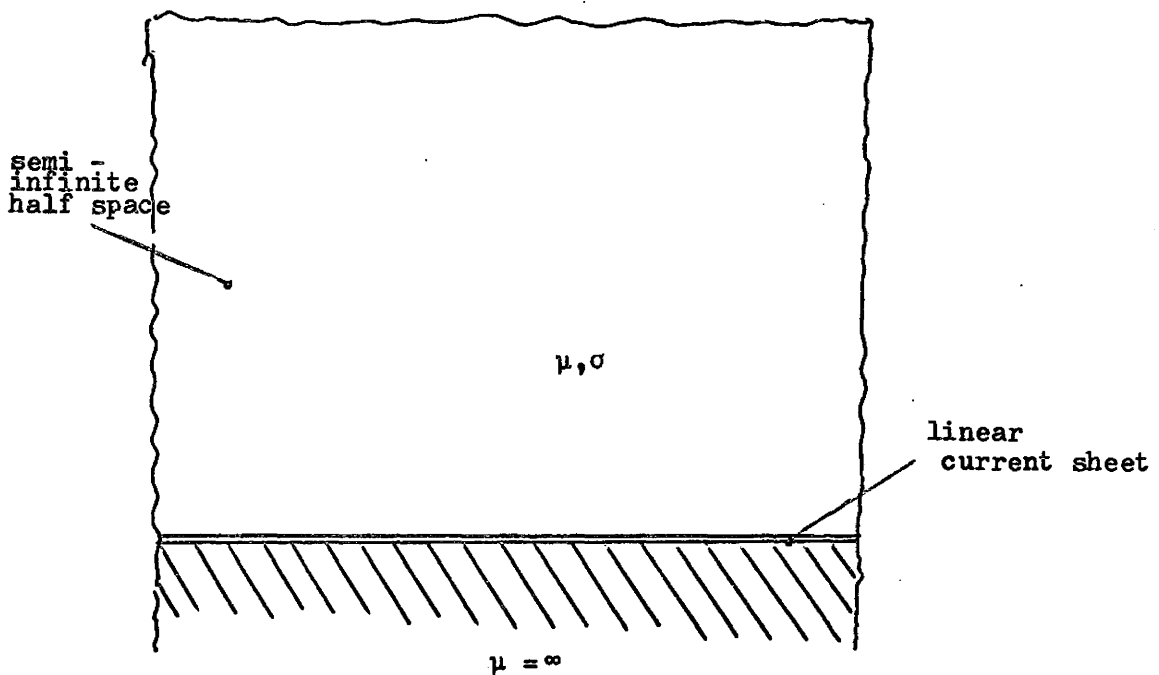


FIG. 4.6-b : Model used in investigating sense of normal force ( attraction or repulsion )

quantities in the x and z directions. The time averaged surface force densities are

$$f_{sx} = -\frac{\mu}{2} \operatorname{Re} \{H_2 H_1^*\} \quad \dots 4.17-a$$

$$f_{sy} = -\frac{\mu}{4} \{ |H_2|^2 - |H_1|^2 \} \quad \dots 4.17-b$$

As indicated in Fig. 4.6-a the field values are evaluated immediately outside the region.

The expression for the x direction force should be consistent with that given in 4.3 since it is due entirely to conduction current.

Using 4.3 and the constitutive equation  $\beta = \mu H$  we find that 4.17-a becomes

$$f_{sx} = \frac{\beta}{\omega} \operatorname{Re} \{E_z H_1^*\}$$

which is the surface force density as found in section 4.3.

The y or normal force is more complicated in its interpretation. Very little general conclusion can be drawn since the calculation demands evaluation of two field quantities at two surfaces.

A feeling for the mechanism involved can be gained by consideration of a semi-infinite half space of ferromagnetic conductor. Due to one surface being at infinity the field decays exponentially in that direction and consequently there is no force contribution at the surface. Furthermore the field intensities at the surface are related by the characteristic impedance. The configuration is as shown in Fig. 4.6-b. From 4.17-b we have:

$$f_{sy} = -\frac{1}{4} \frac{\mu_0}{4} \{ |H_{\sim 2}|^2 - |H_{\sim 1}|^2 \}$$

Applying the constitutive equation  $\beta = \mu H$  and 4.3 we obtain

$$f_{sy} = -\frac{1}{4} \frac{\beta^2}{\omega^2} \frac{1}{\mu_0} |E_{\sim 3}|^2 \left[ 1 - \frac{|H_{\sim 1}|^2}{\frac{\beta^2}{\omega^2} \frac{1}{\mu_0} |E_{\sim 3}|^2} \right] \quad \dots 4.18$$

Recognising  $H_{\sim 1}/E_{\sim 3}$  as the characteristic wave admittance and substituting from 4.13-b we obtain

$$\begin{aligned} f_{sy} &= -\frac{1}{4} \frac{\beta^2}{\omega^2} \frac{1}{\mu_0} |E_{\sim 3}|^2 \left\{ 1 - \frac{|Y|^2}{\beta^2 \frac{\mu^2}{\mu_0}} \right\} \\ &= -\frac{1}{4} \frac{\beta^2}{\omega^2} \frac{\mu_0}{\mu^2} |E_{\sim 3}|^2 \left\{ \frac{\mu^2}{\mu_0} - \frac{|Y|^2}{\beta^2} \right\} \\ &= -\frac{1}{4} \frac{\beta^2}{\omega^2} \frac{\mu_0}{\mu^2} |E_{\sim 3}|^2 \left\{ \mu_R^2 - \sqrt{1 + S^2 R^2} \right\} \quad \dots 4.19 \end{aligned}$$

The above expression is similar to that derived in (38).

The net force is negative for values of  $\mu_R > \sqrt{1 + S^2 R^2}$ . This would be the usual case. If  $\mu_R$  is small then it is possible to have cancellation of normal force at a particular slip. The force would change from levitation to attraction as the speed increased through the critical slip. If the secondary is non-magnetic then the force is given by

$$f_{sy} = -\frac{1}{4} \frac{\beta^2}{\omega^2 \mu_0} |E_{\sim 3}|^2 \left\{ 1 - \sqrt{1 + S^2 R^2} \right\} \quad \dots 4.20$$

This is in agreement with the result in Section 3.3.

#### 4.6 Representation of Slotted Stator

The object of this section is to relate the fundamental component of the tangential electric and magnetic field intensities to the stator voltage and current.

The model is as shown in Fig. 4.7-a. The stator yoke is considered to be infinitely permeable but the reluctance of the stator tooth and crown regions is considered. The appropriate values of permeability are calculated from the results of Fig. 4.2

Consider the stator tooth region which is represented by the equivalent anisotropic medium shown in Fig. 4.7-b.

From Maxwells' equations we have:

$$\nabla \times H = J.$$

In this case the current density is due to the impressed primary current.

From the above we obtain

$$\frac{\partial H_2}{\partial x} - \frac{\partial H_1}{\partial y} = - \frac{J}{\lambda_a} \quad \dots 4.21$$

where  $\frac{J}{\lambda_a}$  is the fundamental component of the primary current density (see Appendix 2).

From Maxwell's equation  $\nabla \times E = - \frac{\partial B}{\partial t}$  we obtain:

$$- j\omega \mu \frac{H_1}{\lambda_1} = \frac{\partial E_3}{\partial y} \quad \dots 4.22-a$$

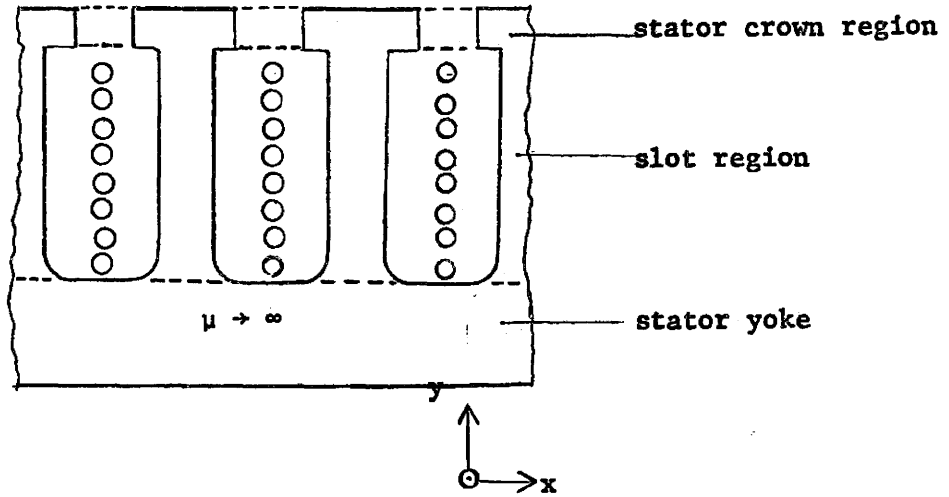


FIG. 4.7-a : Representation of stator region

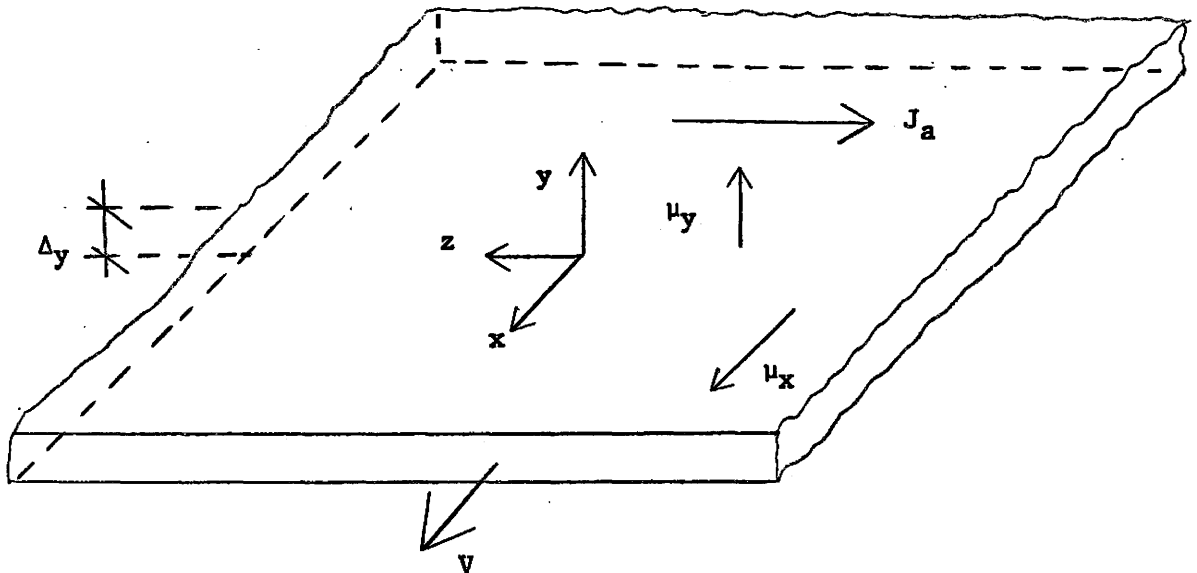


FIG. 4.7-b : Thin slice of tooth region

$$-j\omega\mu_y H_2 = -\frac{\partial E_3}{\partial x} \quad \dots 4.22-b$$

Combining the above with 4.21 we obtain the following differential equation:

$$-\frac{j}{\omega\mu_y} \frac{\partial^2 E_3}{\partial x^2} - \frac{j}{\omega\mu_x} \frac{\partial^2 E_3}{\partial y^2} = -\frac{J}{a} \quad \dots 4.23$$

Substituting  $-\beta^2 E_3$  for  $\frac{\partial^2}{\partial x^2}$ , and multiplying by  $e^{-j(\omega t - \beta x)}$  we obtain:

$$\frac{\partial^2 E_3}{\partial y^2} = \beta_2^2 E_3 - j\omega\mu_x \frac{J}{a} \quad \dots 4.24$$

where  $\beta_2^2 = \frac{\mu_x}{\mu_y} \beta^2$  (as defined in 4.9-b).

The general solution to above is:

$$E_3 = C \cosh \beta_2 y + D \sinh \beta_2 y + \frac{j\omega\mu_x}{\beta_2^2} \frac{J}{a} \quad \dots 4.25$$

Using relationship 4.22-a we obtain:

$$H_1 = j \frac{\beta_2}{\omega\mu_x} \{C \sinh \beta_2 y + D \cosh \beta_2 y\} \quad \dots 4.26$$

Due to the infinite permeability of the stator yoke  $H_1$  must be zero at  $y = 0$ . Consequently  $D = 0$ .

The important quantity for the evaluation of stator voltage is the average value of  $E_3$  over the slot depth.

Consequently we have:

$$E_{3avg} = C \frac{\text{Sinh } \beta_2 d_s}{\beta_2 d_s} + j \frac{\omega \mu_x}{\beta_2^2} J \cdot a$$

which gives:

$$C = \frac{\beta_2 d_s}{\text{Sinh } \beta_2 d_s} (E_{3avg} - j \frac{\omega \mu_x}{\beta_2^2} J \cdot a)$$

Substituting the above value of C in 4.25 and 4.26 we obtain:

$$E_3 = \beta_2 d_s \frac{\text{Cosh } \beta_2 y}{\text{Sinh } \beta_2 d_s} E_{3avg} - j \frac{\omega \mu_x}{\beta_2^2} \left( \frac{\beta_2 d_s}{\text{Sinh } \beta_2 d_s} \text{Cosh } \beta_2 y - 1 \right) J \cdot a \quad \dots 4.27-a$$

$$H_1 = j \frac{\beta_2^2 d_s}{\omega \mu_y} \frac{\text{Sinh } \beta_2 y}{\text{Sinh } \beta_2 d_s} E_{3avg} + d_s \frac{\text{Sinh } \beta_2 y}{\text{Sinh } \beta_2 d_s} J \cdot a \quad \dots 4.27-b$$

If we make the assumption that the slot depth is such that  $\beta_2 d_s \ll 1$  we get the following relationship upon using Taylor series approximations for the hyperbolic functions.

$$\begin{bmatrix} E_3 \\ H_1 \end{bmatrix}_{y=d_s} = \begin{bmatrix} 1 & -j \frac{\omega \mu_x d_s^2}{3} \\ j \frac{\beta_2^2 d_s}{\omega \mu_y} & d_s \end{bmatrix} \begin{bmatrix} E_{3avg} \\ J \cdot a \end{bmatrix}$$

The crown tip region can be represented by the circuit in Fig. 4.4

with  $\sigma = 0$ .

$$\begin{bmatrix} E_3 \\ H_1 \end{bmatrix}_{y=d_c} = \begin{bmatrix} 1 & -j\omega\mu_x^1 d_c \\ +\frac{j\beta^2 d_c}{\omega\mu_y} & 1 \end{bmatrix} \begin{bmatrix} E_3 \\ H_1 \end{bmatrix}_{y=d_s}$$

Furthermore the circuit can be simplified to a single series reactance since the y branch is generally so large that it is virtually an open circuit.

#### 4.7 Discussion:

The development in the previous sections allows the flat linear machine (under the infinite width approximation) to be represented as a tandem connection of analogue circuits. At least one of the extreme boundaries will be a primary. The transformation from primary voltage and current to the field quantities has been shown. Consequently the overall circuit represents an equivalent circuit. The traction and levitation forces and power quantities were derived in terms of circuit quantities.

## CHAPTER V

### SIMULTANEOUS TREATMENT OF FLUX PENETRATION AND LATERAL EDGE EFFECT USING A WAVE IMPEDANCE APPROACH

#### 5.1 Introduction:

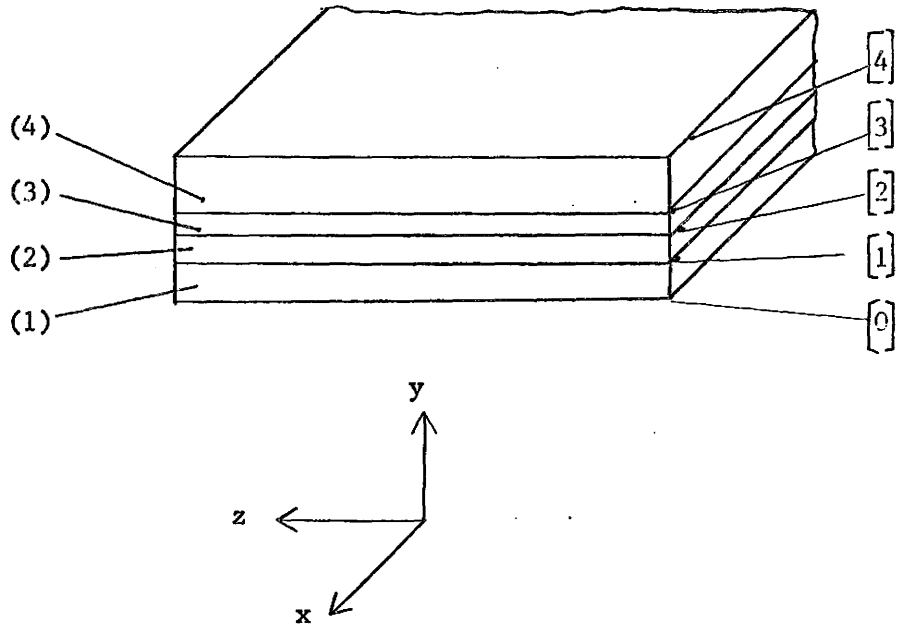
Due to their homogeneity and isotropy, sheet secondary induction motors are more directly amenable to solution than composite secondary devices. However, the analysis has been for the most part, limited to the cases where flux penetration and lateral edge effect are separately neglected. There has been limited work on simultaneous consideration of these effects (22), (27), (45).

Due to the formidability of the expressions found, very little general conclusion is drawn.

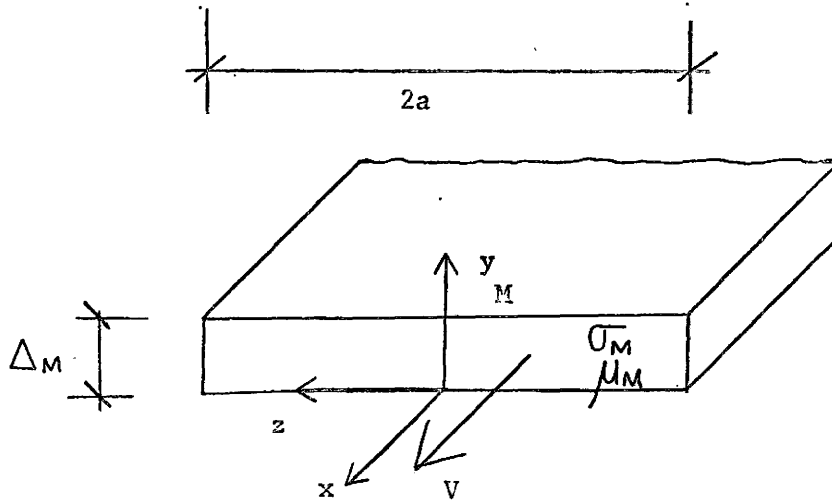
In this chapter the concept of wave impedance is applied to give a general solution for this problem.

#### 5.2 Assumptions:

As in Chapter 4, the machine is considered as consisting of a number of planar regions stacked together. Each region is homogeneous and isotropic. All regions have the same width as the primary (stator). Fringing beyond this width {fig. 5.1-a} is neglected. The primary excitation scheme can be replaced by a linear current sheet backing a smooth iron surface of infinite permeability. The appropriate gap depth is given by Carter's coefficient.



(a) General stack of planar regions.



(b) Co-ordinate system for region (M)

Fig 5.1 : Multiregion representation of finite width machine.

### 5.3 General Development:

Consider the general region M shown in Fig. 5.1-b. The field quantities are described by the magnetic transport equation (ref. Ch. 3):

$$\nabla^2 \bar{B} = \mu_M \sigma_M \left\{ \frac{\partial \bar{B}}{\partial t} - \bar{\nabla} \times \bar{\nabla} \times \bar{B} \right\} \quad \dots 5.1$$

Writing all field quantities in vector phasor form (Appendix 2) and using the property  $\frac{\partial^2 \bar{B}}{\partial x^2} = -\beta^2 \bar{B}$  we obtain:

$$\left\{ \frac{\partial^2}{\partial y^2} + \frac{\partial^2}{\partial z^2} \right\} \bar{B} = \left\{ \beta^2 + j\omega \mu_M \sigma_M \right\} \bar{B} - \bar{\nabla} \times \bar{\nabla}_M \times \bar{B} \quad \dots 5.2$$

Since  $\bar{\nabla}_M = \nabla_M \bar{1}_x$  and  $\bar{\nabla} \cdot \bar{B} = 0$  we obtain, upon multiplying by  $e^{-j(\omega t - \beta x)}$ :

$$\left\{ \frac{\partial^2}{\partial y^2} + \frac{\partial^2}{\partial z^2} \right\} B_1 = \gamma^2 B_1$$

$$\left\{ \frac{\partial^2}{\partial y^2} + \frac{\partial^2}{\partial z^2} \right\} B_2 = \gamma^2 B_2 \quad \dots 5.3$$

$$\left\{ \frac{\partial^2}{\partial y^2} + \frac{\partial^2}{\partial z^2} \right\} B_3 = \gamma^2 B_3$$

where  $\gamma^2 = \beta^2 (1 + j S.R)$

R is the magnetic Reynolds number for region M, and is defined:

$$R = \frac{\omega \mu_M \sigma_M}{\beta^2}$$

$B_1$  is an even function of  $z$  since the linear current sheet is assumed sym-

metrically disposed about  $z = 0$ . The condition  $\nabla \cdot \bar{B} = 0$  then requires the components  $B_2$  and  $B_3$  to be even and odd functions of  $z$ . Consequently, using the method of separation of variables we obtain the general solution:

$$\begin{aligned}
 B_1 &= \sum_{n=1}^{\infty} \{C_{1n} \sinh \gamma_n y + D_{1n} \cosh \gamma_n y\} \cos \alpha_n z \\
 B_2 &= \sum_{n=1}^{\infty} \{C_{2n} \cosh \gamma_n y + D_{2n} \sinh \gamma_n y\} \cos \alpha_n z \quad \dots 5.4 \\
 B_3 &= \sum_{n=1}^{\infty} \{C_{3n} \sinh \gamma_n y + D_{3n} \cosh \gamma_n y\} \sin \alpha_n z
 \end{aligned}$$

where  $\alpha_n = \frac{2n-1}{2a} \pi$  and  $\gamma_n^2 = \alpha_n^2 + \gamma_0^2$

Since  $J_2 = 0$  we have from Maxwell's curl relationship:

$$\frac{\partial B_1}{\partial z} - \frac{\partial B_3}{\partial x} = 0 \quad \dots 5.5$$

Using the property  $\frac{\partial}{\partial x} = -j\beta$ , and multiplying by  $e^{-j(\omega t - \beta x)}$  we obtain:

$$\frac{\partial B_1}{\partial z} + j\beta B_3 = 0$$

Applying this to 5.4 we obtain:

$$\begin{aligned}
 -\alpha_n C_{1n} + j\beta C_{3n} &= 0 \\
 -\alpha_n D_{1n} + j\beta D_{3n} &= 0 \quad \dots 5.6
 \end{aligned}$$

The divergence theorem demands:

$$\frac{\partial B_{.1}}{\partial x} + \frac{\partial B_{.2}}{\partial y} + \frac{\partial B_{.3}}{\partial z} = 0 \quad \dots 5.7$$

Again using the property  $\frac{\partial}{\partial x} = -j\beta$  and multiplying by  $e^{-j(\omega t - \beta x)}$  we obtain:

$$-j\beta B_{.1} + \frac{\partial B_{.2}}{\partial y} + \frac{\partial B_{.3}}{\partial z} = 0$$

which gives the following equations:

$$\begin{aligned} -j\beta C_{.1n} + \gamma_n C_{.2n} + \alpha_n C_{.3n} &= 0 \\ -j\beta D_{.1n} + \gamma_n D_{.2n} + \alpha_n D_{.3n} &= 0 \end{aligned} \quad \dots 5.8$$

It follows from above that all field quantities can be found if one of the C and D series of complex coefficients are known.  $J_1, J_3, E_1$  and  $E_3$  can now be obtained from Maxwells' equations. Writing all quantities in terms of  $C_{.1n}$  and  $D_{.1n}$  we obtain:

$$\begin{aligned} B_1 &= \sum_{n=1}^{\infty} \{C_{.1n} \sinh \gamma_n y + D_{.1n} \cosh \gamma_n y\} \cos \alpha_n z \\ B_2 &= \sum_{n=1}^{\infty} j \frac{\alpha_n^2 + \beta^2}{\beta \gamma_n} \{C_{.1n} \cosh \gamma_n y + D_{.1n} \sinh \gamma_n y\} \cos \alpha_n z \\ B_3 &= \sum_{n=1}^{\infty} -j \frac{\alpha_n}{\beta} \{C_{.1n} \sinh \gamma_n y + D_{.1n} \cosh \gamma_n y\} \sin \alpha_n z \\ J_1 &= \sum_{n=1}^{\infty} -\frac{\alpha_n \beta S R}{\mu \gamma_n} \{C_{.1n} \cosh \gamma_n y + D_{.1n} \sinh \gamma_n y\} \sin \alpha_n z \\ J_3 &= \sum_{n=1}^{\infty} j \frac{\beta^2 S R}{\mu \gamma_n} \{C_{.1n} \cosh \gamma_n y + D_{.1n} \sinh \gamma_n y\} \cos \alpha_n z \end{aligned} \quad \dots 5.9$$

cont...

eqn. 5.9 continued

$$E_1 = \sum_{n=1}^{\infty} + \frac{\omega \alpha_n}{\beta \gamma_n} \{C_{.1n} \text{Cosh } \gamma_n y + D_{.1n} \text{Sinh } \gamma_n y\} \text{Sin } \alpha_n z$$

$$E_3 = \sum_{n=1}^{\infty} - j \frac{\omega}{\gamma_n} \{C_{.1n} \text{Cosh } \gamma_n y + D_{.1n} \text{Sinh } \gamma_n y\} \text{Cos } \alpha_n z$$

#### 5.4 Penetration Effect in The Infinite Depth Case

The usual definition for skin depth is made for the case of semi-infinite plane geometry where the medium is postulated to extend indefinitely in two directions. In chapter 3 the skin depth was determined for a travelling wave. Even at zero frequency or zero conductivity there is a finite skin depth of  $1/\beta$ .

Let us now consider the case where the thickness of the region M tends towards infinity. We wish now to investigate the penetration of a finite width travelling field.

Under this circumstance 5.4 becomes:

$$B_1 = \sum_{n=1}^{\infty} D_{.1n} e^{-\gamma_n y} \text{Cos } \alpha_n y$$

$$B_2 = \sum_{n=1}^{\infty} D_{.2n} e^{-\gamma_n y} \text{Cos } \alpha_n y \quad \dots 5.10$$

$$B_3 = \sum_{n=1}^{\infty} D_{.3n} e^{-\gamma_n y} \text{Sin } \alpha_n y$$

5.5 and 5.7 still apply so consequently we obtain:

$$- \alpha_n D_{.1n} + j \beta D_{.3n} = 0$$

and

$$-j\beta D_{.1n} - \gamma_n D_{.2n} + \alpha_n D_{.3n} = 0$$

All quantities can consequently be expressed in terms of the  $H_{1n}$  series which is the cosine series representing the x component of magnetic field intensity at the surface.

$$\begin{aligned} B_1 &= \sum_{n=1}^{\infty} \{ \mu H_{1n} e^{-\gamma_n y} \} \cos \alpha_n z \\ B_2 &= \sum_{n=1}^{\infty} -j \frac{\alpha_n^2 + \beta^2}{\beta \gamma_n} \{ \mu H_{1n} e^{-\gamma_n y} \} \cos \alpha_n z \\ B_3 &= \sum_{n=1}^{\infty} -j \frac{\alpha_n}{\beta} \{ \mu H_{1n} e^{-\gamma_n y} \} \sin \alpha_n z \\ J_1 &= \sum_{n=1}^{\infty} - \frac{\alpha_n \beta S R}{\mu \gamma_n} \{ \mu H_{1n} e^{-\gamma_n y} \} \cos \alpha_n z \quad \dots 5.11 \\ J_3 &= \sum_{n=1}^{\infty} j \frac{\beta^2 S R}{\mu \gamma_n} \{ \mu H_{1n} e^{-\gamma_n y} \} \sin \alpha_n z \\ E_1 &= \sum_{n=1}^{\infty} + \frac{\omega}{\beta} \frac{\alpha_n}{\gamma_n} \{ \mu H_{1n} e^{-\gamma_n y} \} \cos \alpha_n z \\ E_3 &= \sum_{n=1}^{\infty} -j \frac{\omega}{\gamma_n} \{ \mu H_{1n} e^{-\gamma_n y} \} \sin \alpha_n z \end{aligned}$$

Proceeding in an analogous manner as in section 4 of chapter 4 we define the nth harmonic wave characteristic impedance and admittance:

$$\frac{E_{.3n}}{H_{.1n}} = Z_{.0n} = j \frac{\omega \mu}{\gamma_n}$$

...5.12

$$Y_{.0n} = 1/Z_{.0n}$$

Upon examination of the above it is seen that the harmonic components composing a particular surface distribution of each field quantity are independently attenuated in the  $y$  direction. By analogy with the standing wave case we define the skin depth as that depth representing an attenuation to 36.8% [ $e^{-1} \times 100\%$ ] of the surface value. Consequently, the skin depth for the  $n$ th harmonic is:

$$\delta_{sn} = \frac{1}{\gamma_{nr}} \quad \dots 5.13$$

where  $\gamma_{nr}$  is the real component of  $\gamma_n$  and is defined:

$$\gamma_{nr} = \frac{2}{\sqrt{\alpha_n^2 + \beta^2 + \sqrt{(\alpha_n^2 + \beta^2)^2 + \beta^2(SR)^2}}}$$

In the case of  $a \rightarrow \infty$ ,  $\alpha_n \rightarrow 0$  for all  $n$ . In this case the skin depth reduces to the expression found in Section 3.2

$$\delta: - \frac{1}{\beta} \sqrt{\frac{2}{1 + \sqrt{1 + (SR)^2}}}$$

As the harmonic number increases the interaction of the induced currents and the wavelength become of diminishing importance. In this case we have

$$\lim_{n \rightarrow \infty} \frac{\partial}{\partial s_n} \rightarrow \frac{1}{\alpha_n}$$

Variation of skin depth with Reynolds number, wavelength and secondary width are shown in Fig. 5.2-a,-b,-c respectively. These graphs are for liquid metal pump which explains the large skin depth.

### 5.5 Transfer matrix and General Solution:

The most convenient boundary conditions are the continuity of  $H_1$  and  $E_3$  at the interfaces. The above two conditions satisfy the continuity of all tangential field intensity quantities as well as satisfying the continuity of the normal component of flux density.

Consider the conditions at boundary [0] of region M. Upon substituting  $y = 0$  we obtain:

$$\sum_{n=1}^{\infty} H_{1n} \cos \alpha_n z = \sum_{n=1}^{\infty} \frac{1}{\mu_n} D_{1n} \cos \alpha_n z \quad \dots 5.14-a$$

$$\sum_{n=1}^{\infty} E_{3n} \cos \alpha_n z = \sum_{n=1}^{\infty} j \frac{\omega}{\gamma_n} C_{1n} \cos \alpha_n a \quad \dots 5.14-b$$

where  $H_{1n}$  and  $E_{3n}$  are the nth coefficients of the Fourier series representing  $H_1$  and  $E_3$  at boundary [M-1].

It follows immediately from above that

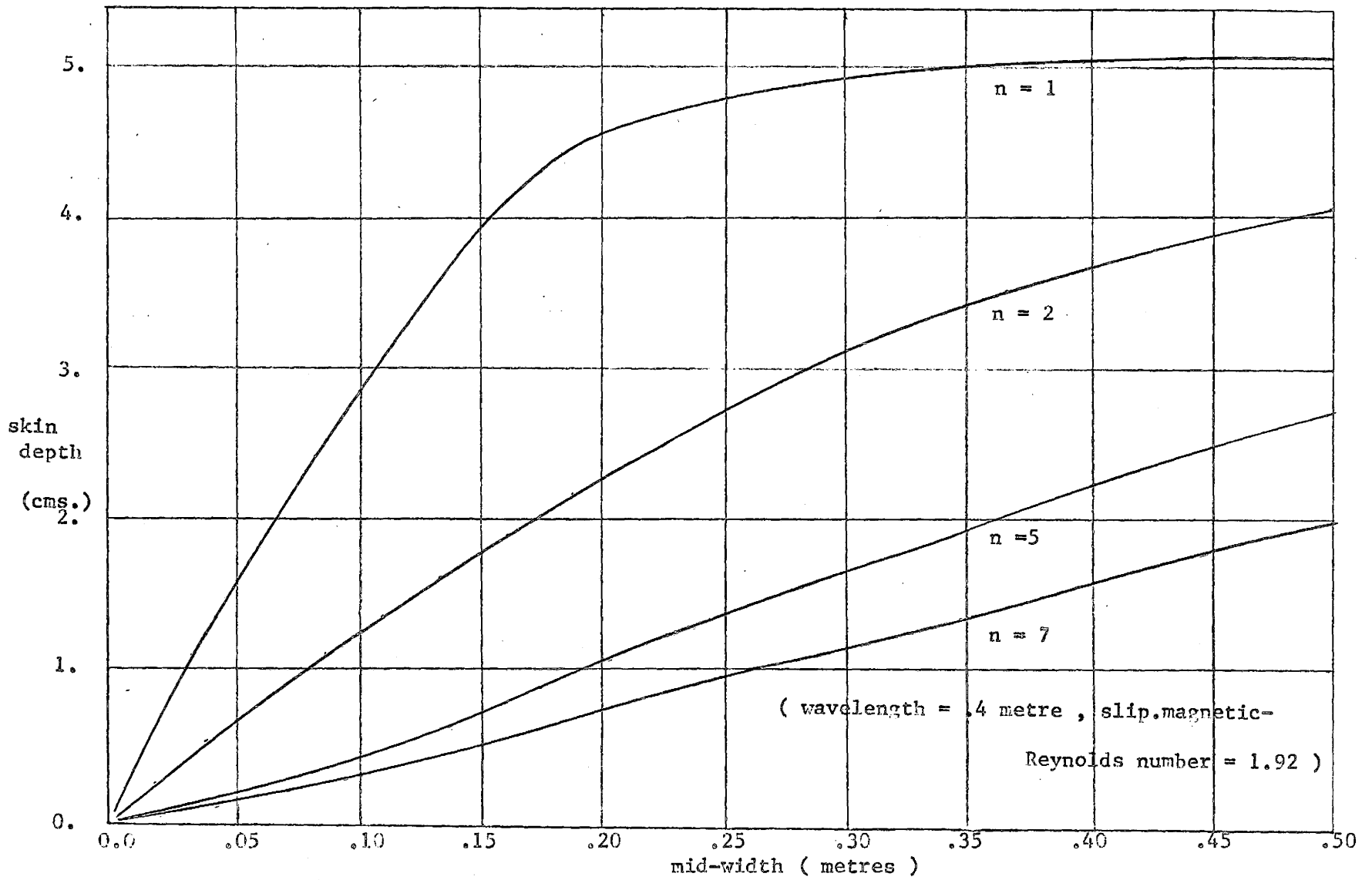


Fig 5.2-a : Variation of skin depth with secondary width.

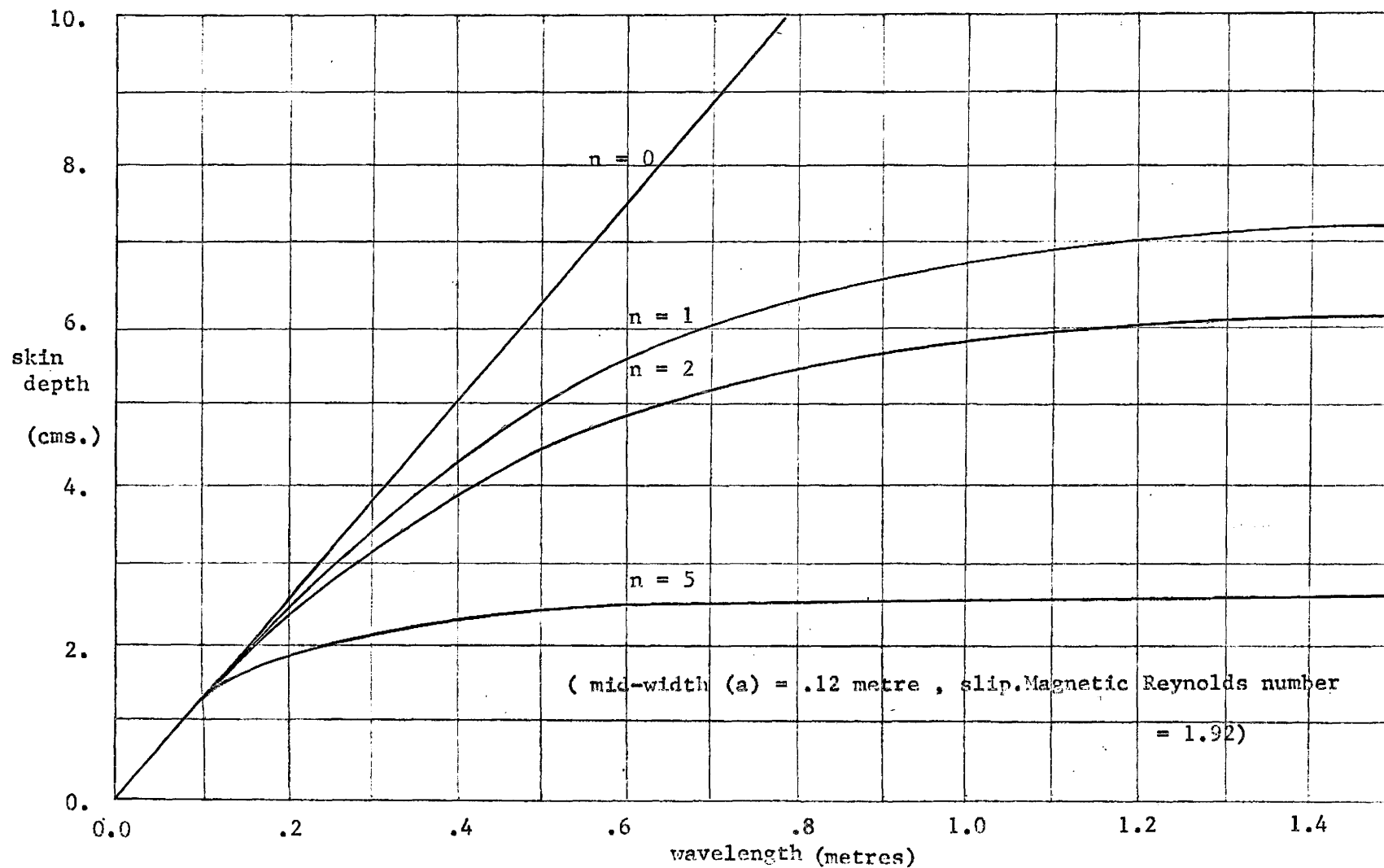


Fig 5.2-b : Variation of skin depth with wavelength.

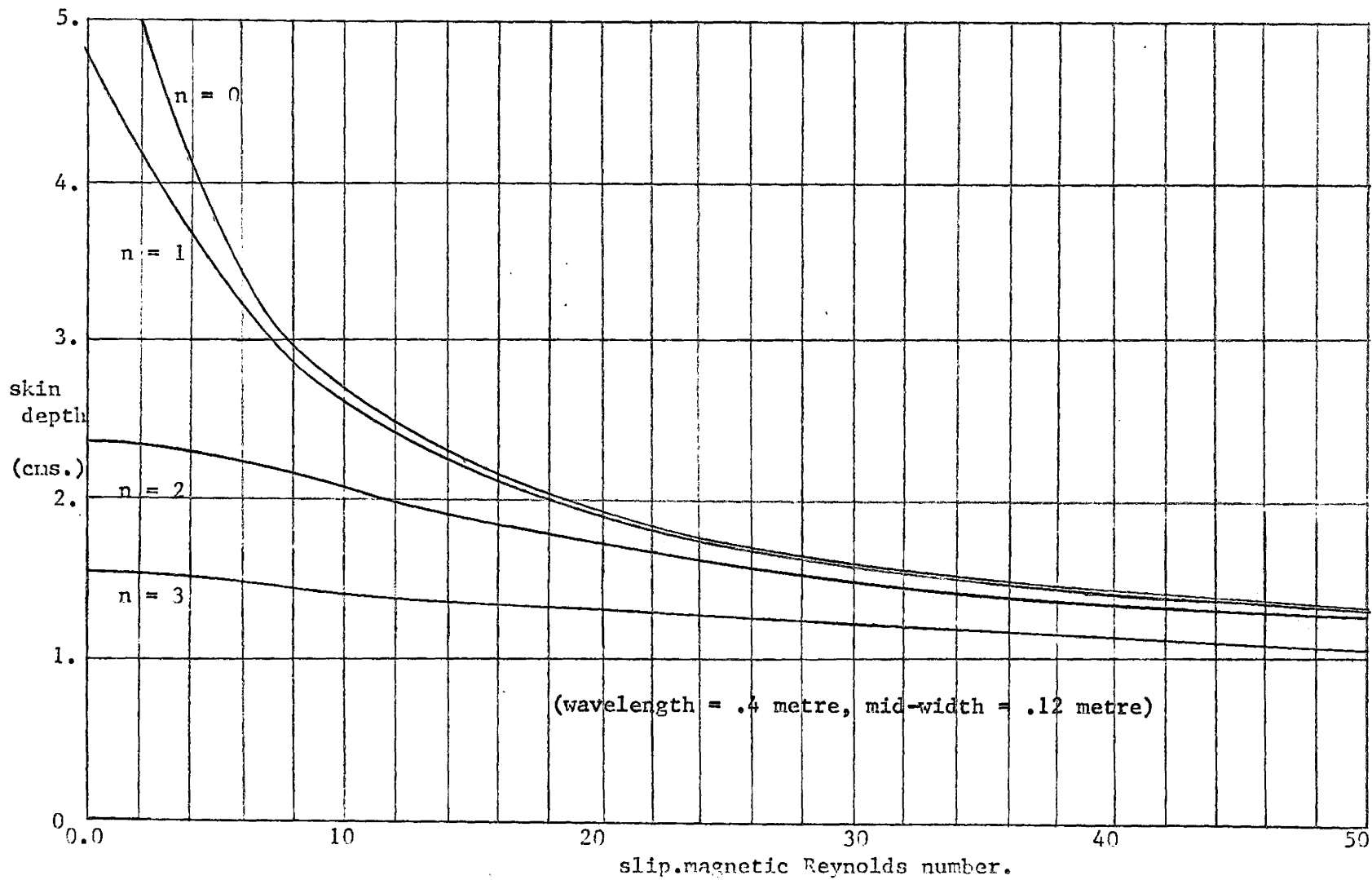


Fig 5.2-c : Variation of skin depth with magnetic Reynolds number

$$C_{.1n} = -j \frac{\gamma_n}{\omega} E_{.3n}$$

...5.15

$$D_{.1n} = \mu_n H_{.1n}$$

All quantities may now be written in terms of  $E_{.3n}$  and  $H_{.1n}$  at boundary M-1. Furthermore the relationship between the values at the two boundaries is given:

$$\begin{bmatrix} E_{.3n} \\ H_{.1n} \end{bmatrix} = \begin{bmatrix} \text{Cosh } \gamma_{Mn} \Delta_M & -j \frac{\omega \mu_M}{\gamma_{Mn}} \text{Sinh } \gamma_{Mn} \Delta_M \\ + j \frac{\gamma_{Mn}}{\omega \mu_M} \text{Sinh } \gamma_{Mn} \Delta_M & \text{Cosh } \gamma_{Mn} \Delta_M \end{bmatrix} \begin{bmatrix} E_{3M} \\ H_{1M} \end{bmatrix} \quad \dots 5.16$$

[M]  [M-1]

where  $\gamma_{Mn} = \sqrt{\alpha_n^2 + \beta^2 (1 + j S_M R_M)}$

$S_M$  = slip of region M

$R_M$  = Magnetic Reynolds number

$\Delta_M$  = thickness of region

The above matrix can be written:

$$T_{.Mn} = \begin{bmatrix} \text{Cosh } \gamma_{Mn} \Delta_M & -Z_{Mn} \text{Sinh } \gamma_{Mn} \Delta_M \\ Y_{.Mn} \text{Sinh } \gamma_{Mn} \Delta_M & \text{Cosh } \gamma_{Mn} \Delta_M \end{bmatrix} \quad \dots 5.17$$

Let us define the above as the  $n$ th harmonic transfer matrix.

It follows that for any number of such layers the values of  $E_{.3n}$  and  $H_{.1n}$  are related at the extreme boundaries:

$$\begin{matrix} \begin{vmatrix} E_{3n} \\ H_{1n} \end{vmatrix} \\ [M_f] \end{matrix} = \begin{matrix} T_{RN} \\ [0] \end{matrix} \begin{matrix} \begin{vmatrix} E_{3n} \\ H_{1n} \end{vmatrix} \\ [0] \end{matrix} \quad \dots 5.18$$

where

$$T_{RN} = \prod_{M, M-1, \dots} T_{Mn}$$

$T_{RN}$  is called the resultant matrix of order n.  $[0]$  and  $[M_f]$  are the two extreme boundaries.

In an open sided configuration one of the air regions is at infinity. In this case it is convenient to write:

$$\begin{matrix} \begin{vmatrix} E_{2M} \\ H_{1n} \end{vmatrix} \\ [M_f-1] \end{matrix} = \begin{matrix} \begin{vmatrix} 1 & 0 \\ j \frac{\sqrt{\alpha_n^2 + \beta^2}}{\omega \mu_0} & 0 \end{vmatrix} \\ [M_f] \end{matrix} \begin{matrix} \begin{vmatrix} E_{2n} \\ 0 \end{vmatrix} \\ [M_f] \end{matrix} \quad \dots 5.19$$

The 2,1 terms of the above matrix is the nth harmonic characteristic wave admittance for the air space.

### 5.6 Boundary Conditions at Stator Surface:

The primary currents are assumed to flow within an infinitesimally thin sheet of width 2a. The sheet is backed by a smooth iron surface of infinite permeability. Carter's coefficient is used in determining the effective air gap.

The divergence theorem must be satisfied for the primary linear current sheets:

$$\frac{\partial h_{\sim 1}}{\partial x} + \frac{\partial h_{\sim 3}}{\partial z} = 0 \quad \dots 5.20$$

The  $h_{\sim 1}$  component represents the end currents i.e. the currents in the winding overhang.

A particular distribution considered was to assume  $h_{\sim 3}$  having a rectangular distribution over the width. The corresponding  $h_{\sim 1}$  consists of delta dirac functions at  $y = \pm a$  see Fig. (5.3-a). This distribution was also considered by Okhremenko (22) and by Preston and Reece (45) the latter also considered the distribution shown in Fig. (5.3-b). A consequence of our particular choice of distribution is that at the inductor surface there are corresponding delta dirac functions in flux density distributions. These do not occur in practice since the above hypothesised smooth stator surface containing infinitesimally thin end conductors does not exist. However, at all points  $y > 0$  the expressions are convergent.

In appendix 1 the relationship between  $h_{\sim 30}$ , the fundamental of linear current sheet and phase "a" current is computed. The Fourier series representing the distribution shown in Fig. 5.3-a is:

$$h_{\sim 3n} = C_n h_{\sim 30} \quad \dots 5.21$$

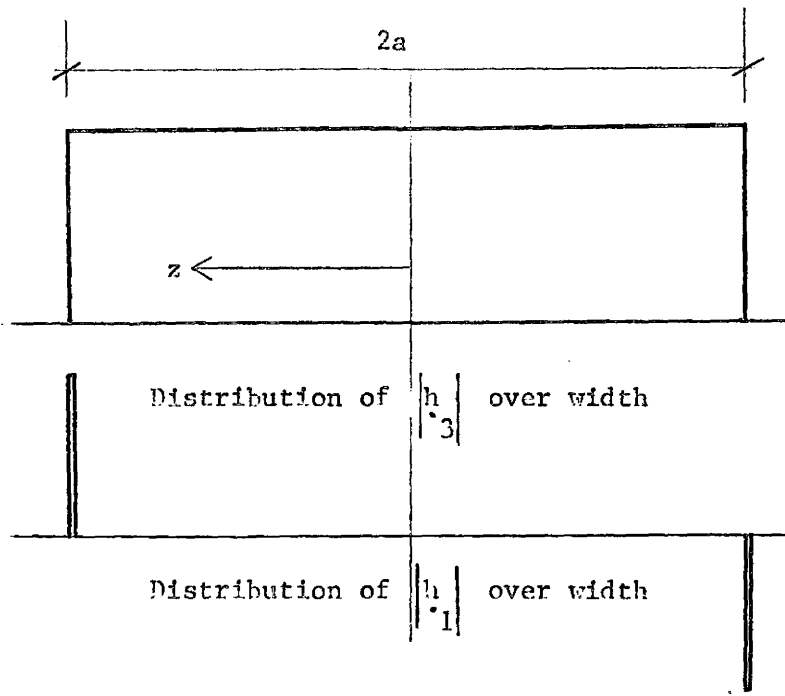


Fig 5.3-a : Primary current sheet distribution

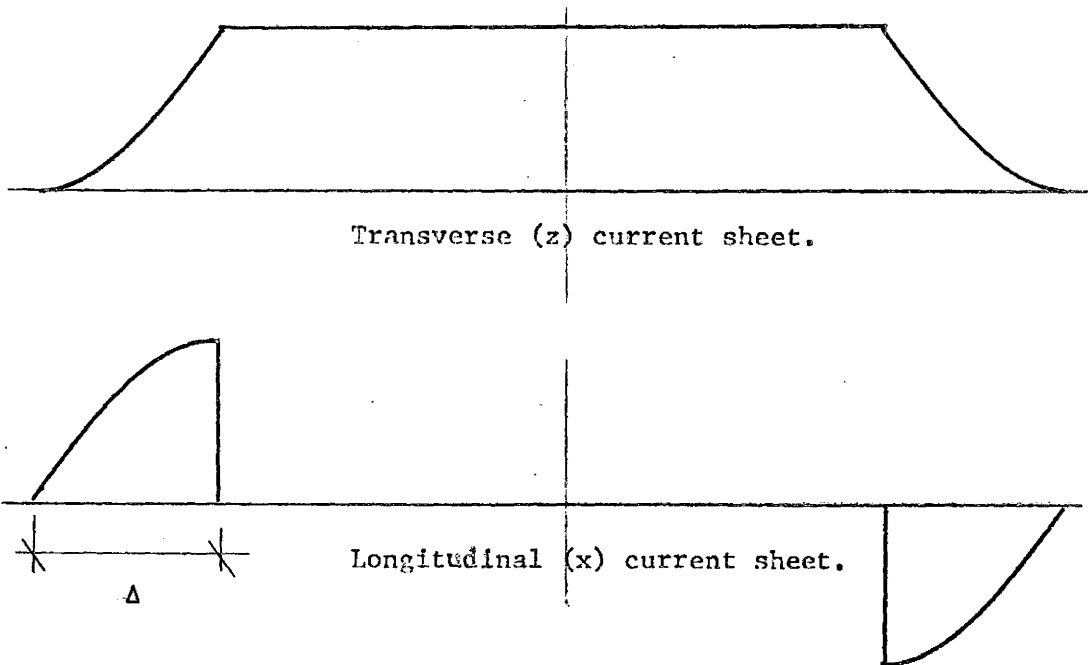


Fig 5.3-b : Primary current sheet distribution suggested in (45) to account for fringing.

no. of terms:	1	3	7	9	15	25	40
error	18.94%	6.69%	2.89%	2.25%	1.35%	.81%	.51%

Fig 5.4 : Truncation error in current sheet representation.

where

$$C_n = (-1)^{n-1} \frac{4}{\pi} \frac{1}{2n-1}$$

The value of  $h_{.1n}$  can now be found by applying the divergence theorem:

$$-j\beta h_{.1} + \sum_{n=1}^{\infty} -\alpha_n C_n h_{.30} \sin \alpha_n y = 0$$

i.e.

$$h_{.1} = \sum_{n=1}^{\infty} j(-1)^{n-1} \frac{2}{a} h_{.30} \sin \alpha_n y \quad \dots 5.22$$

A feeling for the magnitude of the truncation error involved in taking a finite number of terms in the solution can be obtained by finding the error at the boundary.

Using the error criterion suggested in (43, Section 6.8) we obtain:

$$e_N = 1 - \frac{1}{2} \sum_{n=1}^{\infty} C_n^2 \quad \dots 5.23$$

Typical values of the above error number are shown in table 5.4.

### 5.7 Reduction of General Solution in limiting cases:

The results in 5.5 are for the general case where both skin and the lateral edge effect are present. We now individually consider the limiting cases where the results obtained indicate their diminishing importance.

#### (a) Infinitely wide case

Say  $a$ , the mid width,  $\rightarrow \infty$

then  $\alpha_n = \frac{2n-1}{2a} \pi \rightarrow 0$ , all  $n$ .

Consequently:

$$\gamma_n \rightarrow \gamma_0 \text{ all } n.$$

It follows that all harmonic components of the field quantities are attenuated to the same extent.

In this case the  $n$ th harmonic Transfer Matrix (5.17) is identical with that defined in 4.16 where the lateral edge effect is neglected. It follows that for a surface current sheet which is constant over the width the solution takes the form outlined in 4.4.

(b) Finite width "thin" model:

Consider the transfer matrix  $T_{Mn}$  as defined 5.17. For values of  $|\gamma_{Mn} \Delta_M| \ll 1$  we can use the first term of the Taylor series expansion to replace the hyperbolic functions. Consequently we obtain:

$$\begin{bmatrix} T_{Mn} \end{bmatrix} = \begin{bmatrix} 1 & j\omega\mu_M\Delta_M \\ -j \frac{\gamma_{Mn}^2 \Delta_M}{\omega\mu_M} & 1 \end{bmatrix} \quad \dots 5.24$$

The above should give the same results as were obtained in Chapter 2. Consider the application of the above to the model in section 2.2. For simplicity we shall assume that  $c=g$ , i.e. the secondary completely fills the air gap.

From the definition of harmonic transfer matrix we have:

$$\begin{bmatrix} E_{3n} \\ 0 \end{bmatrix}_{y=0} = \begin{bmatrix} 1 & j\omega\mu_0 c \\ -j \frac{\gamma_n^2 c}{\omega\mu_0} & 1 \end{bmatrix} \begin{bmatrix} E_{3n} \\ H_{1n} \end{bmatrix}_{y=-c} \quad \dots 5.25$$

(Due to symmetry, the transverse magnetic field ( $H_1$ ) at the secondary centre = 0)

Consequently we have at the inductor surface:

$$E_{3n} = j \frac{\omega\mu_0}{\gamma_n^2 c} H_{1n} \quad \dots 5.26$$

From 5.9 we have:

$$B_{2n} = - \frac{\alpha_n^2 + \beta^2}{\omega\beta} E_{3n} \quad \dots 5.27$$

Substituting in 5.26 we obtain:

$$B_{2n} = - j \frac{\mu_0}{\beta c} \frac{\alpha_n^2 + \beta^2}{\gamma_n^2} H_{1n} \quad \dots 5.28$$

Upon substituting for  $H_{1n}$  (5.21) we obtain:

$$B_{2n} = - j \frac{\mu_0 h_{30}}{\beta c} (-1)^{n-1} \frac{1}{2n-1} \frac{\alpha_n^2 + \beta^2}{\gamma_n^2} \quad \dots 5.29$$

Using the relationship:

$$\frac{\cosh \gamma_0 z}{\cosh \gamma_0 a} = \sum_{n=1}^{\infty} \frac{2}{a} (-1)^{n-1} \frac{\alpha_n}{\gamma_n} \cos \alpha_n z \quad \dots 5.30$$

over  $-a < z < a$ .

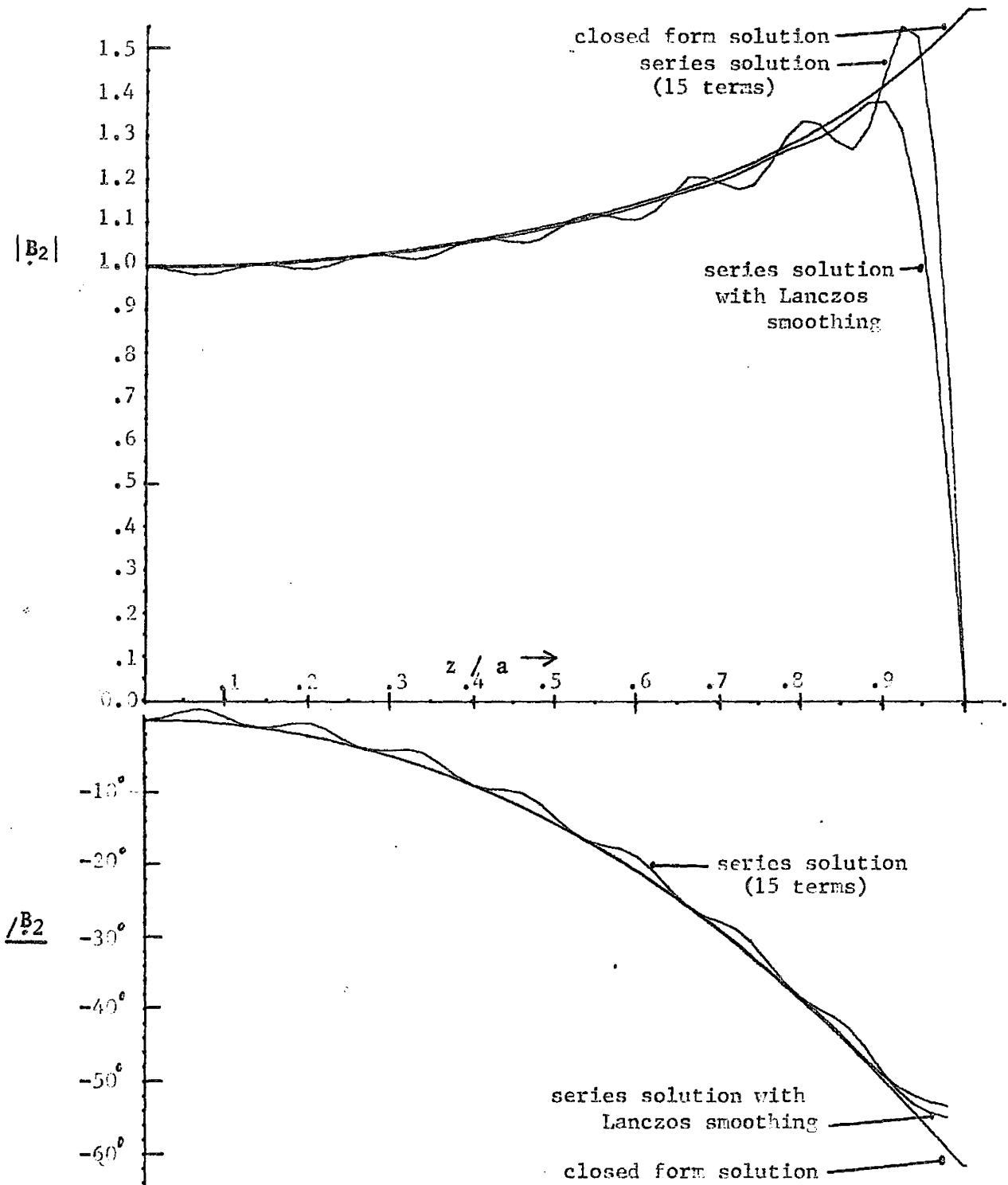


FIG. 5.5 : Equivalence of closed form and series solution.

( Lateral variation of  $B_3$  ,  $a / \lambda = .3$  , S.R = 1.92 ,  $\Delta = .5$  cm )

(which can be derived by taking the Fourier Series for  $\text{Cosh } \gamma_0 z / \text{Cosh } \gamma_0 a$  over the range) we obtain:

$$B_2 = -j \frac{\mu_0 h_3}{\beta c} \frac{1}{1 + j S R} \left\{ 1 + j S R \frac{\text{Cosh } \gamma_0 z}{\text{Cosh } \gamma_0 a} \right\} \quad \dots 5.31$$

This is exactly the result of (2.6-a) when  $G$  is replaced by  $R$  since the air gap is completely filled with secondary.

The equivalence of the two results is shown in fig. 5.5 with  $S, R = 1.92$  and  $a/\lambda = .3$ . Improvement in convergence and smoothing results when the Lanczos sigma factors (47) are applied to the 15 term series solution.

### 5.8 Discussion:

A compact solution to the multi-region travelling wave problem has been derived. Skin and lateral edge effect in the linear induction machine can be simultaneously studied using the solution obtained.

In the general case the stator and secondary will not have the same width. If skin effect is to be included the assumption of zero permeability outside the limits of the stators cannot be used. The fringing field at the stator edges and the field due to the stator end coils must be considered. One way of circumventing the problem is to artificially extend the stator to the limits of

the secondary. The fringing field can then be accounted for in a crude manner by allowing a variation in current in the end region. Such an approximation was made in (45).

A more accurate representation can be made if a solution is found for the fringing region. In this case the problem reduces to matching up the boundary conditions over the secondary width. Further work is being done in this area.

## CHAPTER VI

### CONCLUSIONS

#### 6.1 Summary of the Thesis:

The usual two models of the flat linear induction machine are the "infinite width" model and the "finite width thin" model. Each model has been analysed using traditional approaches.

The "ideal machine" has been described. The Laithwaite Goodness number has been introduced in terms of the equivalent circuit for the "ideal machine". The lateral edge effect has been discussed in detail. The distribution of the field quantities over the width has been shown to depend on the dimensionless parameters:-slip, Goodness number and mid-width/wavelength. In the case of the flat linear induction pump two extra parameters must be considered: the ratio of the side conductor resistance to the liquid metals resistance and the ratio of side conductor thickness to wavelength. The induced current density streamlines have been drawn. The main conclusion is that for values of mid-width/wavelength  $> 1$  the lateral edge effect can be neglected. The uneven flux density distribution resulting in shaded pole action has been determined for the case of a secondary asymmetrically positioned relative to the primary iron.

In the case of the infinite width machine flux penetration effects were studied.

Skin depth in the case of a travelling field was considered. The flux distribution over a single sided machine with and without

secondary conductor was plotted. The results show the dependence of the distribution on the dimensionless parameter slip, Reynold's number and on the wavelength. A travelling field has been shown to exist in the normal direction (upwards from the primary surface). The levitation force due to the resulting induction motor action in the normal direction has been calculated. For a finite thickness machine the distribution of the field quantities and output characteristics has been shown to depend on the dimensionless parameters: slip, magnetic Reynold's number and mid-thickness/ wavelength. It has been shown that a through flux machine with small mid-thickness/ wavelength ( $< .05$ ) is 'ideal'.

An analogue circuit representation has been used previously in describing electromagnetic fields in machines. This thesis develops and extends this idea to give a generalised representation of all flat linear machines under the infinite width assumption. Anisotropy has been considered which allows composite secondary machines to be analysed. Maxwells' magnetic stresses have been used in force calculation. The field in the stator teeth region has been determined. It is shown how the equivalent circuit is obtained from the analogue circuit. The concept forms a very useful bridge between the electromagnetic and circuit theory viewpoint of electrical machines.

The above method has been extended to include the case of simultaneous treatment of lateral edge and skin effect in the case of a homogeneous secondary. Skin effect is investigated in the case of a finite width travelling wave. Each harmonic component of the travelling wave is shown to have different skin depths. the skin

depth decreases with increasing harmonic number. Even in the case of infinite wavelength and zero conductivity a finite penetration depth results. Subject to the constraint that the secondary and stator(s) have the same width a general solution is obtained for the field quantities. It is indicated how this solution can be used to predict the performance of machines where neither of the two limiting approximations are appropriate. In the separate cases where the width becomes large and the thickness small (both compared with the wavelength) the results obtained are shown to be identical with those obtained using existing techniques.

## 6.2 Specific Contributions of This Work:

Some important steps in furthering the knowledge and generalising the theory of linear induction machines have been taken.

### 6.2-a

The induced current paths have been plotted in the case of the finite width machine. A clear insight is given to the lateral edge effect. In Fig 2.9-a the contours for  $S.R = .1$  and  $a/\lambda = .3$  are approximately elliptical in shape. With  $S.R = 1.92$  and  $a/\lambda = .3$  the ellipses are slightly distorted. This distortion is a consequence of the non-uniform phase shift in the  $z$  direction. The increase in non-uniformity with  $S.G$  is shown in Fig. 2.8.

Finally from Fig. 2.7, the phase and magnitude of the flux density is uniform over the centre portion of the channel. The

uniformity of the magnitude of the flux density is indicative of currents being  $z$  directed. The induced current contours for this case appear in Fig. 2.9-c. The steep change in phase angle gives rise to the acute distortion in induced current paths near the edges of the sheet. The validity of the infinite width assumption is apparent from the diagram.

A good appreciation for skin effect in the travelling wave case can be obtained from figures 3.3 and 3.4. Fig. 3.3 shows the usual flux distribution for an open sided machine. Fig. 3.4 shows very clearly the effect of the conducting medium on the penetration depth. The distortion of the contours in the direction of motion results from the phase shift in the  $y$  direction and indicates the presence of the travelling field in the  $y$  direction.

#### 6.2-b

The case of an induction pump with short circuiting side conductors has been taken into account. The case considered is that in which the side conductors are positioned just outside the limits of the primary ( $z = \pm a$  in Fig. 2.1). Fig. 2.12 shows the variation of over the width normal component of flux density as a function of the ratio of the resistivity of side-conductors to the fluids resistivity. The justification of the ideal machine assumption for low values of  $\rho' / \rho$  is shown.

In the practical case the contact resistance between the fluid

may not be negligible and the side conductors may not be positioned at  $(z = \pm a, \text{ Fig. 2.1})$ . In this case modified values of impedance at the interfaces separating the active from the inactive zones will have to be considered.

#### 6.2-c

The Goodness number of Laithewaite has been placed in proper perspective by comparing it with the magnetic Reynold's number. The magnetic Reynold's number is the more fundamental of the two. The Reynold's number is a dimensionless parameter occurring in the magnetic transport equation. The Laithwaite Goodness number on the other hand results from an inspection of the equivalent circuit.

#### 6.2-d

A major step in the representation of induction machines (under the infinite width assumption) as a tandem connection of analogue circuits has been taken. This is in the representation of the stator tooth region as a two port network.

In previous work the linear current sheet idealization had to be used and the primary slot leakage reactance calculated by conventional techniques.

In this thesis the slotted stator region is accounted for just as all other regions as a two port network.

The field quantities  $E_3$  and  $H_1$  (Fig. 4.2) are expressed in

terms of the average electric field intensity in the slot region and the applied current density. The latter two quantities are related to the applied voltage and current respectively. Consequently the driving function has been established.

This extension to the theory allows a complete representation of induction machines as analogue circuits in tandem. From 4.27 we can write:

$$\begin{bmatrix} E_3 \\ H_1 \end{bmatrix}_{d_s} = \begin{bmatrix} \frac{\beta_2 d_s}{\tanh \beta_2 d_s} & -j \frac{\mu_x}{\beta_2 d_s} \left( \frac{\beta_2 d_s}{\tanh \beta_2 d_s} - 1 \right) \\ j \frac{\beta_2 d_s}{\omega \mu_y} & 1 \end{bmatrix} \begin{bmatrix} E_{3avg} \\ H_a \end{bmatrix}$$

where  $H_a = d_s J_{s3}$ .

From the above the obvious choice for the driving function is  $E_{3avg}$  or  $H_a$  depending on whether we have a voltage or current drive. The relationship between  $E_{3avg}$  and the applied voltage and between  $J_{s3}$  ( $H_a = d_s J_{s3}$ ) and the primary current were derived and appear in Appendix 2.

The above transfer matrix was derived by solving the field equations for the stator tooth region. This region was represented by an anisotropic medium with a distributed current density distribution.

The resulting slot leakage reactance given by the analogue circuit can be shown to be consistent with the value calculated conventional machine analysis. The modified procedure for obtaining a solution to

the field equations and the equivalent circuit for any induction machine under the infinite width assumption is:

- (1) The machine is divided into a number of planar regions. The regions may be stratified in the x direction (direction of motion) but each must be homogeneous over its thickness (y direction). The appropriate value of conductivity and permeability is calculated in accordance with the table in Fig. 4.2.
- (2) The transfer matrix (as defined Fig. 4.16-b) for each region is obtained. The Tor  $\pi$  equivalent circuits may be derived.
- (3) The overall analogue circuit is the tandem connection of the individual circuit representing each region.
- (4) Solution for the field quantities in any region reduces to solving an electric circuit. One of the two quantities  $E_{3avg}$  and  $H_a$  will be determined (depending on whether we are considering the external voltage or current to be constant).

#### 6.2-e

One of the main advantages of the Transfer Matrix (Analogue circuit) representation of induction machines is the systematic way in which the boundary conditions are applied. This ensures complete tractability of the results and minimises the danger of using incorrect reference directions etc. The same algorithm can be used to give the results to a wide variety of problems. Another advantage is that the influence of different elements can be appreciated quite simply

137

in an equivalent circuit or Transfer Matrix form.

The solution of the field equations in a three dimensional case is generally in the form of an infinite series solution. Due to the formidability of the resultant expressions attempts to analyse the solutions are usually abandoned.

There was very obviously a requirement for an extension of the Transfer Matrix approach to cover this case.

That goal has been achieved in this thesis for the case where all the regions representing the machine have the same width.

Following the development in the infinitely wide case the solution for a general region is obtained. It has been shown that if the boundary conditions are expressed as Fourier series then each harmonic component of the field quantities at one boundary is related only to the same harmonic component at the other boundary. It follows that the analysis for the complete stack of regions can be determined by solving independently for each lateral harmonic. Consequently an overall harmonic transfer matrix is determined. It expresses the relationship for each harmonic between the electric and magnetic field intensities at one extreme boundary to those at the other.

If the primary current is known then the harmonic components of magnetic field intensity can be obtained from the lateral harmonic components of the linear current sheet representing the primary. If the voltage is fixed it is necessary to assume some current, find the corresponding voltage and then multiply the current by the appropriate

factor. It should be noted that a specific voltage does not uniquely determine the individual lateral space harmonics of electric field intensity. The approach developed permits simultaneous investigation of flux penetration effects (leakage and skin effect) and lateral edge effects. The method is directly amenable to solution by digital computer.

In cases where the width becomes comparable with the wavelength the results have been shown to be consistent with those given by the Transfer Matrix approach (under the infinite width approximation). In cases where the thickness is small relative to the wavelength the results given by the Harmonic Transfer Matrix have also been shown to be consistent with those given by an independent two dimensional approach.

### 6.3 Suggestions for future work in this area:

The inclusion of the phrase "in this area" is intended to differentiate between the general field of linear induction machines and the work presented in this thesis. The latter could be classified as solution of certain electromagnetic boundary value problems which have as one of their applications linear induction machines.

The method outlined in Ch. 5 is subject to the constraint that the secondary has the same width as the stator. For accurate analysis the field in the fringing region and the stator return path outside the iron must be accounted for. Work has already begun on this problem. When completed more accurate predictions will be possible. The assumption

of lateral symmetry may be then discarded and a general analysis of lateral stability in the presence of skin effect and fringing field may be performed.

As developed here the analogue circuit concept applies to all induction machines. It would be most useful to apply this to the case of cylindrical elements. Very compact results would then be available for a wide range of machines such as the solid rotor induction machine.

It would be extremely interesting to investigate deeply the full consequence of the replacement of the stratified structures in Section 4.1 by an anisotropic medium. This would involve the solution of equations with periodically varying coefficients. The solution would indicate space harmonics and clearly define the conditions under which the space harmonics can be neglected.

## APPENDIX 1

### CURRENT DENSITY DISTRIBUTION DUE TO A THREE PHASE DISTRIBUTED WINDING.

Refer to Fig. 2.1. for co-ordinate system. It can be shown that for a balanced 3 $\phi$  system we get:

$$J_3(x,t) = \frac{3n_s n_t d_s}{\tau d_s} \left[ \sum_{n=1}^{\infty} k_{dn} \cos(\omega t - \beta_n x) \right] I_a$$

$n_s$  = number of slots per phase belt.

$n_t$  = number of turns in series/slot.

$\tau$  = pole pitch.

$d_s$  = active slot depth.

$I_a$  - phase current.(origin for  $x$  is at centre of phase-belt'a')

$k_{dn}$  = is the winding distribution factor.

$$= \frac{\sin \frac{n\pi}{6}}{n_s \sin \frac{n\pi}{6} n_s}$$

$$\beta_n = + \frac{\pi}{\tau}, - \frac{3\pi}{\tau}, + \frac{5\pi}{\tau} \text{ etc.}$$

If we neglect the coils distribution in the  $y$  direction then we get the usual linear current sheet distribution.

$$h_3(x,t) = d_s J_3(x,t)$$

The fundamental component is only considered in this work. The neglect of harmonics is in fact generally more acceptable in linear machines. This is because, due to the relatively large air gap higher harmonic fields are attenuated more severely than the fundamental.

The voltage induced is given by integrating the electric field intensity in the z direction, and adding the contribution due to different coils.

The result is:

$$V_a = 2 n_s n_t K_{dl} E_{3avg} \cos(\omega t) \quad \text{volts/metre length}$$

APPENDIX II  
VECTOR PHASORS

Due to alternating currents in a distributed winding, it has been stated in appendix 1, a current distribution exists whose fundamental component is of form:-

$$J_{3m} \cos(\omega t - \beta x).$$

The above represents the boundary conditions distribution and it can be shown (since we are dealing with a linear system) all field quantities take the same x distribution.

It is much easier to work in complex numbers so consequently we write:

$$J_{3m} = \operatorname{Re}\{J_{3m}\} = \operatorname{Re}\{J_{3m} e^{j(\omega t - \beta x)}\}$$

A vector phasor can be obtained from the above by deleting the time-x variation. The time averaged values of quantities involving the product of two phasor quantities G and H is given:

$$1/2 \operatorname{Re} \{ G.H^* \}$$

where Re stands for the 'real part of' and the asterisk denotes the complex conjugate.

## REFERENCES

1. E.R. LAITHWAITE & S.A. NASAR: "Linear Motion Electrical Machines", Proc. IEEE, vol. 58, no. 4, April 1970.
2. A.A. VERTE, "Electromagnetic Transport of liquid metal", translation Izdatel'stvo "Metallugiya", Moscow, U.S.S.R. 1965
3. "A Wound Rotor Motor 1400 ft. long, " Westinghouse Engineer, vol. 6, p. 160, 1946.
4. L.R. BLAKE, "Conduction and Induction Pumps for Liquid Metals", Proc. IEE (London) pt. A, pp. 49 - 67, 1957.
5. ELLIOTT & ALT, "Performance capabilities of Liquid Metal MHD Induction Generators," Energy from MHD, vol. 3, International Atomic Energy Agency, Vienna, Austria, pp. 1859 - 1877, 1968.
6. KANT & BONNEFILLE, "Determination of an ac Liquid Metal MHD Generator," Energy from MHD, fol. 3, pp. 1717 - 1729, 1968.
7. E.R. LAITHWAITE, "Propulsion Without Wheels," Hart, New York, 1968.
8. E.R. LAITHWAITE, "The Engineer in Wonderland", The English Universities House, 1967.
9. E.R. LAITHWAITE, "Induction Machines for Special Purposes", London, George Newnes, 1966.
10. E.R. LAITHWAITE, " The Goodness of a Machine", Proc. IEE (London, vol. 112, pp. 538 - 541, 1965.

11. E.R. LAITHWAITE, "Differences in series and parallel connection in machines with asymmetric magnetic circuits," Proc. IEE (London), vol. 112, pp. 2074 - 2082, 1965.
12. E.R. LAITHWAITE, "Some aspects of electrical machines with open magnetic circuits," Proc. IEE (London) vol. 115, pp. 1275 - 1283, 1968.
13. E.R. LAITHWAITE, & D. TIPPING & D.E. HESMONDHALGH, "The application of induction motors to conveyors," Proc. IEE (London), vol. 107A, pp. 284 - 294, 1960.
14. E.R. LAITHWAITE, "Electromagnetic levitation," Proc. IEE (London), vol. 112, pp. 2361 - 2375, 1965.
15. M. POLOUJADOFF, "Linear induction machines, Part I", IEEE Spectrum, vol. 8, no. 3, pp. 72 - 80, Feb. 1971.
16. M. POLOUJADOFF, "Linear induction machines, Part II", IEEE Spectrum, vol. 8, no. 3, pp. 79 - 86, March 1971.
17. M. POLOUJADOFF, "A simplified theory of the linear induction motor", ETZ, vol. 90, pp. 545 - 548, 1969.
18. M. POLOUJADOFF, "Influence of the shape of the magnetic circuit on the end effect of linear induction motors," Compt. Rend. Acad. Sci. Paris, vol. 269, pp. 1215 - 1218, 1969.

19. E.R. LAITHWAITE, & F.T. BARWELL, "Linear induction motor for high-speed railways", Electronics and Power, vol. 10, pp. 100-103, 1964.
20. D.N. ABOUNDARA & L.K. EDWARDS, "Tomorrow's mass rapid transit-available today", IEEE Spectrum, vol. 4, pp. 61 - 70, Jan. 1967.
21. BOON-TECK OOI & D.C. WHITE, "Traction and Normal forces in the linear induction motor", IEEE Trans. on Power Apparatus and Syst., vol. Pas.-89, no. 4, April 1970.
22. N.M.OKHREMENKO, "An investigation of the spatial distribution of the magnetic fields and electromagnetic effects in induction pumps," Magnetohydrodynamics, vol. 1, no. 3, pp. 72 - 80 , 1965.
23. N.M. OKHREMENKO, "Transverse fringe effects in flat linear induction pumps, Magnetohydrodynamics, vol. 1, no. 3, pp. 64 - 71 , 1965.
24. N.M. OKHREMENKO, "Travelling-field induction pumps," Magnetohydrodynamics, vol. 1, no. 4, pp. 1 - 14, 1965.
25. TSIH C. WANG, "Linear Induction Motor for High-speed Ground Transportation", IEEE Trans. on Industry and general applications, vol. IGA-7, no. 5, Sept./Oct. 1971.
26. T.C. WANG & S.J. DUDZINSKY, "Theoretical and experimental study of a liquid metal MHD induction generator", AIAAJ, vol. 5, pp. 107 - 112, 1967.

27. T.A. VESKE, "Solution of the electromagnetic field equations for a plane linear induction machine with secondary boundary effects", *Magnitnaya Gidrodinamika*, vol. 1, no. 1, pp. 87 - 96, 1965.
28. Y.A. VALUEV, Method of Selecting the optimal parameters of a flat linear induction pump with lateral shorting bars", *Magnitnaya Gidrodinamika*, vol. 3, no. 1, pp. 109 - 114, 1967.
29. H. BOLTON, "Transverse edge effect in sheet-rotor induction motors", *Proc. IEE*, vol. 116, no. 5, May 1969.
30. H. BOLTON, "Forces in induction motors with laterally asymmetric sheet secondaries", *Proc. IEE*, vol. 117, no. 12, December 1970.
31. A.P.RASHCHEPKIN, "Field in the gap of induction machines for a variable linear winding load", *Magnetohydrodynamics*, vol. 1, no. 3, pp. 71 - 75, 1965.
32. A.P.RASHCHEPKIN, "Symmetrization of the winding of an induction machine with an open magnetic circuit", *Magnitnaya Gidrodinamika*, vol. 2, no. 2, pp. 116 - 122, 1966.
33. S.A. NASAR, "Electromagnetic fields and forces in a linear induction motor taking into account edge-effects," *Proc. IEE (London)*, vol. 116, pp. 605 - 609, 1969.
34. D.J. CERINI & D.G. ELLIOTT, "Performance Characteristics of a Single-Wavelength liquid metal MHD induction with End-Loss Compensation", *AIAA Journal*, vol. 6, no. 3, March 1968.

35. D.A. WATT, "The design of electromagnetic pumps for liquid metals", The Institution of Electrical Engineering, no. 2763, Dec. 1958.
36. G.F. NIX & E.R. LAITHWAITE, "Linear induction motors for low-speed and standstill application", proc. IEE, vol. 113, no. 6, June 1966.
37. J. GREIG, E.M. FREEMAN, "Travelling-wave problem in electrical machines", Proc. IEE, vol. 114, no. 11, November 1967.
38. E.M. FREEMAN, "Travelling waves in induction machines Input impedance and equivalent circuits", Proc. IEE, vol. 115, no. 12, Dec. 1968.
39. E. MISHKIN, " Theory of the squirrel cage induction machine derived directly from Maxwells' field equations", Quart. Journ. Mech. and Appl. Math., vol. 7, pt. 4, 1954.
40. A.L. CULLEN, T.H. BARTON, "A simplified electromagnetic theory of the induction motor, using the concept of wave impedance", IEE, vol. 105, no. 8, 1958.
41. C.J. CARPENTER, "Surface-integral methods of calculating forces on magnetized iron parts", IEE, no. 342, Aug. 1959.
42. N. KESAVAMURTHY, P.K. RAJAGOPALAN, "Equivalent Circuit and evaluation of eddy-current loss in solid cores subjected to alternating and rotating magnetic fields", IEE, no. 385, June 1960.
43. E. DELLA TORRE & C.V. LONGO, "The Electromagnetic field", Allyn and Bacon Inc. 1969.

44. HUGHES & YOUNG, "The electromagnetodynamics of fluids", Wiley, 1966.
45. T.W. PRESTON, A.B. REECE, "Transverse edge effects in linear induction motors," Proc. IEE, vol. 116, no. 6, June 1969.
46. A.A. VERTE, "Electromagnetic Transport of liquid metal", translation Izdatel' stuo Metqlllugiya, Moscow, 1965.
47. LANCZOS "Applied Analysis" Prentice Hall 1961.